Ionotropic and metabotropic signalling in neuronal development and differentiation

A thesis submitted for the degree of Doctor of Philosophy

by

Alexander W J Harrison MSc (DIC)

2012

Cardiff School of Biosciences

Cardiff University

Abstract

This thesis investigates ionotropic and metabotropic signalling mechanisms in developing neurons from human embryonic stem cell and primary sources. Focus is placed on the measurement of functional activity using primarily whole-cell patch-clamp and Ca^{2+} imaging techniques

These signalling mechanisms were investigated in undifferentiated human embryonic stem cells, hESC-derived neurons, fetal primary human neurons and neonatal primary mouse neurons. The results of this research are separated into three chapters. Preliminary work carried out on iPSC-derived neurons is also included as an indication of future direction

Chapter 3: P2 Receptors in hESCs

Purinergic signalling was shown to be active in undifferentiated hESC populations. Specifically, the activity of $P2Y_1$ receptors was confirmed pharmacologically. This is a novel observation and indicates a mechanism for physiologically relevant signalling molecules to modify $[Ca^{2+}]_i$

Chapter 4: Functional Characterisation of hESC-Derived and Primary Neurons

Functional characteristics associated with neuronal development were measured in human embryonic stem cells during terminal neuronal differentiation in a chemically-defined medium. The presence and activity of voltage-gated Na^+, K^+ and Ca^{2+} channels were recorded, alongside data on neuronal excitability (V_m, iAP induction and threshold and spontaneous electrical activity). These data were also recorded in fetal hWGE- and neonatal mWGE-derived neurons for comparison. hESC-derived neurons were shown to be functionally more similar to fetal hWGE-neurons suggesting an immature neuronal phenotype

Chapter 5: GABAergic Signalling in hESC-Derived and Primary Neurons

GABAergic signalling in hESC-, mWGE- and hWGE-derived neuronal populations was investigated. Focus was placed on hWGE-derived neurons and the developmental state of GABAergic responses. In fetal hWGE-derived neurons, a percentage of cells displayed an 'inhibitory' response to $GABA_AR$ activation. This is a novel observation with implications in human neuronal development. *In vitro* modulation of GABAergic signalling was also shown, providing potential tools for future research into this phenomenon

Chapter 6: Future Developments and General Discussion

iPSC-derived neuronal populations were shown to display basic neuronal functional properties. This work will form the basis of future studies on these cells

Acknowledgements

I would like to thank everyone who I worked with during my PhD for making it a very enjoyable experience.

Thanks to Alysia for teaching me how to grow hESCs, to Bill and Seva for teaching me to patch and to Seb for teaching me Ca^{2+} imaging.

I would also like to thank Claire, Sophie and Shona for kindly providing cells on numerous occasions.

Thank you to Nick and Paul for giving me this opportunity and for all the help and support you have provided over the years.

Jules, thank you for being there throughout, keeping me sane and giving me a life I look forward to getting back to.

Finally I would like to dedicate this thesis to Alice Kate Glenister, forever smiling and forever keeping me motivated.

Abbreviations

BDNF - Brain-Derived Neurotrophic Factor

CCE - Capacitative Calcium Entry

CNS - Central Nervous System

DIV - Days in vitro

ECS - Extracellular Solution

hWGE - Human Whole Ganglionic Eminence

iAP - Induced Action Potential

ICS - Intracellular Solution

iPSC - Induced Pluripotent Stem Cell

LGE - Lateral Ganglionic Eminence

mESC - Mouse Embryonic Stem Cell

MGE - Medial Ganglionic Eminence

MTOP - Medical Termination of Pregnancy

mWGE - Mouse Whole Ganglionic Eminence

NSC - Neural Stem Cell

PLL - Poly-L-Lysine

PPD - Post-Plate Down

sAP - Spontaneous Action Potential

STOP - Surgical Termination of Pregnancy

SVZ - Subventricular Zone

Vm - Membrane Voltage

VZ - Ventricular Zone

Contents

Chapter 1. Introduction

Regenerative medicine is the practice of producing healthy cells or tissue for the replacement or repair of damaged tissue in the host. Stem cells have been widely publicised as a potential source of cells for tissue transplantation. Similarly, the ability to grow and differentiate cells *in vitro* provides the potential for producing developmental and disease models which mimic *in vivo* phenotypes. Such models may provide valuable information about developmental processes and may also offer a platform for high throughput drug screening and testing. Ionotropic and metabotropic signalling within stem-cell populations remains relatively uncontrolled *in vitro* yet offers the potential for improved differentiation. The following thesis focuses on ionotropic and metabotropic signalling within stem cell and progenitor populations, specifically with respect to neuronal development.

1.1. Tissue Transplantation

Tissue transplantation has long been used as a method to alleviate or eliminate the symptoms of disease. It is commonplace for patients with kidney, heart, liver or skin defects to undergo transplantation surgery to replace defective with healthy tissue although progress with neuronal transplantation has been limited (Starzl, 2000). In the early 20th century, the first successful corneal transplantation was carried out by Dr Eduard Zirm (Zirm, 1906), whilst whole-organ transplants have been used successfully since the 1950s to replace organs which have become defective (Murray *et al.*, 1956). There are several types of transplantation, defined by the source of donor tissue: autograft - where donor and recipient are the same individual (*e.g.* skin grafts, tendon replacement); allograft – where the donor is a non-identical individual species-matched to the recipient; isograft – where donor

and recipient are genetically identical individuals (*e.g.* identical twins), and; xenograft – where the donor is of a different species to the recipient (*e.g.* the use of porcine valves in heart transplantation). Organ donation, in these many forms, is often a complicated procedure both physically and ethically. It is also, with the exceptions of autografts and isografts, subject to rejection of donor tissue by the host immune system. This problem, due to histoincompatibility between the donor and recipient human leukocyte antigen system (HLA), is one of the major obstacles to successful tissue transplantation (Kahan, 2009).

The use of immunosuppressants, such as cyclosporine-A, has been shown to reduce the destruction of donated tissue by the recipient's immune system. However, the suppression of the immune system dramatically increases the risk of infection and malignancy within the patient (Starzl, 2000). Together with the difficulties in finding donors with matching HLAs, rejection of transplants makes the process of tissue transplantation a difficult and lengthy challenge which, at best, is still far from perfect as a treatment for the original disorder or disease (Kahan, 2009).

Since autografts employ donor tissue originating from the recipient, they are not subject to rejection and, consequently, carry less risk than the more commonly employed allografts. The obvious downside to autografts is the availability of tissue. Being unable to provide tissue for direct replacement of organs restricts this type of donation to the movement of tissue from one area in order to repair other areas, as in skin grafts or muscle and tendon repair (Starzl, 2000; Marrale *et al.*, 2007). To combat the problems of both tissue availability and compatibility, the use of stem cells as a source of donor tissue is widely considered as a potentially realistic prospect. With recent advances in the production, maintenance, differentiation and

manipulation of stem cells, it is becoming more apparent that, with further research and development of techniques, it may be possible to produce tissue for donation that has been specifically engineered for the intended purpose (Dominguez-Bendala *et al.*, 2002).

Although there is exciting potential for stem cells to provide tissue for transplantation, current knowledge and techniques are as yet underdeveloped. Embryonic stem cells (ESCs) are now widely cultured in many laboratories and multiple established cell lines are now available. Furthermore, there are established protocols for the differentiation of these cells into various important tissue types, and clinical trials involving the transplantation of stem cells into human patients, although uncommon, are in progress (Bongso & Fong, 2009; Cristante *et al.*, 2009; Menasche, 2009). However, there is still a requirement for more information about the biological characteristics and functional properties of these cells. Studying their integration into patient organ systems, observing similarities between differentiation *in vitro* and *in vivo* of various cell types and assessing the effectiveness of differentiated cells at performing functions necessary for their use is important in order to realise fully their clinical potential (Blum & Benvenisty, 2008).

It is possible that treatment of neurological disorders through the introduction of tissue may potentially alter the patient's personality and psychological characteristics. Even if exogenous neuronal tissue was effectively integrated into the existing network, it may not necessarily improve cognitive function. Not enough is known about neuronal networks and the complicated system of integration of newly generated neurons *in vivo* let alone that of exogenous tissue introduced

through surgery. In some cases of neuronal degradation, there is preliminary evidence that suggests transplantation of new tissue may lessen the disease-associated psychological and motor effects observed in many patients. This area is still in its infancy and a greater understanding of the integration and of both the beneficial and detrimental effects of neuronal grafting will be of tremendous value to this area (Lindvall & Kokaia, 2006).

1.2. Stem Cells as Disease Models

In addition to their use in transplant therapy, it has been suggested that stem cells may be useful in producing *in vitro* models of disease. This would allow improved study of diseases and how they affect cell populations in systems more accessible to various investigative techniques, such as whole cell patch clamp. Once established, these models may provide important information that could otherwise be unobtainable, or ethically unreasonable, using animal or patient studies, respectively. They may also be useful for high-throughput drug discovery and drug toxicity testing that employ large libraries of drugs to be screened for advantageous or negative effects on specific stem cell-derived cell types. Using these models to test the efficacy of candidate drugs before clinical trials may reduce the ethical complications in setting up such trials (Scheffler *et al.*, 2006).

1.3. Neuronal Transplantation

The transplantation of neuronal tissue has been studied since the late 1800s when W. G. Thompson transplanted cortical tissue from feline and canine brains into canine host brains (Markakis & Redmond, 2005). The low level of transplant success, and the minimal requirements for a transplant to be considered successful,

was a clear indication of the necessity for improvement and further research. At this early stage, a successful transplant had only to show signs that the tissue had survived a short period of time within the host system. Integration and interaction were not required. As the implications of neural transplantation became more focused on the potential clinical advantages, rather than mere scientific curiosity, research into this area became more commonplace.

The focus of recent research into neural transplantation has largely centred on the treatment, or improvement to pathology, of patients with neurodegenerative conditions effecting specific cell types or brain regions including Huntington's disease (Hauser *et al.*, 1999; Bachoud-Levi *et al.*, 2001; Gaura *et al.*, 2004), Parkinson's disease (Perlow *et al.*, 1979; Bjorklund *et al.*, 1980; Dunnett *et al.*, 1981) and stroke damage (Savitz *et al.*, 2004) in particular (Markakis & Redmond, 2005). Research into spinal injury has also received considerable attention (McDonald & Becker, 2003), but, whilst showing many similarities, is considered to be a different area of research and will not be considered further herein.

Neuronal grafting, as it is referred to in this thesis, consists of injecting suspensions of neuronal progenitor cells into the relevant region of the host brain.

1.3.1. Fetal Neural Tissue Transplantation

Early studies have shown that immature postnatal tissue provides a greater success rate than mature tissue for survival of transplanted tissue in rodent models (Markakis & Redmond, 2005). This idea was further refined to show that prenatal tissue conferred a considerable improvement of graft survival in rodent models (Le Gros Clark, 1940).

As with many areas of research, the use of animal models as research tools has been the focus of the majority of efforts. Animal models provide a means to understand and research the process of tissue transplantation without endangering further the health of people with neurological disorders using procedures that are not yet fully optimised. Following the success for fetal grafts in animal models of Parkinson's disease, where functional improvements were first observed (Bjorklund & Stenevi, 1979; Perlow *et al.*, 1979), research into grafting as a therapy for Huntington's disease also began with the use of animal models. Originally, it was shown that fetal rat tissue grafted into quinolinic acid excitotoxicity-lesioned rodent striatum (a model for the degeneration seen in Huntington's disease), could survive in the host brain up to 16 weeks and that choline acetyltransferase and glutamic acid decarboxylase levels, normally decreased in the diseased state, were restored in the graft-treated striata of rats compared to the control (sham-operated) rats. Not only were physical properties restored to the striatum, but functional properties were also improved; striatal-lesioned rats recieveing grafts had reduced locomotor-hyperactivity symptoms post-graft (Deckel *et al.*, 1983; Isacson *et al.*, 1984). The combined improvement of physical and functional properties led to the study of behavioural improvements, and it was observed that the performance of graft-treated, lesioned rodents at delayed alternation in the T-maze was improved when compared to a sham-operated, lesioned rodent control. Nocturnal hyperactivity, seen in lesioned rodents, was also reduced when graft-treated (Deckel *et al.*, 1986; Isacson *et al.*, 1986). The apparent success in rodent models led to the introduction of clinical trials in humans, although these are still relatively low

in number and restricted in their depth (Piccini *et al.*, 1999; Lindvall & Bjorklund, 2004; Trounson *et al.*, 2011).

Success rates of clinical trials of fetal tissue transplantation have been variable (Markakis & Redmond, 2005). Freed and colleagues compared grafted and sham-operated patients, without immunosuppressive treatment, and observed no significant improvement in the grafted patients' pathology or neurological function over a 12 month period post-transplantation (Freed *et al.*, 2001). Conversely, Lindvall and Bjorkland pooled results from four separate studies (Hagell *et al.*, 1999; Hauser *et al.*, 1999; Brundin *et al.*, 2000; Freed *et al.*, 2001) and concluded that modest improvements to motor control were observed in graft-treated patients. Results for fetal mesencephalon-derived cells in Parkinsonian primate graft trials showed significant functional benefits in the host and were reported to have high survival of transplant tissue (Bakay & King, 1986; Redmond *et al.*, 1986). It has been suggested that the high variation seen in clinical outcomes may reflect that seen in the pre-clinical treatment of the fetal tissue used, the disease state of patient cohorts and the exact methods of treatment making conclusive comparisons difficult to justify. The lack of consistency between trials means that the true value of grafting as a treatment for neurodegenerative diseases is currently difficult to assess (Lindvall & Bjorklund, 2004).

The discovery, and subsequent culture, of proliferative populations of multi-potent cells from fetal and adult mammalian brain that are capable of self-renewal and differentiation into any of the three major CNS lineages, neurons, astrocytes and oligodendrocytes, provides two clinically relevant options (Reynolds & Weiss, 1992; Ma *et al.*, 2009). Firstly, the presence of endogenous neurogenic centres may

enable recruitment of the patient's own cells *in vivo* for the repair or replacement of neuronal tissue. Secondly, the ability to culture cells, under proliferative conditions, which are semi-fate-determined potentially provides a source of cells that can be produced in the scale needed for tissue transplantation and which are already 'primed' for neuronal differentiation (Uchida *et al.*, 2000; Schwartz *et al.*, 2003). Such fetal NSCs are currently being used in multiple clinical trials (Aboody *et al.*, 2011).

1.3.2. ESC-Derived Neuronal Transplantation

ESC-derived neurons and neuronal precursors have been used for transplantation in numerous animal models in order to establish their potential as a source of tissue for therapeutic use. One study showed that hESC-derived NSCs were incorporated into multiple regions of neonatal mouse brain. These grafts were shown to differentiate into neuronal and astrocytic populations (Zhang *et al.*, 2001). Another study showed mESC-derived NSCs 'survived, migrated, and differentiated into various types of neurons in different brain regions including cerebral cortex, hippocampus, and amygdala' (Wernig *et al.*, 2004). Further work on hESC-derived NSCs grafted into the lateral ventricles of neonatal rat brain showed that these grafts exhibited migration into grey and white matter of the host brain within weeks of transplantation (Reubinoff *et al.*, 2001). H9 hESC-derived NSCs displayed improved differentiation potential upon transplantation into neonatal rodent hippocampus and injured adult rodent striatum and spinal cord (Joannides *et al.*, 2007b).

Unfortunately, due to the tumourigenic potential of ESC-derived NSCs, clinical trials with these cells are rare. Currently, there are only 4 clinical trials on-going within

the USA. Geron Inc. are looking to treat subacute thoracic spinal cord injuries with hESC-derived oligodendrocyte progenitor cells. This trial is in Phase I and aims to have 10 patients enrolled between 2010 and 2012 (http://clinicaltrials.gov/ct2/show/NCT01217008, accessed on 27th September 2011). Advanced Cell Technologies have two Phase I/II studies, one on 12 patients investigating the clinical benefits of hESC-derived retinal pigment epithelial cells on juvenile macular degeneration. The other is looking at the same cells as treatment for age-related macular degeneration in another 12 patients. Finally, California Stem Cell are studying type 1 spinal muscular atrophy after transplantation of hESC-derived motor neuron progenitor cells, although this study is currently on hold. The results of these clinical trials are not yet complete and many more trials will be required to show that these cells can fulfil the expectations that have been placed on them by so many (Ben-David & Benvenisty, 2011).

As the research into graft-treatment improves, and as their use in a clinical environment becomes more of a reality, it is of greater importance that we fully understand the process of neural development and integration, both *in vivo* and *in vitro*. Such research will in itself provide the crucial information needed to improve the efficiency and clinical outcome of transplantation therapies.

The improved outcome of grafted tissue derived from the region of the donor brain which corresponds to that which it is hoped it will replace in the host brain (*i.e.* striatum of Huntington's Disease patients and the dopamine containing neurons of the ventral mesencephalon for Parkinson's Disease) and the improvement of graft success seen when using fetal tissue at a developmental stage which is close to the time of birth of the specific neurons to be transplanted highlights the importance of

the production of hESC differentiation protocols aimed at replicating the characteristics of these fetal populations.

The focus of this thesis is on the study of both hESC-derived neurons and of neurons derived-from striatal regions of fetal human and neonatal mouse. It is hoped that comparisons between these populations will provide insight into future directions for the improvement of hESC-differentiation.

1.4. Striatal Development

Striatal development begins, as does all neuronal development, with neural induction. This process is the thickening of the ectoderm of the gastrula to form the neural plate. The rounding and subsequent fusing of the neural plate forms the neural tube in a process called neurulation. Neural precursor cells, which will give rise to the central nervous system, line the neural tube forming the pseudostratified columnar epithelium. Through a process of patterning along the rostro-caudal axis, the neural tube is subdivided into distinct regions: the hindbrain (rhombencephalon); midbrain (mesencephalon); and the forebrain (prosencephalon), which is separated into the diencephalon and the telencephalon (Barker & Barasi, 1999). In the developing embryo, the telencephalon can be subdivided into the pallium and subpallium, the pallium developing into the cerebral cortex and other dorsal structures, and the subpallium giving rise to, among other ventral structures, the globus pallidus and the striatum (Rubenstein *et al.*, 1998). This whole process takes approximately 6 weeks in humans with the striatum appearing at around Carnegie stage 18 (O'Rahilly & Muller, 1999).

During telencephalic development, two ganglionic eminences begin to protrude into the ventricles. These are the medial ganglionic eminence (MGE) and the lateral ganglionic eminence (LGE). Together, these regions of precursor proliferation provide the cells for the striatum and other structures. The LGE produces the GABAergic MSNs and interneurons and the MGE provides the cholinergic interneurons and GABAergic neurons that migrate tangentially to the cortex. More specifically, the neuroepithelium of these eminences form the ventricular zone (VZ), a region of sustained proliferation and mitotic activity. Further in (away from the ventricle) from the VZ is the subventricular zone (SVZ), also a region of proliferation, which lacks the organised epithelial structure of the VZ. The neural precursors in these zones undergo asymmetric division, producing an identical neural precursor capable of further division, and a mitotically inactive neuroblast which migrates away from the region towards the mantle zone. This neuroblast migrates and then differentiates to become a mature striatal neuron (Olsson *et al.*, 1998; Jain *et al.*, 2001; Hebert & Fishell, 2008).

As has been mentioned, the main neurogenic region of the adult brain is the subventricular zone of the striatum (Ming & Song, 2011). As the region from which new neurons are generated, migrating through the rostral migratory stream to the olfactory bulb where they are integrated as functional components of the CNS. To be able to direct hESC-differentiation toward the development of neurons which mimic those utilised endogenously for the replenishment of neuronal tissue would likely provide an improvement in success rates in hESC-derived tissue transplantation. Furthermore, the observed specific loss of striatal medium spiny neurons (MSNs) in Huntington's Disease makes the production of tissue similar in

phenotype to striatal neurons clinically relevant. In order to refine directed protocols that direct the differentiation of hESCs towards specific subtypes of neuronal populations, it is important to understand the developmental processes which occur *in vivo* during the endogenous maturation of these cell types.

The striatum makes up part of the basal ganglion and has been linked to motor, cognitive and limbic functions (Alexander *et al.*, 1990; Parent & Hazrati, 1995). It consists of the ventral striatum, containing the nucleus accumbens and part of the olfactory tubercle, and the dorsal striatum, containing the caudate nucleus and the putamen. Approximately 90% of the striatum is made up of MSNs. These projection neurons primarily use γ-aminobutyric acid (GABA) as a functional neurotransmitter and project into both the direct pathway, through the globus pallidus, and the indirect pathway to the substantia nigra via the internal pallidum. The remaining 10% is mostly made up of aspiny interneurons, which are either cholinergic or GABAergic and can be further subdivided (Jain *et al.*, 2001).

For striatal MSNs, the dopamine- and cAMP-regulated phosphoprotein (Darpp32) is the most commonly used antigen for immunohistochemical identification. Although there are others reported, like Ctip2 (Arlotta *et al.*, 2008), these are not as widely used, or universally accepted.

1.5. Embryonic Stem Cells

ESCs are undifferentiated, self-renewable, pluripotent cells, isolated from the inner cell mass of an embryo at the blastocyst stage that can be cultured in an undifferentiated state indefinitely or, through the activation of differentiation pathways, can give rise to mature cells of various types (Dhara & Stice, 2008).

Human ESCs (hESCs) are widely accepted as having great potential in the treatment of a number of diseases and disorders involving cell loss (Thomson *et al.*, 1998). These cells are capable of differentiation into any cell type in the human body. True totipotent stem cells are also capable of forming cells of the placenta, but the more widely used pluripotent embryonic stem cells (ESCs) are capable of becoming all the cells within the three somatic germ cell lines, mesoderm, ectoderm and endoderm. In recent years, there has been increased focus on the controlled differentiation of these cells into specific cell types with the aim of employing them in transplant therapies for certain degenerative diseases or other disorders requiring tissue replacement (O'Brien & Barry, 2009).

1.6. Fetal Stem Cells

Fetal stem cells are, to a degree, already fate determined, and they are often more suitably named fetal precursor cells. Taken from the developing fetus, these cells provide tissue that is pre-programmed to mature into specific cell types depending on the fetal location from which they were extracted. Whilst currently providing the gold standard of immature tissue for neuronal transplant therapy, fetal stem cells are limited in availability and are often seen as ethically unreasonable for large scale clinical use (Ogawa *et al.*, 2009).

1.7. Adult Stem Cells

As with fetal stem cells, adult stem cells are fate-determined precursor cells. Until recently, it was not realised how many adult stem cells populations were present in the body. It is now accepted that these cells exist, usually in a state of quiescence, and that they can provide a source of renewable tissue to replace mature, non-

dividing adult cells (Ma *et al.*, 2009). Although adult stem cells are not seen as a potential cell source for therapy, their presence and activity within the body is encouraging as it suggests there are mechanisms in place for the integration of immature cells into functional adult tissue.

1.8. Induced Pluripotent Stem Cells

The discovery that mature, differentiated cells can be directed back to an undifferentiated, pluripotent 'stem cell' state through the expression of certain proteins has given further weight to the potential of stem cells to be a source of tissue for clinical use. To take a sample of tissue directly from a patient and use it to produce functional tissue for autologous transplantation therapy entirely removes the problems associated with ethics and immunological rejection. It is likely that sharing identical genetic origins would allow the tissue to be more easily and fully integrated than any other tissue source. This technique is still in its infancy, and the current procedure requires the transfection of exogenous DNA into the cells to induce pluripotency (Takahashi & Yamanaka, 2006). The foremost problem, as with any random integration of DNA, is the potential for disruption of oncogene and tumour suppressor gene function, resulting in cancer. Much is being done to establish methods of induction which negate the need for transfection, and should the outcome be an effective and safe method of inducing pluripotency in differentiated cells, this would likely be a huge advancement in the field of cell transplantation therapy (Chen & Liu, 2009; Normile, 2009). These induced pluripotent stem cells (iPSCs) have the potential to provide cell lines derived from patients with genetic disorders for use in disease modelling. The *in vitro*

developmental profile of these cells may also provide data relevant to the *in vivo* progression of the disease from which the donor patient suffers.

1.9. Electrophysiology and Ion Channel Study

The study of ion channels and electrical signalling in cells began in earnest in the late 1930s when Hodgkin and Huxley first measured action potentials and membrane potential in the squid giant axon (Hodgkin & Huxley, 1939). Using techniques which were at their infancy, it was determined that cells of the nervous system had negative resting membrane potentials and that they could, upon stimulation, fire an action potential, where membrane potential was seen to rise, reversing and reaching a peak, then falling below original baseline before re-establishing the same baseline.

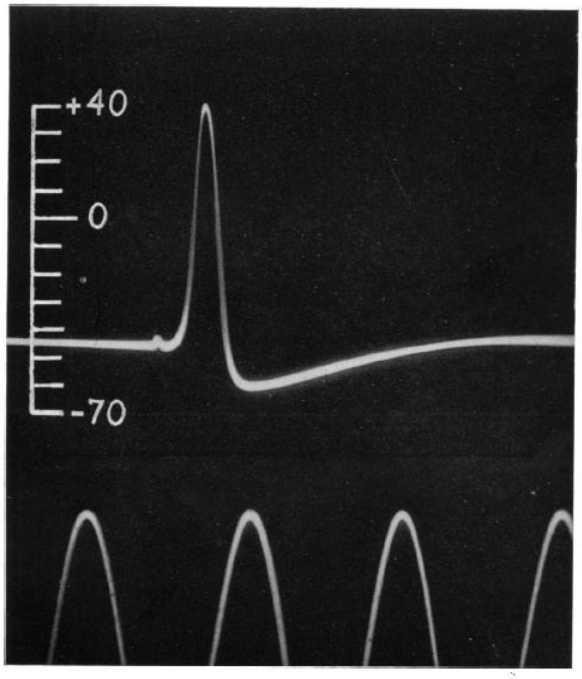

Figure 1.1. The First Recording of an Action Potential: Shown is an action potential recorded between the inside and outside of a squid giant axon. Below the recorded trace is a time marker displaying 500 oscillations per s. The vertical scale indicates the potential of the internal electrode (mV), the sea water outside being taken as zero (figure directly copied from (Hodgkin & Huxley, 1945)

Hodgkin and Huxley reported in their paper of 1945 entitled 'Resting and action potentials in single nerve fibres' that the traditional (at that time) concept, that action potentials arise from a transient breakdown in membrane potential, was not correct and that the inside of the nerve fibre becomes positive during an action potential due to a reversal of the membrane potential (Figure 1.1). Without knowing about the movement of ions across the membrane through selective pores, this was a near perfect explanation of what we now know happens during this event. It should also be mentioned that another group, Curtis and Cole, using different methods, observed similar results (Curtis & Cole, 1942), and in fact their

work provided information that allowed Hodgkin and Huxley to improve their model (Hodgkin & Huxley, 1945).

As technology developed and new methods were made available, observations on the nature of this electrical signalling in nerve fibres allowed the establishment of ion channels as a mechanism for ionic movement in and out of the fibre. Hodgkin and Huxley went on to propose that there was a voltage-sensitive aspect to the ion channel activity and that in order for this to be the case there must be a voltage sensitive component to the channel (Hodgkin & Huxley, 1952a). Through the 1950s and 1960s, the development of such techniques as dialysis (Brinley & Mullins, 1967), internal perfusion (Baker *et al.*, 1961; Oikawa *et al.*, 1961) and the use of permeable chambers and tubing to change the internal solution of the axon (Chandler *et al.*, 1965) allowed further observations to be made leading to advances in our knowledge of selectivity and the presence of Na^+, K^+ and Ca^{2+} channels. The discovery and use of certain toxins and channel blockers (such as tetrodotoxin (TTX) for Na^+ channels and tetraethyl ammonium (TEA) for K^+ channels) that could selectively inhibit the action of specific channels provided the proof for this theory (Tasaki & Hagiwara, 1957; Narahashi *et al.*, 1964; Armstrong & Binstock, 1965). Although the function of these channels and their selectivity was now becoming more understood, the actual structure was still unknown. Work by Rojas and Luxoro in 1963 showed, using protease treated axons, that these channels are proteins embedded in the membrane (Rojas & Luxoro, 1963). Isolation of the Na^+ channel from electric eel electrocytes (Agnew *et al.*, 1978) provided information about the size and structure of this channel. Single channel recordings were first made using artificial bilayers into which protein channels could be placed (Bean *et al.*, 1969a;

Bean *et al.*, 1969b). This paved the way for more functional studies and increased efforts into the exact mechanisms at work such as the Na^+ channel 'ball and chain' hypothesis (Goldman & Schauf, 1972; Armstrong & Bezanilla, 1977; Bezanilla & Armstrong, 1977).

In 1976 Erwin Neher and Bert Sakmann developed a technique using a pipette pressed against denervated frog muscle fibres. This allowed them to record single-channel currents from the membrane. This work, eventually winning them the Nobel prize in 1991, revolutionised electrophysiology and our knowledge of nervous transduction. Through modifications and experimental trial, the method was refined, altered and presented as 'The extracellular patch clamp: a method for resolving currents through individual open channels in biological membranes' in a paper of the same title (Neher *et al.*, 1978). The later development of this protocol to enable efficient seal formation and physical access to the cell via applied suction (whole-cell access) allowed for the control over ionic driving forces through the use of solutions with known ionic concentrations on both sides of the membrane (Hamill *et al.*, 1981).

The patch clamp method was to become the most important advancement in the field of electrophysiology, allowing direct recording of ion channel activity in almost any given cell type, and later in intact tissue (Sakmann *et al.*, 1989). The ability to study channels *in situ* was of tremendous importance to the study of neurons and neurological activity.

1.10. Ca^{2+} Imaging

Ca^{2+}-sensitive, fluorescent dyes have been used to image Ca^{2+} for 50 years (Shimomura *et al.*, 1962). Originally, this process was highly laborious, requiring relatively large volumes of solution. For measurements of intracellular Ca^{2+}, the cell membrane had to be broken and the cytoplasm collected. Later developments allowed the use of microelectrodes or injection of aequorin, a luminescent Ca^{2+}-binding protein from jellyfish, through the cell membrane, a process that often left the cell damaged and the data unreliable. The pioneering work of Roger Tsien and his colleagues in the late 1970s provided membrane-soluble, efficient dyes that could be used for the measurement of intracellular Ca^{2+} in living cells far more simply and with a higher success rate than previously. The production of the Ca^{2+}-sensitive fluorescent dye Quin2 paved the way for the development of Ca^{2+} imaging as it is now. By using membrane-permeable ester derivatives of the dye, cells incubated in its presence would take up the dye, cleave it of its esters via intracellular esterases and, in doing so, both 'activate' the dye and render it membrane-impermeable, allowing recordings of intracellular Ca^{2+} to be made. This dye was not without its problems though and, as Ca^{2+} concentration was determined by the intensity change of the dye, the observed signal was also dependent on a number of variables other than the Ca^{2+} concentration. The signal was directly affected by the dye concentration and the thickness of the cell at the region being measured. The excitation wavelength of Quin2 is also only 339 nm, this is relatively short and as a result autofluorescence of the cell components interfered with the signal. One way around this problem was to load the cells with very high levels of the dye (greater than millimolar concentrations), however, this was found

to have significant deleterious effects on Ca^{2+} signalling itself due to Ca^{2+}-buffering by the dye. Non-specific heavy metal binding also altered the Ca^{2+} signal strength as the heavy metals, especially magnesium, quenched the Quin2 without inducing fluorescence. A direct result of these flaws was the improvement of the dye and eventual synthesis of 'a new generation of Ca^{2+} indicators with greatly improved fluorescence properties' (Grynkiewicz *et al.*, 1985). The article of that title is currently the second most cited paper in the journal of biological chemistry (Current as of 27th September 2011; http://www.jbc.org/reports/most-cited), indicating exactly how important these compounds have become for this research area. The development of Ca^{2+}-sensitive dyes that respond to changes in Ca^{2+} by a shift in the wavelength rather than the intensity allows for the intracellular Ca^{2+} concentration to be determined by a ratio of the emissions when excited at both wavelengths. This significantly reduces any effect on the signal from Ca^{2+}-independent factors, such as dye concentration, bleaching and cell thickness. The increased specificity in these compounds reduced the non-specific heavy metal binding and associated signal loss. Of these compounds, Fura 2 (or more specifically, its derivative Fura 2-acetoxymethyl ester (AM)) has become the most widely used Ca^{2+}-sensitive fluorescent dye in the field of intracellular Ca^{2+} imaging and is used for cytosolic free Ca^{2+} measurements in this thesis.

1.11. Aims and Objectives

The study of stem-cell differentiation often focuses on changes at the gene expression and protein level. Immunohistochemical analysis of cell cultures provides population data about the cell types present. The influence of signalling mechanisms on the control of cellular development is prominent. This thesis aims

to investigate multiple signalling mechanisms in clinically relevant cell types with a view to further understanding the importance of these pathways in neuronal development. It aims to draw comparisons between hESC- and primary-derived neurons in order to better evaluate the functional maturation of hESC-derived neuronal populations with regard to endogenously differentiated cells.

Chapter 2. General Methods

2.1. Tissue Culture

All tissue culture was carried out in a laminar flow hood using standard aseptic techniques. Cells were maintained in culture in a humidified incubator at 5% CO_2 and 37 ^{o}C.

2.1.1. Human Embryonic Stem Cells:

Pre-cultured and frozen stocks of the hESC H9 line (WiCell Research Institute, Madison; WI, USA) between passages 60 and 90, derived in accordance with local and national guidelines, were used throughout as the source for hESCs.

2.1.2. H9 Embryonic Stem Cell Feeder-Free Culture:

2.1.2.1. Media Ingredients:

ADF:

Advanced DMEM:F-12 (Dulbecco's Modified Eagle Medium⁄Ham's F-12) was supplemented with lipid concentrate, transferrin (300 µl in 500 ml medium, 12.5 mg/ml stock, Sigma), insulin (700 µl in 500 ml medium, 10 mg/ml stock, Sigma) β-mercaptoethanol (100 µM, Sigma), penicillin/streptomycin (pen/strep) and L-glutamine (All from Invitrogen, CA, USA unless stated).

ADF-FA:

50 ml ADF (As above) was supplemented with fibroblast growth factor 2 (FGF2, 50 µl in 50 ml medium, 10 µg/ml stock, Peprotech, UK) and ActivinA (50 µl in 50 ml medium, 10 µg/ml stock, R&D Systems, MN, USA)

ADF-SB:

50 ml ADF (as above) supplemented with 50 µl SB-431542 (ActivinA inhibitor, Ascent Scientific Ltd, UK)

For ADF-SB-F2(Hep):

50 ml ADF-SB supplemented with 12.5 µl FGF2 and 5 µl heparin (5 µg/ml stock, Sigma)

ADF-10F2(Hep)-10E:

50 ml ADF supplemented with 25 µl FGF2, 5 µl heparin, 50 µl epidermal growth factor (EGF, 10µg/ml stock, Millipore, MA, USA)

SFDM II:

48.5 ml mixture of DMEM and Advanced DMEM:F12 (1:3 ratio) supplemented with 2% B27 (+ retinoic acid), 1% pen/strep and 500 nM (additional) retinoic acid (all Invitrogen).

For SFDM II + BDNF:

SFDM II (as above) supplemented with 50 µl BDNF (10µg/ml stock, Peprotech)

2.1.2.2. Pre-Coating Plates:

2 ml fetal calf serum (Invitrogen) was pipetted onto 6 cm Nunclon plates and incubated at 37 ^{o}C for 24 h before use.

2.1.2.3. Thawing:

Cells were removed from frozen storage and allowed to thaw before a small amount of 37 ^{o}C ADF-FA was added and the suspension transferred to a 15 ml

Falcon tube. This was spun at 500 g for 2 min, the supernatant was removed and the pellet was resuspended in 5 ml ADF-FA. This was then transferred to Nunclon 6 cm plate (pre-coated in FCS (Invitrogen) and washed twice with PBS).

2.1.2.4. Maintaining:

Medium was removed daily and replaced with 3 ml ADF-FA until colonies were large and ready for splitting.

2.1.2.5. Splitting:

Medium was removed and 2 ml collagenase IV (Invitrogen)/media mix (1 mg/ml) was added. This was incubated at 37 ^{o}C for 40 min-1.5 h (depending on the age of the collagenase mix). Once the colonies were loosened from the plate surface, a further 2 ml ADF-FA was added and the suspension was transferred to a 15 ml Falcon tube. This was spun at 500 g for 2 min, the supernatant was removed and the pellet resuspended in 1 ml ADF-FA, a 200 µl pipette was used to break up the pellet and the colonies by repeat pipetting. 4 ml ADF-FA was then added to the tube and this was transferred to a 6 cm Nunclon plate (pre-coated in FCS and washed twice with phosphate-buffered saline (PBS, Invitrogen) before use).

2.1.2.6. Freezing:

Freezing medium (10% DMSO (Sigma) in FCS) was made to 1 ml per 6 cm plate and a corresponding number of 1 ml Cryotubes (Nunclon) were pre-labelled. Collagenase was added as per splitting. When colonies lifted off the plate by themselves they were transferred into a 15 ml Falcon tube as intact colonies and centrifuged at 500 g for 2 min. The supernatant was removed and the pellet resuspended in the freezing media. 1 ml of the suspension was quickly transferred

into each Cryotube and placed into a slow-freezing isopropanol chamber. This was placed at -80 ^{o}C, left overnight and transferred into liquid nitrogen storage for future use.

2.1.3. H9 Neurosphere Protocol:

For initial differentiation down a neuronal lineage, hESCs were grown as neurospheres for 32 days as described below.

2.1.3.1. Day 0-8:

hESCs were collagenase-treated as in a normal split for hESCs, the suspension was spun at 500 g for 2 min in a 15 ml Falcon tube and the supernatant was removed. The pellet was resuspended in 200 µl ADF (without Fgf2) which was pipetted into the centre of a Sterilin dish. The colonies were allowed to settle so that some medium could be removed to improve chopping efficiency. As much as possible of the 200 µl media was removed without removing the cells. The tissue chopper (McIlwain, UK) was then used to chop the colonies into equal fragments using setting 1.5, chopping was repeated in a 90^{o} angle to the first run to ensure fragments were equally sized. Warm ADF-SB plus the ROCK inhibitor Y-27632 (Ascent Scientific Ltd, UK) was then added to the cells using amounts as follows:

1 x 6 cm H9 ESCs into 7.5 ml ADF-SB + ROCK Inhibitor (10 µM)

These cells were then transferred to a fresh Sterilin plate.

2.1.3.2. Feeding:

Neurospheres, suspended in medium in a Sterilin plate, were transferred to a 15 ml Falcon tube. This was spun at 150 g for 3 min. The supernatant was removed and the pellet resuspended in the appropriate amount of medium for the desired

dilution (after making spheres, the amount of medium was often reduced at first feed then, as the population increased, the amount was increased). Feeding was carried out every 2 days.

2.1.3.3. Day 8-30:

Cells were fed (as above) with ADF-SB-F2(Hep)

2.1.3.4. Day 30+:

Cells were fed with ADF-10F2(Hep)-10E

2.1.4. H9 Plate Downs/Terminal Neuronal Differentiation:

For terminal differentiation of neural precursors to mature neurons, and for electrophysiology and Ca^{2+} imaging, day 32 neurospheres were plated onto 13 mm glass coverslips pre-coated in poly-l-lysine (PLL, Sigma) and laminin at a density of 1.5×10^3 per slip as described below.

2.1.4.1. Preparing Poly-l-Lysine (PLL)-Laminin Slips:

Coverslips (13 mm diameter VWR, PA, USA) were autoclaved on filter paper.

Coverslips were placed into 24-well Nunclon plates using sterile forceps (flamed). PLL (2 µg/ml) was added and incubated overnight at 4 ^{o}C. The PLL was removed, the coverslips were washed with water and left to dry at room temperature over-day in the tissue culture hood. These plates could then be stored until required.

The day before setting up the differentiation experiment, 80 µl of laminin (10 µg/ml) was pipetted to the centre of each coverslip as single droplets. Water was added to the area between wells to prevent excessive drying out. These plates were incubated overnight in the tissue incubator at 37 ^{o}C. When the cells for plating

down were ready, the laminin droplet was removed and the culture media with the cells was added without allowing the remaining laminin layer to dry out.

2.1.4.2. For Single-Cell Plate Downs:

Neurospheres for dissociation were spun down at 150g for 3 min. These were resuspended in 1 ml Accutase and incubated at 37 ^{o}C for 5 min. 1 ml more Accutase was added and clumps were broken apart by repeat pipetting before incubating for a further 5 min. The resulting single cell suspension was spun down at 500 g for 2 min. The pellet was resuspended in SFDM II+BDNF and counted. Cells were diluted and plated according to the dilution required *e.g.* 1,500 cells per well. Dilutions were made to allow for the correct number of cells to be in between 80 and 150 µl. The correct amount was then added to each cover slip and incubated for at least 3 hours before the plate was flooded with 1 ml of SFDMII+BDNF.

Plated down cells were fed every 3 days by replacing half the media each time. Cells were grown for up to 7 weeks post-plate down (PPD).

2.1.5. H9 Embryonic Stem Cell mefi-Culture:

H9 hESCs cultured on irradiated mouse embryonic fibroblasts (mefi) were provided by Shona Joy (Cardiff University). The information provided here is for the purpose of clarity.

2.1.5.1. H9 Media

412.5 ml Knockout DMEM was supplemented with 75 ml serum replacement, non-essential amino acids, L-glutamine, 2.5 ml pen/strep, 3.5 µl β-mercaptoethanol and 4 ng/ml FGF2.

H9 hESC colonies were grown on low density mefi cultures on gelatin coated tissue culture plates. When these colonies were ready for harvesting they were collagenase-treated, as described in section 2.1.2.5. Complete colonies were suspended in H9 media and pipetted in a droplet onto FBS coated glass coverslips maintaining a medium colony density.

2.1.6. Human Fetal Neurons

The fetal tissue used throughout this thesis was collected and prepared by either Claire Kelly or Sophie Precious (Cardiff University). Once the cells were plated they were passed on for functional characterisation. The information provided here is included for the purpose of clarity.

Human fetal tissue was obtained following termination of pregnancies in maternal donors. All tissue was collected and used following the guidelines of the Polkinghorne and Department of Health reports and with Bro Taf Local Research Ethics Committee approval. In all cases, full, informed consent was provided by the maternal donor following consent for termination of pregnancy. Consent was obtained as part of the MRC-sponsored, South Wales initiative for transplantation (SWIFT) program.

Fetal tissue was obtained from fetuses ranging in age from 6 to 12 weeks post-conception

Surgical Termination of Pregnancy (STOP) and Medical Termination of Pregnancy (MTOP) tissues were collected as described previously (Kelly *et al.*, 2011).

Following extraction and identification, fetal parts were transferred to a 50 ml Falcon tube containing hibernation media (Hibernate E, Invitrogen). The WGE was

dissected and the tissue either processed immediately or stored in hibernation media overnight at 4 ^{o}C.

WGE fragments were incubated in TrypLE express (Invitrogen) for 20 min at 37 ^{o}C for dissociation. DNAase (Sigma, 0.01%) was added and the tissue incubated for a further 5 min at 37°C.

The tissue was then spun down at 150 g for 3 min, washed twice with DMEM/F-12 and then spun down at 150 g for 3 min. The pellet was resuspended in 200 µl DMEM/F12 and triturated to produce a single cell suspension (Kelly *et al.*, 2011).

This suspension was used to plate neurons using the same method applied to hESC-derived neurons described in section 2.1.4.

2.1.7. Postnatal Mouse Neurons

Postnatal day 1 mice were sacrificed by decapitation and their brains were surgically removed for processing. Whole brains were transferred to a dish containing ice cold Hank's buffered saline solution (HBSS, Invitrogen). The WGE was located, removed and chopped into small pieces surgically. These pieces were placed in HBSS in a 15 ml Falcon tube and allowed to settle to the bottom. The HBSS was removed from the tube leaving only the WGE fragments. 1.5 ml trypsin (0.5% in PBS without Ca^{2+} or Mg^{2+}) was added to the Falcon tube and incubated for 10 min at 37 ^{o}C. 500 µl DNAase (Sigma, 0.04%) was added to the trypsin/mWGE mixture and incubated for a further 5 min at 37 ^{o}C.

The mWGE tissue was then spun down at 150 g for 3 min, washed twice with DMEM/F-12 and then spun down at 150 g for 3 min. The pellet was resuspended in 200 µl DMEM/F12 and triturated to produce a single cell suspension.

This suspension was used to plate mWGE-derived neurons using the same method applied to hESC-derived neurons described in section 2.1.4.

2.2. Functional Characterisation

All whole-cell patch-clamp and Ca^{2+} imaging work was carried out at room temperature (23 ± 1 ^{o}C). Cells were prepared on glass coverslips as described in the relevant method sections.

2.2.1. Physiological Solutions

The same physiological extracellular solution (ECS) was used in both whole-cell patch-clamp and Ca^{2+} imaging. The intracellular solution was only used in patch-clamp studies.

2.2.1.1. Extracellular Solution (ECS):

Ingredient	Final Concentration
NaCl	135 mM
KCl	5 mM
HEPES	5 mM
Glucose	10 mM
$MgCl_2$	1.2 mM
$CaCl_2$	1.25 mM

pH made to 7.4 with NaOH

2.2.1.2. Intracellular Solution (ICS):

Ingredient	Final Concentration
KCl	117 mM
NaCl	10 mM
HEPES	11 mM
EGTA	11 mM
$MgCl_2$	2 mM
$CaCl_2$	1 mM
Na_2. ATP	2 mM

pH made to 7.2 with KOH

2.2.1.3. K^+ Channel Blocker and Na^+ Replacement Solutions

Tetraethyl ammonium-Cl (TEA, Sigma) was used for blocking K^+ channels. 20 mM TEA was dissolved in standard ECS on the day of use.

For block of Na^+ channel activity standard ECS with equimolar replacement of NaCl with NMDG-Cl (NMDG, Sigma) was made.

Note: When using NMDG-Cl as an equimolar NaCl replacement in external solution pH is very high requiring HCl to bring to pH 7.4 in place of NaOH

2.2.1.4. Liquid Junction Potential

The liquid junction potential using the standard extracellular and intracellular solutions was calculated to be 2.2 mV. Where appropriate, this value was subtracted from the recorded data offline. For the majority of experiments this value was not deemed large enough to significantly alter the data, in these cases the junction potential was ignored.

2.2.2. Whole-Cell Patch-Clamp

2.2.2.1. Electrodes

Silver/silver Cl^- (Ag/AgCl) electrodes for patch-clamp were produced by electrolysis of NaCl with a 9 V battery using pure silver wire (0.25 mm diameter, Clark Electromedical Instruments, UK) as the cathode. These electrodes were Cl^--coated as required. An Ag/AgCl pellet (Clark Electromedical Instruments) connected to the patch-clamp headstage was used as the bath (reference) electrode.

2.2.2.2. Patch Pipettes

Thin-walled, filamented, borosilicate glass tubes (World-Precision Instruments, UK) were pulled using a two-stage pipette puller (PP-830, Narishige, Japan) to give patch pipettes with a measured tip resistance of 3-6 MΩ when filled with the internal pipette solution. These pipettes were used to establish whole-cell configuration of the patch clamp technique.

2.2.2.3. Whole-Cell Patch-Clamp Technique

Plated down cells grown on glass coverslips were transferred into a perfusion chamber mounted on the stage of an Olympus CK40 inverted microscope equipped with phase-contrast optics mounted inside a Faraday cage on an anti-vibration air table (Wentworth Laboratories Ltd., Oxford, UK). Continuous perfusion of the cells with ECS was maintained by a gravity-fed system using a 50 ml disposable syringe as a reservoir connected to the bath with gas-impermeable tubing (Cole-Parmer, UK). Continuous perfusion was maintained at a rate of approximately 2-4 ml per min. A gravity-fed rapid solution changer (RSC, RSC-200, Bio-Logic, France) was used to apply various solutions directly to the cells when required allowing for solution

changes as fast as 20 ms. The RSC enabled 9 different solutions using either 50 or 10 ml disposable syringe reservoirs connected to separate, parallel glass tubes (Bio-Logic) with capillary tubing (Cole-Parmer, UK). Flow rates of between 0.5 and 1.5 ml per minute were maintained depending on reservoir height. Switching of solutions was enabled via electromagnetic stopper valves and a step motor to move the appropriate glass tube in line with the patch-clamped cell. The RSC system enables full automation of solution application protocols enabling greater reproducibility with repeated experiments. Waste solution was removed via vacuum suction through a flame-pulled glass tube connected to a waste Buchner flask with Tygon tubing.

Patch-clamp pipettes were partially filled with ICS, pushed through a 0.22 µm pore filter (Gelman Sciences, UK) using carbon-fibre flexible needles (MicroFil, WPI). Filled pipettes were mounted on a CV 201AU headstage attached to an Axopatch 700A Amplifier (Axon Instruments; Forster City, CA, USA) and DigiData 1320 A/D interface.

The patch-pipette tip was then lowered towards the cell to be patched using the macromanipulation controls of a manipulator (Burleigh, Canada). A slight positive pressure was applied through the headstage mount via tubing attached to a syringe allowing control of the patch-pipette pressure. This positive pressure prevented the accumulation of particles from the bath onto the pipette tip preventing efficient seal formation. Upon insertion into the bath solution, a seal test was applied using the pClamp software. This 10 mV step for 10 ms, applied at 50 Hz, allowed for measure of the resistance between the pipette and reference electrodes. At this stage any pipette voltage offset was zeroed using the Multiclamp Commander

software. When the pipette tip was within the micromanipulation limits of the cell to be patched the micromanipulation controls were used to bring the cell into contact with the cell membrane.

Upon contact of the patch-pipette tip with the cell membrane there was an observable reduction in the amplitude of current flowing through the set-up indicating the increased resistance due to the membrane covering the tip. At this stage, the positive pressure in the patch-pipette was removed and a slight negative pressure was applied. This negative pressure, coupled with slight adjustment of the micromanipulator to gain better contact with the cell, was used to form a tight seal on the cell membrane. A holding potential of -60 mV was then applied across the system to prevent depolarisation upon whole-cell access. The negative pressure, pipette positioning and holding potential aided formation of a seal which was greater than 1 GΩ in resistance. Only cells in which a GΩ or greater resistance was achieved were taken on to the whole-cell configuration. Upon GΩ formation, any residual capacitance currents (pipette capacitance) were compensated using the fast and slow-capacitance compensation in the Multiclamp Commander software.

Whole-cell was achieved by the gentle increase of negative pressure in the patch-pipette until noticeable capacitance transients appeared in the seal test current trace. These transients, indicative of the membrane capacitance, were automatically or manually compensated and measured using the whole-cell compensation feature in the Multiclamp Commander software. Series resistance was measured and only cells displaying a series resistance lower than 10 MΩ were used for further study. The negative pressure applied to gain whole-cell access was

often removed upon successful whole-cell formation, however, in some cases this was left on to prevent loss of the cell.

Voltage- or current-clamp were used to apply voltage or current protocols, generated using Axon Laboratory's pClamp 9 software, to the patched cell. These were recorded on-line for further analysis using the pClamp software. Offline data review and analysis was performed using Axon Laboratory's Clampfit 9, Microsoft Office Excel and Prism4.

2.2.2.4. Voltage Clamp Protocols:

Voltage step p-n: Cells were held at -70 mV and sequentially stepped, for 200 ms, to voltages between -120 mV and +60 mV in 10 mV increments taking 19 separate sweeps to complete. Data were recorded with an online p-n subtraction protocol where, for each sweep, four steps preceding the recording were carried out which were equal in size of step to one quarter of the step for that sweep. The measured increase in current for each of these steps were summed and subtracted from the current during the main voltage step for that sweep. This enabled the subtraction of the linear (leak) component of the voltage-induced current.

Modifications to the voltage-step protocol for measurement of GABA reversal potentials involved changes to the starting and ending voltages, the number of sweeps and the length of the voltage step. These changes are indicated in the text where appropriate.

2.2.2.5. Current Clamp Protocols:

Gap free: Cells were held in current clamp with zero current injection for recording of resting membrane potentials (V_m) and observation of any spontaneous action

potentials. Recordings were made using the 'Gap free' protocol immediately after whole-cell access to reduce the effect of the pipette ICS dialysing with the actual cytosolic solution and thus influencing the resting membrane potential in anyway. Recordings were made for 90 s for a mean calculation of V_m and to allow for spontaneous action potentials to be recorded.

Current steps: Variable current injection was used to hold the membrane potential close to -80 mV. A sequential injection of current for 100 ms from 0 pA to 180 pA in 10 pA increments taking 19 sweeps was used in an attempt to elicit an action-potential like response upon the membrane potential reaching and passing the action potential threshold value.

2.2.2.6. Whole-Cell Patch-Clamp Data Analysis

Data obtained using the 'voltage step p-n' protocol under voltage clamp conditions was analysed in Clampfit 8/9. Briefly, the minimum peak current between 1 and 20 ms of the voltage step for each sweep was taken as the inward current and the mean current value between 180 and 195 ms of the voltage step for each sweep was recorded as the outward current. In all cases currents were normalised to cell size by dividing the current over the cell capacitance to give the current density (pA/pF).

Data from the 'current step' protocol were analysed in Clampfit 8/9 and exported to Excel for further processing. A segment of the trace including the action potential threshold from the first sweep which induced an action potential response that exceeded 0 mV was exported to Excel where dV/dt was calculated and plotted against V_m.

The average V_m during a 90 s 'Gap Free' recording in current clamp was taken as the resting membrane potential. In cells displaying spontaneous activity, an estimation of the baseline was made from the trace.

2.2.3. Ca^{2+} Imaging

The ratiometric Ca^{2+} sensitive dye Fura-2-AM (Molecular Probes, Eugene, OR, USA) was used for Ca^{2+} imaging experiments. This dye was purchased as a dry powder in 50 µg aliquots. Before use, these aliquots were dissolved in 50 µl DMSO (Sigma) by vortex. They were then incubated at 37 ^{o}C for 1 h to ensure the dye was fully dissolved. 1 µl of the 1 mg/ml Fura-2-AM stock was added to 250 µl of normal cell growth media and mixed. Cells on glass coverslips were then added to the well and incubated for 30 min at 37 ^{o}C and 5% CO_2 in a humidified tissue culture incubator. Both stocks and media containing the dye were kept, where possible, out of direct light to prevent photo-bleaching of the dye. This incubation allowed for Fura-2-AM to be taken up by the cells, cleaved and turned into the active dye Fura-2.

Fura-2-loaded cells were placed in a specialised perfusion chamber, designed to allow direct access of the microscope oil-immersion lens with the bottom of the coverslip, mounted upon an Olympus IX71 equipped with a Cairn monochromator-based fluorescence system (Cairn Instruments, Faversham, UK) and were continuously superfused with ECS. Fura-2 was alternately excited using fluorescence light emitted from the monochromator at 340 and 380 nm. Images at 510 nm were acquired at 0.33 or 0.2Hz by a slow-scan CCD camera (Kinetic Imaging Ltd, Nottingham, UK). Solutions, agonists and antagonists were locally applied to the cells using the gravity-driven rapid solution changer (see section 2.2.2.3.).

2.2.3.1. Ca^{2+} Imaging Data Analysis

Raw data, in the form of emission intensities at 510 nm, during alternate excitation at 340 or 380 nm, were recorded and stored using the Andor IQ 1.3 software package (Andor Technology, Belfast, UK).

Following background subtraction, emission ratios (340/380) were calculated off-line using Microsoft Office Excel (Microsoft, Redmond, Washington, US).

Where indicated, data were normalised to the first 10 frames to allow further analysis and for comparisons.

Chapter 3. P2 Receptors in hESCs

3.1. Introduction

3.1.1. Purinergic Signalling

Purinergic signalling is the physiological utilisation of both purine and pyrimidines for the process of extracellular signalling. Purines, and their derivatives - such as adenosine, ATP and ADP - and pyrimidines, and their derivatives - *e.g.* UTP and UDP - released from healthy cells, via diffusion, exocytosis and transport, and from dying or damaged cells, are employed for extracellular signalling via purinergic receptors located on the plasma membrane (Burnstock, 2006). This system provides a mechanism for extracellular signalling that has not only been employed by nearly all tissue types in mammals, but has been implicated in a huge number of other organisms from virtually all major phyla (Burnstock & Verkhratsky, 2009). There are three classes of purinergic receptor, P1, P2X and P2Y. The P1 family of receptors are sensitive to adenosine, whereas P2X and P2Y are nucleotide-sensitive receptors. Both P1 and P2Y receptors are metabotropic, seven-transmembrane G-protein coupled receptors, P1 receptors modulating cAMP production, P2Y receptors working through either cAMP or inositol triphosphate (IP_3) to release Ca^{2+} from intracellular stores. P2X receptors are ionotropic nucleotide receptors which, upon binding of the relevant ligand, open to allow cations to pass through the cell membrane(Burnstock & Williams, 2000).

3.1.2. P1 Receptors

Currently, four subtypes of the adenosine receptors making up the P1 receptor class have been confirmed. These subtypes, A_1, A_{2A}, A_{2B} and A_3, are all G-protein coupled

receptors and are encoded by separate genes. The subtypes A_1, A_{2A} and A_3 show high affinity for adenosine whereas A_{2B} shows low affinity for this nucleoside. A_1 and A_3 act via G_i and G_o, A_{2A} and A_{2B} act via G_s (with A_{2B} also acting via Gq). Through these G-proteins, these receptors modulate a number of cellular signalling molecules including adenylyl cyclase, PLC and protein kinase C (PKC) leading to downstream effects on gene expression and protein activity (Ralevic & Burnstock, 1998; Klinger *et al.*, 2002).

3.1.3. P2X Receptors

The ligand-gated non-selective cation channels of the P2X family are formed when three subunits form a stretched trimer (North, 2002). So far, seven of these mammalian subunits have been identified and classified $P2X_{1\text{-}7}$. The seven subunits show 30-50% homology at the protein level. Each subunit consists of intracellular N- and C- termini, two transmembrane regions (TM1 and 2) and a large extracellular loop containing a hydrophobic region (H5) and an ATP binding site. There is evidence for the presence of both homo- and hetero-trimer formation between these subunits. The family of functional P2X receptors displays great variability with regards to pharmacological characteristics and physiological functions (Ralevic & Burnstock, 1998; Bianchi *et al.*, 1999).

3.1.4. P2Y Receptors

Of the metabotropic, G-protein-coupled P2Y receptors there are eight known subunits. $P2Y_{1,2,4,6,11,12,13}$ and $P2Y_{14}$ make up a complex family showing a large amount of pharmacological and physiological variation. Of these subtypes, only $P2Y_{1,2,4,6}$ and $P2Y_{11}$ have been found in human tissues. The primary agonists of heterologously expressed human P2Y-receptors are ADP ($P2Y_1$), UTP/ATP ($P2Y_2$),

UTP ($P2Y_4$), UDP ($P2Y_6$) and ATP ($P2Y_{11}$). These subtypes characteristically display an extracellular N-terminus, an intracellular C-terminus and seven transmembrane regions. Each P2Y receptor is coupled to a single heterotrimeric G-protein. This is primarily G_q (also referred to as $G_{q/11}$). However, $P2Y_{11}$ can also bind G_s and $P2Y_{12}$ binds primarily to G_i. Activation of these receptors by their associated ligand elicits activation of phospholipase C (PLC), resulting in an increase in inositol trisphosphate (IP_3) formation and the subsequent mobilisation of intracellular Ca^{2+}. This Ca^{2+} mobilisation can lead to direct and indirect stimulation of various signalling molecules such as PKC, phospholipase A_2 (PLA_2) and Ca^{2+}-activated K^+ channels. $P2Y_{11}$ has also been linked with stimulation of adenylate cyclase, resulting in increased cyclic adenosine monophosphate (cAMP) production. Through such mechanisms, activation of these receptors influences a number of intracellular pathways and expression cascades, the increase of PKC, for example, provides a mechanism for modulation of intracellular proteins through phosphorylation (Ralevic & Burnstock, 1998; von Kugelgen & Wetter, 2000; Marinissen & Gutkind, 2001).

3.1.5. Extracellular Release of Purines and Pyrimidines

Until relatively recently, it was assumed that ATP release from cells occurred only as a result of cellular damage and the subsequent loss of membrane stability. However, it is now understood that cells may release ATP as a response to other factors such as hypoxia, physical stress, inflammation and cellular exposure to certain agonists (Bodin & Burnstock, 2001). In its role as a neurotransmitter, ATP has been shown to be co-packaged in vesicles and co-released at the presynaptic membrane with other classical transmitters (Pankratov *et al.*, 2006). Vesicular

release of ATP has also been demonstrated in other, non-excitable cells types. However, since the presence of ATP permeable ion channels has also been suggested, it may be that both methods are present and provide distinct physiological roles (Burnstock, 2006).

The presence of multiple nucleotidases and hydrolysing enzymes shortens the half-life of extracellular ATP considerably within the body. These enzymes produce the ATP derivatives ADP, AMP and adenosine. These may function as agonists for multiple purinergic receptors with different affinities, and it is likely that the specific dynamic of local ATP release and degradation is physiologically relevant to the functional output of the signalling event that is required (Dubyak & el-Moatassim, 1993; Shukla *et al.*, 2005; Yegutkin, 2008). More recently, confirmation of UTP and UDP release by healthy or damaged tissue has been observed. These experiments have shown UTP that release from mechanically stimulated murine airway epithelial cells directly stimulates Ca^{2+} waves in this tissue (Homolya *et al.*, 2000). Similarly, circulating UTP concentrations in humans during acute myocardial infarction were also shown to have risen (Lazarowski & Boucher, 2001).

3.1.6. Physiological and Developmental Roles of Purinergic Signalling

Purinergic signalling has been shown to play a role in a huge number of physiological processes. Early work on the effect of these compounds on biological systems focussed largely on modulation of cardiovascular parameters, including lowering of blood pressure, vasodilatation and hypotension (Drury & Szent-Gyorgyi, 1929). Effects on platelet aggregation, mast cell function, intestinal contraction, immune response and pain sensing were later observed (Born, 1962). Further investigation revealed a role for purinergic signalling in neurotransmission and

neuromodulation (Burnstock & Kennedy, 1986). Purinergic signalling is not restricted to fast-acting effects on tissues and organs, a number of roles in slow-acting alterations to cellular physiology have also become apparent. Effects of purinergic signalling on cell cycle progression, proliferation, apoptosis, migration and differentiation have all been proposed and observed in various cell populations (Ralevic & Burnstock, 1998; D'Ambrosi *et al.*, 2001; Burnstock, 2002; Greig *et al.*, 2003).

In human fetal astrocyte cultures from 1st trimester brainstem and diencephalon, both ATP and ATPγS (a hydrolysis-resistant ATP analogue) were shown to increase DNA synthesis, as measured by [^{3}H]thymidine incorporation (Neary *et al.*, 1998). In the same cells, ATP-induced increases in the mitogen-activated protein kinase (MAPK) known as extracellular signal-related protein kinase (ERK) were also observed. This increase was reduced by inhibition of P2 signalling with suramin, but was unaffected by P1 inhibition with 8-(p-sulfophenyl)-theophylline suggesting that P2 receptors were, at least partially, responsible for the response. ERK is linked with modulation of cellular proliferation and differentiation in various tissues. Activated MAPK has been shown to translocate to the nucleus where it can activate transcription factors, potentially modifying the expression of genes involved in cell growth (Seger & Krebs, 1995). In adult rat dorsal root ganglionic neurons *in vitro*, $P2Y_2$ signalling has been linked, via ERK signalling, to neuronal survival through its anti-apoptotic effects. Conversely, $P2Y_1$ activation in human prostatic carcinoma (PC-3) cells was induces apoptosis, as measured by caspase-3 activity, lactate dehydrogenase (LDH) release, and annexin-V staining, all of which are linked to apoptotic events (Wei *et al.*, 2011).

In cultured human umbilical vein endothelial cells, $P2Y_1$ has been shown to stimulate migration, as measured in *in vitro* wound repair assays, an effect inhibited by MRS2179, a $P2Y_1$ receptor antagonist (Shen & DiCorleto, 2008). Furthermore, neural stem cells, prepared from 8- to 12-week-old C57BL/6N wild-type mice display increased migration in the presence of ATP, ADPβS and UTP. Again, this result was linked to a purinergic signalling-regulated increase in ERK activity (Grimm *et al.*, 2010).

Although it is now understood that purinergic signalling plays an important part in a large number of biological processes. It is apparent that more information is needed to elucidate their complete function and to understand more fully the extent of their activity. This knowledge, along with an increase in the use of microarray studies providing large-scale genetic expression data, has led to research into the presence and effect of purinergic signalling within stem cell populations.

3.1.7. P2 Receptors in Undifferentiated Human Embryonic Stem Cells

In 2004, Wang *et al.* presented evidence for the expression of P2 receptors within human stem cell populations (Wang *et al.*, 2004). Although this work was carried out on CD34+ stem and progenitor cells from bone marrow, it provided the basis for further investigation into the expression and function of P2 receptors in stem cells. Within the CD34+ line, both $P2Y_1$ and $P2Y_2$ mRNA were abundant. Furthermore, $P2X_1$, $P2X_4$ and, to a lesser degree $P2X_7$, were also shown to be expressed. As a number of these receptors have been linked to cellular functions such as proliferation (Neary *et al.*, 2001; Ryu *et al.*, 2003), migration (Scemes *et al.*, 2003), differentiation (D'Ambrosi *et al.*, 2001) and apoptosis (Burnstock & Williams, 2000;

Greig *et al.*, 2003), it was hypothesised that purinergic signalling may influence stem cell differentiation (Verfaillie, 2002; Wang *et al.*, 2004).

Another group observed that adult neural stem cells from C57BL/6N mice subventricular zone express functional P2 receptors, which, upon activation, elevate intracellular cytosolic free Ca^{2+} concentration ($[Ca^{2+}]_i$) and increase proliferation in these cells (Mishra *et al.*, 2006). In this study, $P2Y_1$ and $P2Y_2$ were shown to be responsible for purinergic-signalling dependent modulation of cellular proliferation. $P2Y_1$ knockout neural stem cells showed 53% reduction in cell number when compared to wild-type. Similarly, 5 μM MRS 2179, a selective $P2Y_1$ antagonist, reduced the cell number by 27% compared to the control. The addition of ADPβS and UTP resulted in increased cell counts. It was concluded that $P2Y_1$ had the dominant effect on proliferation and that this action may be applicable to the study of human embryonic stem cell differentiation and development (Mishra *et al.*, 2006).

$P2Y_1$ was also suggested as the key mediator of proliferation and also of differentiation. In this study, murine P19 embryonal carcinoma cells were used to study the effects of purinergic signalling on progenitor cell proliferation and neuronal differentiation. It was shown that during the process of neuronal differentiation in these cells several P2X and P2Y receptors were differentially expressed, most notably $P2Y_1$, although $P2Y_2$ and $P2X_4$ expression was also shown to change (Resende *et al.*, 2008).

A recent review compiles a list of further experimental evidence which suggests that purinergic signalling is involved in a number of processes in multiple cell types.

However, there is still a lack of knowledge and evidence for the role of these receptors in embryonic development (Burnstock & Ulrich, 2011). In order to realise the potential benefit, with regards to both disease modelling and therapeutic outcomes, that modulation of these receptors in stem cells offers, it is necessary to elucidate further their expression, function and the consequences of their activation.

Currently, there is no information available on the functional activity of P2 receptors within human embryonic stem cell lines. The information available has been gathered from mesenchymal, hematopoietic, mouse stem and progenitor cell lines. It was therefore decided to investigate the functional activity of P2 receptors within undifferentiated H9 hESCs.

3.1.8. Aims of Chapter

In order to better understand the degree of purinergic signalling within hESC populations, and to apply knowledge gained from research into other stem-cell sources, purinergic signalling in undifferentiated hESCs was investigated. Particular attention was be paid to Ca^{2+} mobilisation as a direct effect of purinergic receptor activation as this has been shown to directly affect cellular properties. Pharmacological evaluation of subtypes of purinergic receptors and their mechanisms of action was carried out.

3.2. Non-Standard Methods

The Ca^{2+} imaging technique used in this chapter is discussed fully in section 2.2.3. of Chapter 2: General Methods. Details of the individual agonist/antagonist application

protocols are discussed in the results text and highlighted in the corresponding figures.

3.2.1. Extracellular Solutions:

Extracellular solution: as described in section 2.2.1.1.

50 mM KCl ECS: as per standard ECS, but with 50 mM KCl and 90 mM NaCl

Ca^{2+} Free ECS: as per standard ECS, but with no added $CaCl_2$ and 1 mM EGTA supplement

3.2.2. Reagents

Adenosine 5′-triphosphate disodium salt (ATP): Sigma, stocks of 100 mM dissolved in standard ECS, stored at -20 ^{o}C

Adenosine 5′-diphosphate monopotassium salt (ADP): Sigma, Stocks of 100 mM dissolved in standard ECS, stored at -20 ^{o}C

Uridine 5′-triphosphate tris salt (UTP): Sigma, stocks of 100 mM dissolved in standard ECS, stored at -20 ^{o}C

Uridine 5′-diphosphate disodium salt (UDP): Sigma, stocks of 100 mM dissolved in standard ECS, stored at -20 ^{o}C

α,β-methyleneadenosine 5'-triphosphate trisodium salt (αβme-ATP): Sigma, stocks of 100 mM dissolved in standard ECS,stored at -20 ^{o}C

2′(3′)-O-(4-Benzoylbenzoyl)adenosine 5′-triphosphate triethylammonium salt (Bz-ATP): Sigma, stocks of 10 mM dissolved in standard ECS, stored at -20 ^{o}C

[[(1*R*,2*R*,3*S*,4*R*,5*S*)-4-[6-Amino-2-(methylthio)-9*H*-purin-9-yl]-2,3-dihydroxybicyclo[3.1.0]hex-1-yl]methyl] diphosphoric acid mono ester trisodium salt (MRS2365): Tocris, supplied pre-dissolved at a concentration of 10mM in H_2O, stored at -20 ^{o}C

Adenosine: Sigma, stocks of 100 mM in dissolved in ECS, stored at -20 ^{o}C

8,8'-[Carbonyl*bis*[imino-3,1-phenylenecarbonylimino(4-methyl-3,1-phenylene)carbonylimino]]*bis*-1,3,5-naphthalenetrisulfonic acid hexasodium salt (Suramin): Tocris, stocks of 50 mM in H_2O, stored at -20 ^{o}C

Pyridoxalphosphate-6-azophenyl-2',4'-disulfonic acid tetrasodium salt (PPADS): Tocris, stocks of 50 mM dissolved in H_2O, stored at -20 ^{o}C

2-Aminoethoxydiphenylborane (2-APB): Tocris, stocks of 100 mM dissolved in DMSO, stored at -20 ^{o}C

1-[6-[((17β)-3-Methoxyestra-1,3,5[10]-trien-17-yl)amino]hexyl]-1H-pyrrole-2,5-dione (U-73122): Sigma, stocks of 5mM in DMSO

3.2.3. hESC Culture

For the experiments in this chapter, the H9 line of hESCs was cultured on MEFi until larger, healthy colonies were available for experiments as described in section 2.1.5. These cells were provided for me by another member of our lab (Shona Joy) and were not plated by myself. The method is included here for the purpose of reference.

When ready for Ca^{2+} imaging, H9 colonies were lifted through collagenase treatment (as described in section 2.1.5. These cells were then plated onto glass coverslips (13 mm diameter VWR cat. no 631-0149) pre-coated with Matrigel.

hESC colonies on glass coverslips were incubated overnight at 37 ^{o}C at 5% CO_2/95% air in a humidified tissue culture incubator to allow firm attachment to the Matrigel. Ca^{2+} imaging experiments were carried out within 36 h of plating.

Only those colonies which appeared healthy and undifferentiated (large, compact colonies with no 'spiking' of peripheral cells and a clearly defined colony edge with a morphology characteristic of hESCs) were used for further experiments.

3.2.4. Data Analyses

Ca^{2+} imaging data were analysed as described in section 2.2.3.1.

Statistical analyses were carried out using Prism4 software as described in the relevant text.

3.3. Results

In order to assess the functional characteristics of P2 receptors in the H9 hESC cell line, it is important to measure the functional output of these receptors. Measurement of P2X receptor function can be carried out using both standard whole cell patch-clamp (to measure ionic currents) and Ca^{2+} imaging (to measure Ca^{2+} influx). P2Y receptor function, as $G_{q/11}$-coupled receptors, can be measured by observing IP_3-dependent Ca^{2+} release from intracellular stores in response to agonists.

Unlike murine stem cells, it is not currently possible to maintain undifferentiated hESCs in culture as single cells for prolonged periods. Due to the formation of gap-junctions between stem cells in culture, and the subsequent issues associated with patch-clamping large numbers of electrically coupled cells, little work has been carried out on hESC electrophysiology. For this reason, the focus of the following chapter is on the characterisation of P2 receptor physiology in the H9 line of hESCs using standard Ca^{2+} imaging methods to measure $[Ca^{2+}]_i$.

3.3.1. Extracellular Application of ATP Induces Intracellular Ca^{2+} Rise in hESCs

Fura-2 loaded H9 cells were imaged using the standard Ca^{2+} imaging method (See section 2.2.3.) 100 µM ATP was applied externally and the fluorescence measured (Figure 3.1). In all cells, $[Ca^{2+}]_i$ increased transiently in response to ATP. Three distinct Ca^{2+} responses were observed and labelled 'A', 'B' and 'C' accordingly. 'A' type responses were fast activating, reaching a peak and inactivation within the 160 s application of ATP. 'B' types were fast activating, reaching a peak and partially inactivating to a plateau which subsequently declined to baseline within the 160 s application of ATP. Type 'C' transients were fast activating, reaching a peak and partially inactivating to a plateau which was maintained throughout the 160 s application of ATP.

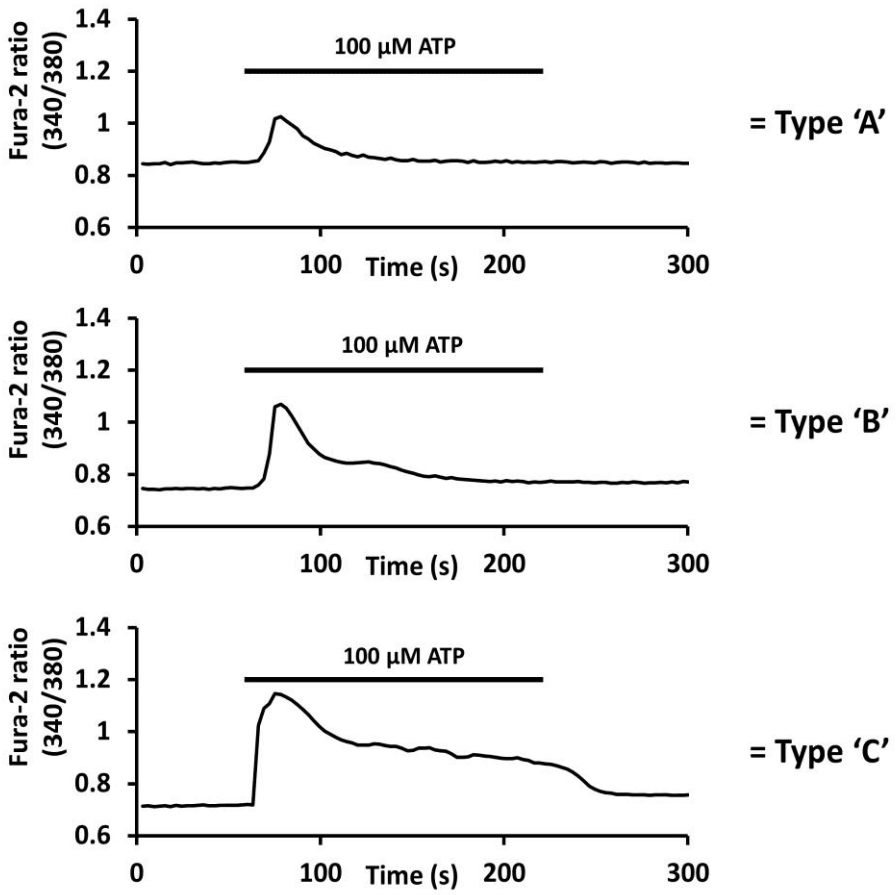

Figure 3.1. Extracellular ATP induces transient intracellular Ca^{2+} increases: The extracellular application of 100 µM ATP for 160 s (black bars) resulted in an increase of intracellular free Ca^{2+}, as reported by an increase in the Fura-2 fluorescence ratio (340/380). Three distinguishable Ca^{2+} transients were observed and named type 'A', 'B' and 'C'.

In all cells (*n* = 79), the first application of ATP elicited a greater response than subsequent applications. This desensitisation of the ATP response is shown in Figure 3.2. It is apparent that those cells labelled as type 'A' show a greater level of desensitisation than those labelled 'B', which, in turn desensitise more readily than those labelled 'C'.

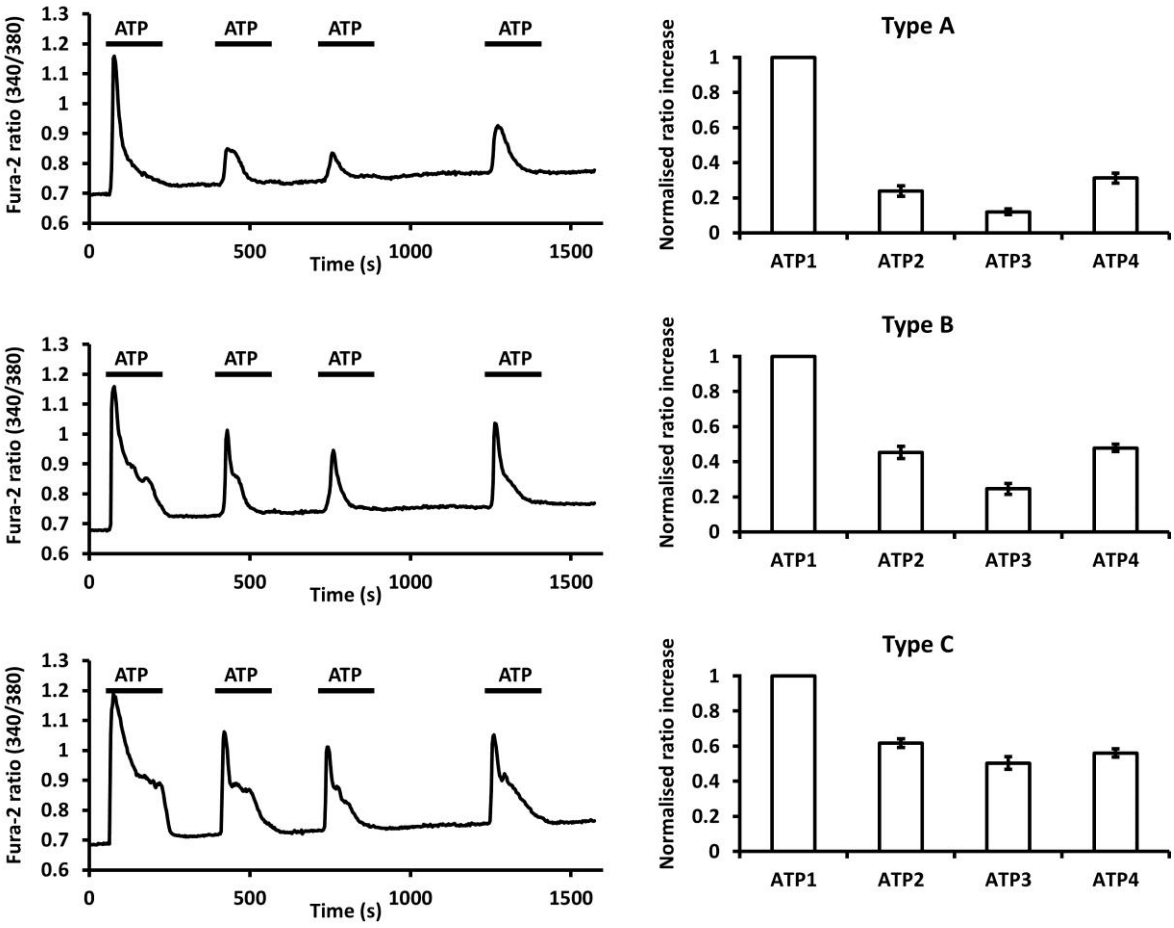

Figure 3.2. Desensitisation of ATP induced Ca^{2+} transients: Sequential applications of 100 µM ATP for 160 s (black bars) resulted in a desensitisation of intracellular free Ca^{2+} transients as reported by an increase in the Fura-2 fluorescence ratio (340/380). The responses from the raw traces (Examples: Left) were normalised to the initial ATP response and plotted for each response 'type' (Bars: Right). Type 'A', n=34. Type 'B', *n* = 32. Type 'C', *n* = 13 (Error bars represent standard error of the mean (SEM)).

In order to establish a concentration response curve for the transient Ca^{2+} response to P2 receptor activation, incrementally increasing concentrations of ATP were applied to the cells and the fluorescence ratio measured (Figure 3.3). The responses were averaged, normalised to the peak response in an attempt to calculate EC_{50}. Due to the high level of desensitisation which was observed in the response to the higher concentrations of ATP applications it was impossible to record accurately an

EC_{50}. However, it is clear that the half maximal activation is between 3 and 30 µM, a range consistent with previously reported values for P2 receptors.

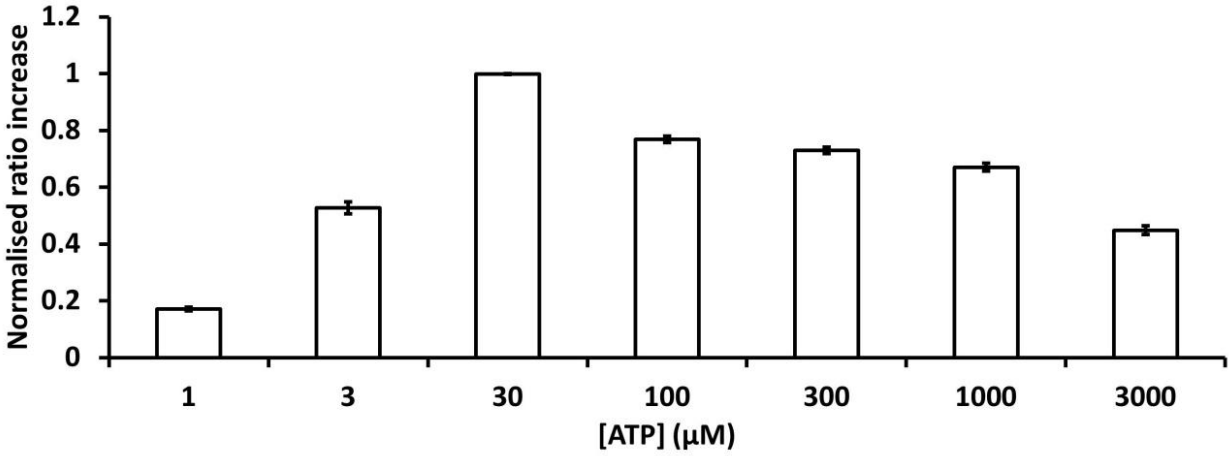

Figure 3.3. Concentration response curve for ATP: The Fura-2 ratio increase observed during transient Ca^{2+} rise in response to various concentrations of ATP was measured (top graph, averages). A sigmoidal concentration response curve was fitted to the data (bottom graph). Error bars represent SEM (not visible in concentration response curve as behind markers), *n* = 116.

3.3.2. ATP Induced Ca^{2+} Transients in hESCs are Dependent on P2 Receptor Activation

To determine if the response to ATP was a result of P2 receptor stimulation, the specific P2 antagonists suramin and pyridoxal-phosphate-6-azophenyl-2′,4′-disulfonate (PPADS) were pre- and co-applied with ATP and the effect on the Ca^{2+} transients observed (Figure 3.4). These antagonists completely and reversibly removed any observable Ca^{2+} transients suggesting that P2 receptors are responsible for the rises seen in the absence of the blockers.

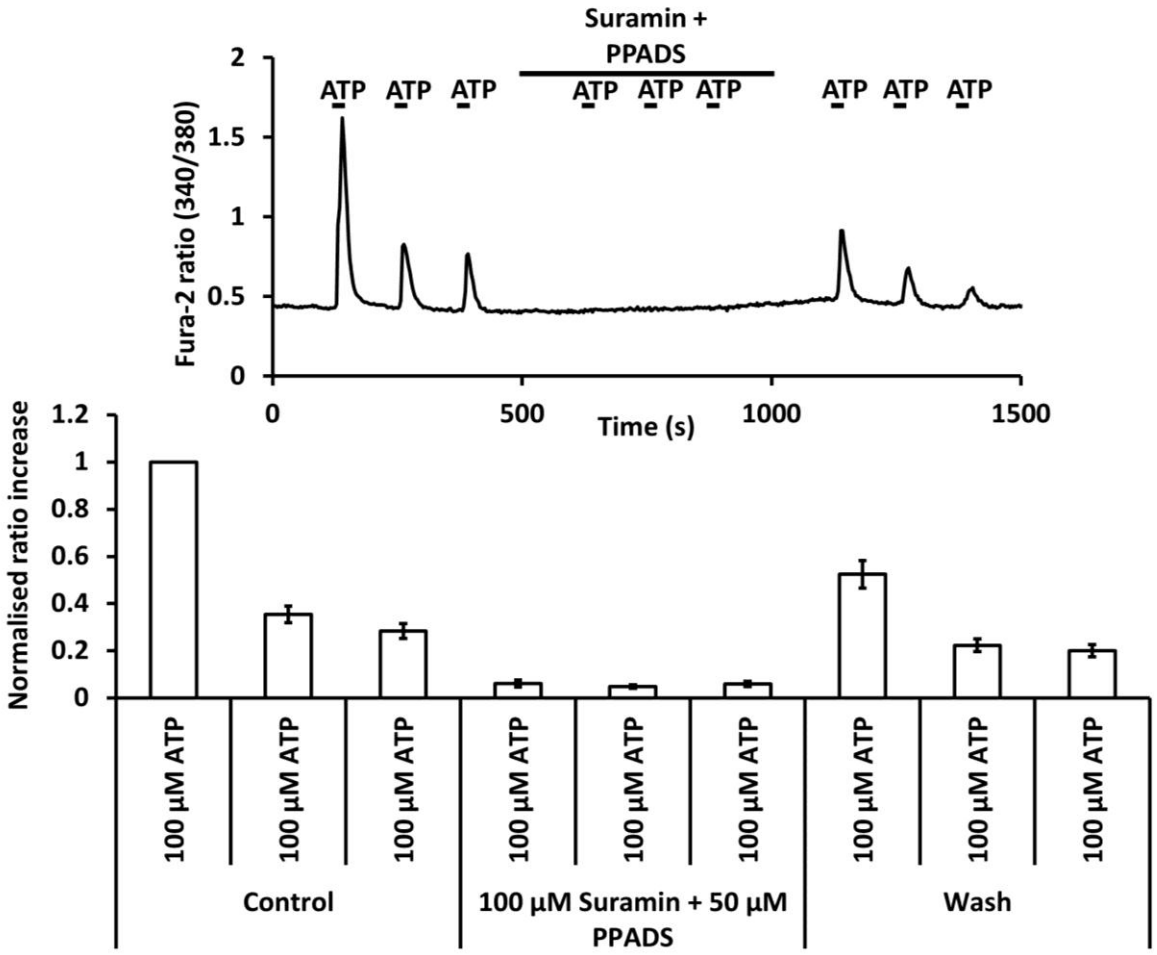

Figure 3.4. ATP-induced Ca^{2+} transients are P2 receptor dependent: Suramin (100 µM) and PPADS (50 µM) fully blocked the effect of ATP (100 µM, 15 s applications). The top example trace indicates the experimental protocol (black bars indicate application times). The bottom graph provides average responses normalised to the initial ATP response (Error bars represent SEM, *n* = 78).

3.3.3. ATP-Induced Ca^{2+} Transients in hESCs Involve Release of Ca^{2+} from Intracellular Stores

In order to establish whether the Ca^{2+} transients resulted from an influx of Ca^{2+} from the extracellular solution or from release from the Ca^{2+} store, Ca^{2+} was removed from the extracellular solution and ATP applied to the cells (Figure 3.5). 3 applications of ATP in the normal extracellular solution were followed by five applications in a "zero" Ca^{2+} solution. After a waiting period in normal extracellular solution (in case the cells should undergo store-operated Ca^{2+} entry), a further three

ATP applications were applied. As before, all of the cells responded to ATP with a transient rise in intracellular Ca^{2+}. When the extracellular Ca^{2+} was removed, the cells initially responded to the ATP with a Ca^{2+} transient similar in size to that of the initial ATP responses. The height of the next ATP response was reduced greatly and subsequent ATP responses were further diminished until no observable response occurred. Upon replacing the extracellular Ca^{2+}, no store-operated capacitive Ca^{2+} entry was observed in any cells. Further ATP applications (once more in the presence of extracellular Ca^{2+}) elicited transient Ca^{2+} responses from all cells.

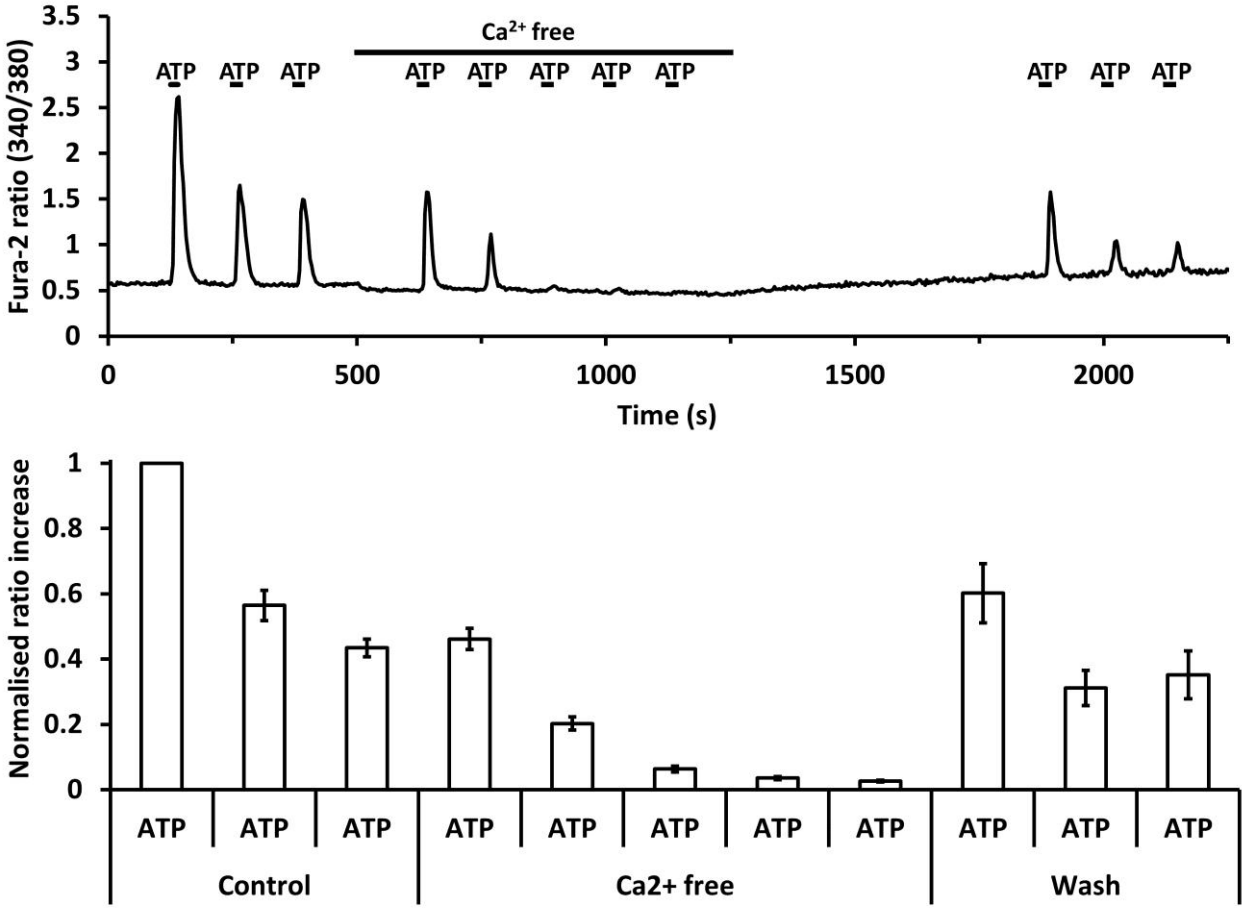

Figure 3.5. ATP induced Ca^{2+} transients are independent of extracellular Ca^{2+}: Ca^{2+} transients persist, but sequentially reduce in Ca^{2+} free solution. Multiple ATP applications in 1.25 mM Ca^{2+} (control) and Ca^{2+}-free solutions were applied as indicated (Black bars, top graph, example trace). The averages of each response normalised to the initial ATP response are shown (bottom graph, Error bars represent SEM, *n* = 56)

The capacity for the cells to respond to ATP applications with a rise in intracellular Ca^{2+} in the absence of extracellular Ca^{2+} suggests the release of Ca^{2+} from intracellular stores. This suggests that a G-protein coupled receptor (P2Y) has been activated. This does not show that the responses observed in the presence of extracellular Ca^{2+} are not also the result of P2X, only that P2Y is more than likely present in these cells. That the transient response depletes over multiple applications is indicative of Ca^{2+} store depletion. Such an event, in cells with the

appropriate intracellular mechanisms, would normally lead to capacitive Ca^{2+} entry (CCE). This was not observed in any of the cells suggesting this mechanism is either not in place in these cells or inactive in the experimental situation. The apparent absence of CCE in these cells is of interest and may reflect an absence of the necessary coupling mechanisms required for CCE, such as STIM1 or ORAI (Várnai *et al.*, 2009).

To determine the signalling pathway responsible for the Ca^{2+} transients observed upon application of ATP, blockers of the common pathway for P2Y G-protein coupled Ca^{2+} release were employed. 2-aminoethoxydiphenylborane (2-APB), a potent blocker of the IP_3 receptors(Maruyama *et al.*, 1997), and 1-[6-[[(17β)-3-methoxyestra-1,3,5(10)-trien-17-yl]amino]hexyl]-1*H*-pyrrole-2,5-dione (U-73122), a blocker of PLC signalling (Bleasdale *et al.*, 1990), were pre- and co-applied to hESCs loaded with Fura-2. As in the previous experiments, 15 s applications of 100 µM ATP were repeated in the presence and absence of each antagonist. The resulting effect on intracellular Ca^{2+} was observed (Figure 3.6). In all cells (n = 35), a Ca^{2+} transient was observable even in the absence of extracellular Ca^{2+}. In all cells, this transient response was abolished by the application of either 2-APB or U-73122. This suggests that the pathway common to P2Y receptor signalling, where ligand binding leads to G-protein coupled activation of PLC and subsequent hydrolysis of PIP_2 to IP_3, resulting in a release of Ca^{2+} from intracellular stores. The observed block of Ca^{2+} transients upon block of this pathway suggests that these transients are dependent upon this signalling cascade.

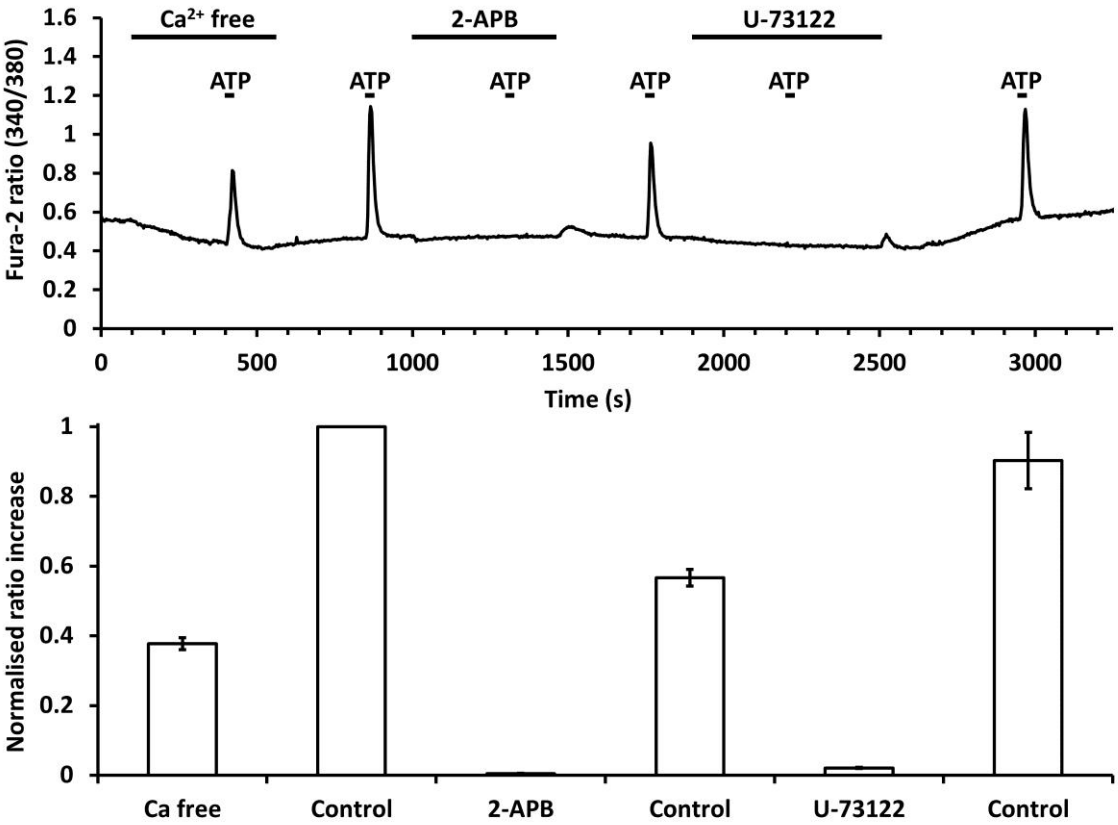

Figure 3.6. ATP induced Ca^{2+} transients are dependent on PLC and IP_3 signalling: hESCs, loaded with Fura-2 were perfused in control, Ca^{2+} free, 2-APB (100 µM) or U73122 (10 µM) as indicated (black bars). ATP (100 µM) applications were made in the indicated solutions and the Ca^{2+} transients observed. The top trace shows an example trace and the bottom graph gives the average responses, normalised to the control ATP response, of all cells (*n* = 35). Error bars indicate SEM.

3.3.4. Ca^{2+} Transients in hESCs are Induced by Multiple P2 Receptor Agonists

In order to investigate further the subtypes of P2 receptors in these cells, a variety of P2 agonists were applied to the cells and the Ca^{2+} response measured (Figure 3.7). A panel of agonists were chosen to best highlight the subtypes of P2 receptors present in the stem cell population. These were chosen from the information available from the British Journal of pharmacology's Guide to Receptors and Channels (Alexander *et al.*, 2009), and from other work on purinergic signalling in

the literature. ATP, αβme-ATP, UTP, ADP, UDP and BzATP were all applied and the effect on intracellular $[Ca^{2+}]_i$ concentrations observed.

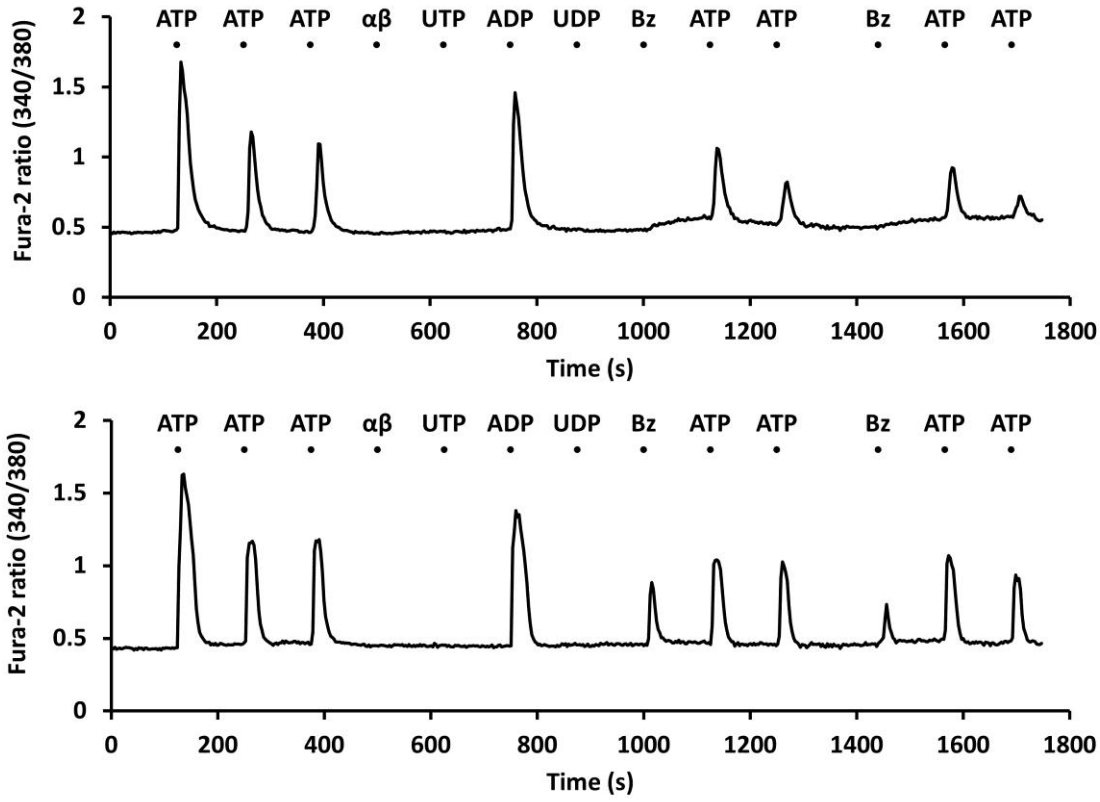

Figure 3.7. Ca^{2+} transients in response to various P2 agonists: Example traces from the application of multiple P2 receptor agonists. ATP, αβme-ATP, UTP, ADP, UDP (all 100 µM) and BzATP (10 µM) were applied to H9 hESC loaded with Fura-2 according to the protocol indicated (black dots, 15 s applications). Ca^{2+} transient responses were recorded from each cell individually. Examples show a trace from two cells, one responding (Bottom trace) and one not responding (top trace) to BzATP (*n* = 174).

As previously shown, all cells responded to 100 µM ATP. Similarly, all cells responded to 100 µM ADP. Approximately 38% (66/174) of cells responded to BzATP (Figure 3.8). None of the cells responded to αβme-ATP, UTP or UDP.

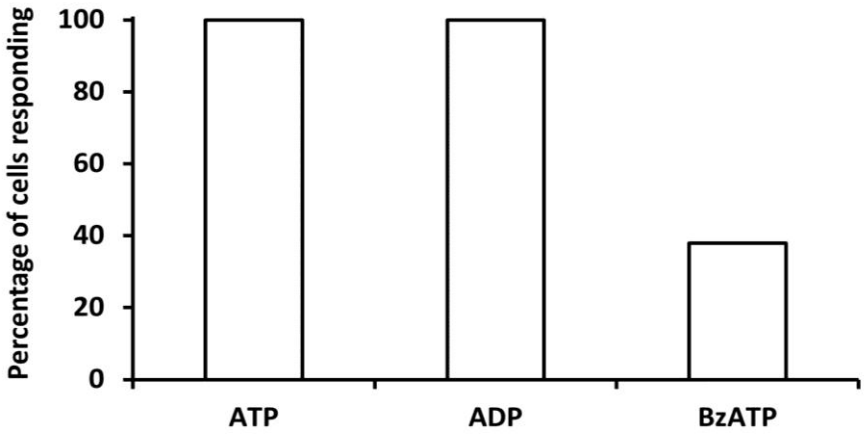

Figure 3.8. Percentage of cells responding to various P2 agonists: The percentage of cells responding to 100 µM ATP, 100 µM ADP and 10 µM BzATP are shown, *n* = 174.

As all cells responded to both ATP and ADP (at 100 µM), to establish the order of potency of the two agonists multiple applications were made in turn and the Ca^{2+} transients observed (Figure 3.9). It is clear that these cells respond more readily to ADP than to ATP at this concentration (Each ADP response is significantly larger than adjacent ATP responses when analysed using a one-tailed, paired t-test, $P < 0.001$, indicated as $***$ on the graph).

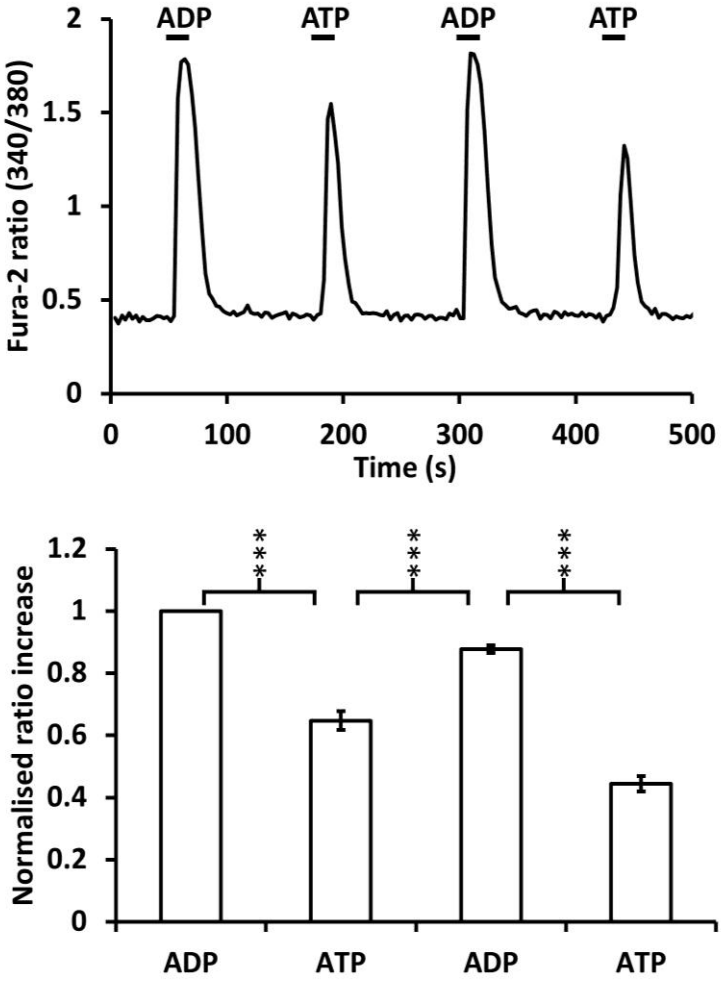

Figure 3.9. Ca^{2+} transients are larger in response to ADP than ATP: The average fluorescence ratio (380/340 nm) increases resulting from P2 receptor activation by either 100 µM ATP or 100 µM ADP is shown (Bottom graph, significance indicated; *** = $P < 0.001$, t-test, Error bars represent SEM, n = 77). An example trace from a single cell is included (top graph).

3.3.5. $P2Y_1$ Receptors are Functionally Active in hESCs

The observation that ADP responses in these cells are greater than those of ATP, along with the evidence to suggest that P2Y receptors are present and data showing that these receptors do not respond to UTP or UDP, indicates that $P2Y_1$ may be present. In order to investigate this idea more completely, the $P2Y_1$ specific agonist, MRS2365, was applied in experimental conditions identical to those already employed establish the ATP response. Figure 3.10 shows an example trace of a cell responding to MRS2365 with a Ca^{2+} transient similar to those observed in the presence of ATP. 77 % (30/39) of the cells observed responded with a Ca^{2+} transient indicating $P2Y_1$ activation.

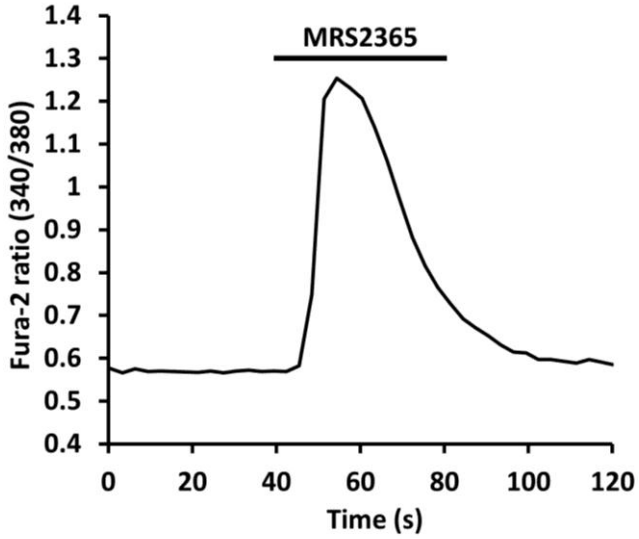

Figure 3.10. $P2Y_1$ specific agonist, MRS2365, induces Ca^{2+} transients in hESCs: MRS2365 (100 nM) was applied extracellularly to hESCs loaded with Fura-2. The resulting transient Ca^{2+} increase was measured. 77 % (30/39) of cells observed showed Ca^{2+} transients in response to this agonist. An example trace is shown with the application time indicated (black bar).

3.3.6. hESCs do not Respond to P1 Receptor Agonists with an Observable Change in Intracellular Ca^{2+}

The P1 receptor agonist, adenosine (100 µM), was applied to cells loaded with Fura-2. An application of adenosine for 60 s was repeated in triplicate on 67 cells. No effect on the Fura-2 ratio (340/380 nm) was ever observed in any of the cells.

3.4. Conclusions

Purinergic signalling in organisms provides a mechanism for extracellular purines and pyrimidines to influence cellular processes via purinergic receptor activation. By measuring intracellular Ca^{2+} alterations in response to extracellular applications of ATP and other purinergic receptor agonists, purinergic signalling has been shown to be functionally active within undifferentiated H9 hESC cultures *in vitro*.

Furthermore, functionally active $P2Y_1$ has been observed within these cells indicating a mechanism present which could allow influence by purinergic receptor agonists on hESC development.

Showing that extracellular application of ATP induces a transient rise in $[Ca^{2+}]_i$ suggests that purinergic signalling is possible within hESC populations. A rise in Ca^{2+} provides a mechanism by which protein activity and gene expression which can be acutely modulated to influence a wide variety of cellular functions. As highlighted in the introduction to this chapter, previous work in purinergic signalling has provided evidence for effects on cell cycle progression, growth, apoptosis, proliferation, migration and differentiation in several cell types. Influences on these processes would likely have major consequences for stem cell pluripotency and differentiation.

It was observed that three 'phenotypes' of response to extracellular ATP application were present (Figure 3.1). This suggests heterogeneity within the hESC population indicative of variability in receptor subtypes, expression levels or mechanisms of signalling. Whether this is due to separate and distinct populations of cells within the hESC culture or variation within the population due to such factors as cell cycle phase requires further investigation and could provide greater insight into the cellular composition of hESC cultures.

That the ATP induced Ca^{2+} rise was dependent upon extracellular Ca^{2+} during repeated applications is consistent with G protein-coupled receptor dependent release of Ca^{2+}_i from intracellular stores, *i.e.* in the absence of $[Ca^{2+}]_{i,}$ the stores cannot be replenished before the next application of agonist. The predicted EC_{50}

within the region of 3-30 μM is not dissimilar to published possible physiological extracellular concentrations of between 5 and 50 μM during ATP release events (Dubyak & el-Moatassim, 1993; Soslau & Youngprapakorn, 1997; Sørensen & Novak, 2001). This suggests that control over the purinergic pathway present in these cells is possible during physiological purine release. Whether a high (μM) phasic release event is required for transient activation, or a low (nM) tonic presence of the agonist could elicit a longer term effect will require further investigation. In human blood samples, nanomolar ATP has been shown to stimulate platelet aggregation, whereas micromolar ATP was shown to inhibit significantly aggregation (Soslau & Youngprapakorn, 1997). This work suggests a mechanism is present for a physiologically relevant, dual mode of action for purinergic signalling. Such a mechanism may be present within stem cell populations. This is an important consideration when planning future experiments as comparison of full activation (μM) and full block (i.e. with an antagonist, or genetic knock-down) may mask a possible physiological role of these agonists at the nM level.

Co-application of suramin (100 μM) and PPADS (50 μM) was shown to block completely the transient rise in Ca^{2+} observed during extracellular application of ATP (Figure 3.4). This suggests that the rise in Ca^{2+} was the result of purinergic receptor activation. In order to establish whether this transient rise in Ca^{2+} was due, in part, to P2Y receptor activation, ATP was applied to the cells in the absence of extracellular Ca^{2+} (Figure 3.5). This prevented the influx of Ca^{2+} through P2X receptor activation and allowed measurement of the P2Y activity as release of Ca^{2+} from intracellular stores. That the transient Ca^{2+} increase was not abolished by the absence of extracellular Ca^{2+} suggests that P2Y receptors are present and active in

these cells. It does not suggest that P2X are not present, and it is important to consider that they may also be expressed in these cells.

To confirm that P2Y receptors were active and responsible for the rise in Ca^{2+} observed upon ATP applications, antagonists of the signalling pathways used in receptor activation induced intracellular Ca^{2+} release were pre- and co-applied with ATP in these cells (Figure 3.6). 2-APB, a potent blocker of IP_3 induced Ca^{2+} store release, prevented a rise in intracellular Ca^{2+}. It is important to note that this antagonist also inhibits store-operated Ca^{2+} influx so will prevent the replenishment of exhausted Ca^{2+} stores (Bootman *et al.*, 2002). For this reason, and to reduce artefact of store reduction and receptor desensitisation, a replenishment time of 135 s post ATP application, in the control extracellular solution (1.25 mM Ca^{2+}) was included in the protocol. With no other Ca^{2+} store release event before co-application of ATP with 2-APB, the effect of inhibition of store-operated Ca^{2+} influx would be minimised. A second antagonist, U 73122, a blocker of PLC, prevents the PLC mediated rise in IP_3 and hence blocks the same pathway as 2-APB via an alternative mechanism (Bleasdale *et al.*, 1990). In these cells U 73122 prevented an observable rise in Ca^{2+} upon application of ATP suggesting that this mechanism was in use during the ATP-mediated rise. The effect of both of these antagonists, along with the independence of the ATP-mediate Ca^{2+} regarding extracellular Ca^{2+} strongly suggests the activity of ATP-induced release of Ca^{2+} from intracellular stores, thereby indicating P2Y activity in these cells.

To investigate further the subtypes of purinergic receptors present in these cells, the following agonists were chosen based on published data; ATP, αβme-ATP, UTP, ADP, UDP (all 100 µM) and BzATP (10 µM) (Alexander *et al.*, 2009). The Ca^{2+}

transients seen in response to these agonists was observed and recorded As observed in the previous experiments, 100% of cells responded to ATP suggesting that purinergic signalling was active in all cells (Figure 3.7 and Figure 3.8). Similarly, 100% of cells responded to ADP. None of the other agonists elicited an alteration in $[Ca^{2+}]_i$, with the exception of BzATP, which resulted in a Ca^{2+} transients in approximately 38% of cells. Bz-ATP is commonly associated with $P2X_7$ as it has a 10-fold greater potency than ATP for this receptor (Surprenant *et al.*, 1996). However, it has also been linked with activation of $P2X_1$, $P2X_2$ and $P2Y_1$ ((Evans *et al.*, 1995; King *et al.*, 1996; King *et al.*, 1997). Whilst it may not be apparent which of the purinergic receptor subtypes is responsible for the rise in intracellular Ca^{2+} during extracellular Bz-ATP application, it is apparent that, due to the selective nature of the responses, with only 38% of cells responding, there are two functional populations with respect to responses to Bz-ATP. Further work is needed to elucidate the cause of this divide, whether it is the presence of alternative receptors (such as $P2X_7$) or modulation in the expression or post expression processing of receptors expressed in all cells. It may be that the observed difference in response is due to cell cycle phase. The cells in neuronal populations are in a proliferative state, therefore there are cells present in all stages of the cell cycle at any given time. Cell cycle phase-dependent gene expression may result in the appearance of certain receptors in some cells and not others (Jaksch *et al.*, 2008).

It is known that $P2Y_1$ responds to ADP with higher affinity than ATP (Alexander *et al.*, 2009). Repeated, alternating applications of equimolar (100 µM) ATP and ADP (Figure 3.9) indicate that ADP displays a higher potency for increasing intracellular Ca^{2+} than ATP. Further to this, a high proportion of the cells exhibited sensitivity to a

highly selective $P2Y_1$ agonist MRS2365. 30 out of 39 cells showed a transient rise in intracellular Ca^{2+} upon extracellular application of 100 nM MRS2365 (Figure 3.10).

hESCs respond to purinergic stimulation with a transient rise in intracellular Ca^{2+} that is independent of extracellular Ca^{2+}, dependent on the PLC and IP_3 signalling pathway, greater in response to ADP than ATP and also occurs, in the majority of cells, in response to a potent and selective agonist of $P2Y_1$. This suggests that it is highly likely that these cells express functional $P2Y_1$ receptors. This evidence does not serve to suggest that other purinergic receptors are not present and highlights that these undifferentiated stem cell cultures are heterogeneous in their responses to purinergic stimulation.

The apparent presence and function of at least one purinergic receptor ($P2Y_1$) in undifferentiated H9 hESCs is indicative that purinergic signalling may not only be endogenously modulating early cellular development, but also that there may be the potential to modify purinergic signalling in hESCs and possibly other stem cell populations (*i.e.* iPSCs). The recently found evidence linking purinergic signalling to key developmental events such as proliferation, survival, migration and differentiation (Burnstock & Ulrich, 2011) provides the further possibility that controlling purinergic signalling in these cells could be beneficial for both disease modelling and the production of large-scale, consistent stem cell cultures for therapeutic uses.

An interesting link between $P2Y_{1,2,4}$ and $P2Y_6$ and Rho Kinase activation has been published (Sauzeau *et al.*, 2000). Rho-kinase upregulation promotes apoptosis and the inhibition of this upregulation is already in common use during stem cell

passage to promote cell survival (Koyanagi *et al.*, 2008): coincidentally, a time associated with high cell damage and ATP release. That there is a direct link between $P2Y_1$ activation and this pathway may provide a starting point for future investigation into the beneficial effects of controlling purinergic signalling in undifferentiated stem cell cultures.

Chapter 4. Functional Characterisation of hESC-Derived and Primary Neurons

4.1. Introduction

Mature neurons are terminally differentiated, preventing them from producing new neurons through cell division (De Filippis *et al.*, 2007; Galli *et al.*, 2008; Goffredo *et al.*, 2008; Hellstraom *et al.*, 2009). In the majority of stem-cell studies, neurons are typically characterised by their expression of certain markers, such as β-tubulin III, NeuN and Map2. However, this type of characterisation does not fully reflect their cell physiology.

4.1.1. Neuronal Physiology

The key function of neurons is to rapidly convey electrical signals over relatively long distances. In order to do this, a number of ion channels and transporters are necessary. These provide the required cellular machinery to produce the electrical signal, and the means to transmit it. Whilst there are a great many ion channels and transporters, only those which are commonly associated with neuronal activity will be discussed here.

In neurons, the voltage-gated, inwardly rectifying channels and two-pore domain K^+ channels (K_{2P}) are the main neuronal K^+ ion channels. The voltage-gated K^+ channels are a diverse group of channels which selectively allow the movement of K^+ across the cell membrane when V_m reaches their activation threshold. Upon depolarisation, and reaching this threshold, a conformational change in a voltage sensor (the S4 voltage sensor) results in a further conformational change in the ion

channel allowing K^+ to move down its electrochemical gradient. Inward rectifier K^+ channels function to re-establish the resting membrane potential after an excitatory event. Hyperpolarisation, observed after an action potential spike, removes a magnesium ion from a specific binding site within the channel. This magnesium ion acts as a channel blocker and its removal allows the influx of K^+ through the channel and thus re-establishment of the resting membrane potential (Nichols & Lopatin, 1997; Doyle *et al.*, 1998; Gouaux & MacKinnon, 2005). K_{2P} channels are constitutively open providing leak pathways for K^+ ions. The activity of these channels stabilises membrane potentials at values approaching E_K depending on their prevalence and activity (Goldstein *et al.*, 2005). These channels serve to modulated neuronal excitability through their control of V_m (Plant *et al.*, 2005).

The voltage-gated Na^+ channels initiate and propagate action potentials within neurons. As with the voltage-gated K^+ channels, a certain membrane potential will activate these channels, opening a pore for the influx of Na^+. Increases of V_m which exceed the threshold of these channels results in fast activation. This activation is followed by fast-inactivation and results in the transient current observed during voltage-gated Na^+ channel activity. The presence and activity of voltage-gated Na^+ channels contributes to excitability within neuronal populations (Kallen *et al.*, 1993; Sato *et al.*, 2001).

Voltage-gated Ca^{2+} channels are involved in most aspects of neuronal development and function. The influx of Ca^{2+} through these channels controls the integration of synaptic input, synaptic transmission, repetitive synaptic firing as well as modulation of gene expression (Catterall, 2011).

As the most abundant anion in organisms, regulation of Cl^- is vital to cellular function. In neurons it is also key to the establishment and maintenance of the resting membrane potential and excitability. There are many varieties and subtypes of Cl^- channels with a number of functions and mechanisms of activation. Cl^- channel gating can be regulated by membrane potential, cell swelling, ligand binding, ATP hydrolysis, phosphorylation and by other ions, such as Ca^{2+} (Jentsch *et al.*, 2002). In neurons, the ClC-2 channels and the γ-aminobutyric acid (GABA) channels are highly important functionally. ClC-2 has been implicated in the maintenance of $[Cl^-]_i$, whilst GABA is the main inhibitory neurotransmitter in the brain. Through the opening of this ligand-gated Cl^- channel upon binding with GABA, and the resulting Cl^- efflux from mature neurons, the resting membrane potential hyperpolarises, pushing it further from the action potential threshold and, therefore, inhibiting excitatory activity within the cell (Gold & Martin, 1984; Wisden & Seeburg, 1992). As the MSNs of the striatum are GABAergic and as GABA appears to play a role in neuronal development, this neurotransmitter is considered in more detail later in the thesis.

There are also a number of ligand-gated ionotropic and metabotropic channels which are associated with neuronal function.

Of the ligand-gated ionotropic receptors, there are the classically excitatory, cation-selective (such as nicotinic acetylcholine, 5-HT3, ionotropic glutamate and P2X), and classically inhibitory, anion-selective (such as $GABA_A$ and glycine) receptors. These receptors are associated with modulation of fast synaptic transmission in neurons, however, more it is now understood that they mediate a number of physiological functions in non-excitatory cells (Alexander *et al.*, 2009).

The ligand-gated metabotropic receptors act via coupled G-proteins to modulate many cellular functions. There are numerous G-protein coupled receptors. These include the adenosine, P2Y and $GABA_B$ receptors which are discussed within this thesis. Many of these receptors are targets for drugs in currently in development or testing (Marinissen & Gutkind, 2001; Alexander *et al.*, 2009).

4.1.2. Neuronal Differentiation and Ion Channel Development

There is an uneven bias within the research area of neuronal differentiation towards classical cell biology aspects of differentiation, such as the effect of neurotrophic factors and the expression of neuronal genes and proteins as markers of differentiation, and away from the electrophysiological aspects, such as the appearance of spontaneous activity on the formation of functional synapses. The search entry 'embryonic stem cell neuronal differentiation gene expression' returns 632 papers in PubMed. The entry 'embryonic stem cell neuronal differentiation electrophysiology' returns only 47 (http://www.ncbi.nlm.nih.gov/pubmed: current as of 25th September 2011). Although this is not an adequate comparative tool for assessing research interests, it does highlight the bias. Whilst it could be argued that the expression of certain markers is vital for the production of specific neuronal subtypes for clinical purposes, it could also be suggested that it is the functional activity, alongside environmental cues, that most likely determine the fate of a differentiating neuron *in vitro*.

It has been shown that embryonic stem cells (ESCs), differentiating *in vitro* down a neuronal lineage, develop electrochemical characteristics that are neuronal in nature, such as fast activating and inactivating action potentials (Song *et al.*, 2002). The appearance of voltage-gated Na^+, K^+ and Ca^{2+} channels, alongside the

development of neuronal action potential-like responses to threshold activation in current-clamp have been reported (Strubing *et al.*, 1995; Cho *et al.*, 2002; Bibel *et al.*, 2004; Biella *et al.*, 2007; Joannides *et al.*, 2007c). However, standardised protocols, for both functional studies and differentiation treatments, are not used. Whilst this is important from the standpoint of developing new techniques and investigating their effects on differentiation, it prevents the direct comparisons of data sets from multiple papers and the comparison of various cell lines that have received different environmental stimuli.

Electrical activity within neuronal populations is not only the end-point of differentiation and maturation. It is now understood that electrical signalling plays an important part in neuronal progenitor proliferation, migration, ion channel expression, neurotransmitter specification, axon path-finding, dendritic outgrowth and terminal differentiation (Spitzer, 2006). The importance of transient rises in $[Ca^{2+}]_i$ during neural induction (Webb *et al.*, 2005) and the involvement of electrical activity in synapse formation and neuronal survival (Mennerick & Zorumski, 2000; Zito & Svoboda, 2002) suggest that electrical signalling is not only present during, but is also a requirement of, proper neuronal development.

$GABA_AR$ activation in neuronal progenitors of the mouse SVZ results in depolarisation and subsequent Ca^{2+} influx (Wang *et al.*, 2003). This mechanism, alongside multiple similar endogenous mechanisms, provides a method for non-synaptic spontaneous activity. Glutamate receptors are activated by vesicular release of their appropriate ligands (NMDA, kainate and AMPA) in pre-neuronal populations (Blanton *et al.*, 1990; Flint *et al.*, 1999). The release of such neurotransmitters, and the presence of their receptors in immature neuronal

populations, enables the use of signalling pathways allowing the control of electrical signalling via the cellular environment. This signalling can, in turn, influence cellular properties. Most notably, alterations to $[Ca^{2+}]_i$ during development result in downstream changes in gene expression and the activity of numerous proteins (Komuro & Rakic, 1996; Spitzer, 2006).

Electrical signalling also provides a mechanism for cell synchronicity within large populations. In embryonic mouse, serotonin stimulates synchronised $[Ca^{2+}]_i$ transients in cranial motor neurons (Hunt *et al.*, 2005). Similarly, voltage-gated Na^+ and Ca^{2+} channel activity in prenatal mouse cortex results in large-scale $[Ca^{2+}]_i$ transients which become more synchronised during development, peaking at birth (Corlew *et al.*, 2004).

In adult neuronal precursors of the hippocampus, NMDA-mediated increases in $[Ca^{2+}]_i$ repress genes which induce glial differentiation whilst stimulating *NeuroD*, a gene which promotes neuronal maturation. Similarly, the depolarising action of GABA on these adult neural progenitors induced an increase in *NeuroD* expression (Deisseroth, 2004).

4.1.3. Aims of Chapter

There is a lack of comparative data obtained in both hESC-derived and primary tissue sources. As has been stated, by far the most common source of tissue for neuronal transplantation has come from fetal brain, specifically from the neurogenic SVZ (Kelly *et al.*, 2011; Trounson *et al.*, 2011). One of the aims of the following chapter is to address the issue of tissue source comparison and, in doing so, compare functional characteristics of hESC-derived neurons during terminal

differentiation with fetal human WGE- and neonatal mouse WGE-derived cells *in vitro*. Focus is placed on the ontogeny of voltage-gated channel activity and excitability. The inclusion of data obtained from neonatal mouse WGE provides reference to cells which are more mature than their fetal counterparts. It is obvious that human tissue would be preferential for this comparative analysis. However, the availability of viable neonatal human neuronal tissue is low, and the ethical and legal ramifications of its use meant that, for this work, mouse WGE was substituted.

4.2. Non-Standard Methods

4.2.1. Neurosphere Plating Efficiency Protocol

Neurospheres, grown as described in section 2.1.3. of Chapter 2: General Methods, were dissociated using one of three techniques.

4.2.1.1. Mechanical Dissociation

Neurospheres were transferred from the Sterilin plate into a 15 ml Falcon tube. These were spun down at 150 g for 2 min. The media was removed and 2 ml fresh neurosphere media added. The neurospheres were then triturated by repeated pipetting using a 1000 µl pipette tip until the majority of the visible neurospheres were dissociated. Large clusters of cells were allowed to sink to the bottom of the Falcon tube before the supernatant, containing single cells and small cell clusters, was transferred to another 15 ml Falcon tube and spun down at 500 g for 2 min. This supernatant was discarded and the pellet was resuspended in the plate-down medium (SFDMII, see section 2.1.2.1.) and used for plate-downs as described in section 2.1.4.

4.2.1.2. Chemical Dissociation

Chemical dissociation was carried out using a method derived from that described by Sen and colleagues (Sen *et al.*, 2004). The medium (PPRF-M4) described in that publication was designed for mouse cells and was based on DMEM:F12 in 1:1 ratio. As the cells in this experiment were only exposed to this medium for min and were then replated in the standard medium, it was decided that the supplements described in the original paper were not necessary; thus basal medium of DMEM:F12 in a 1:1 ratio and relevant pH was used. All pH values were measured using a pH meter (pH 210, HANNA Instruments) before medium was filtered through a 0.2 µm syringe filter (Minisart, Sartorius Stedim Biotech, Cat. No. 17844Q) for sterilisation.

Neurospheres were harvested essentially as described with mechanical dissociation with the exception that, after the first spin down, the spheres were resuspended in 200 µl DMEM:F12 in a 1:1 ratio. 200 µl of alkaline medium (DMEM:F12 in a 1:1 ratio, made to pH 11.6 with NaOH) was added to the sphere suspension and mixed. After 120 s, the solution was very lightly triturated with a 1000 µl pipette (with the tip widened by removing the end with sterile scissors). The suspension was left for a further 5 min, then gently mixed as before. A further 200 µl of acidic medium (DMEM:F12 in a 1:1 ratio, made to pH 1.7 with HCl) was added and the suspension was gently triturated until the neurospheres had visibly dissociated. The suspension was then spun down at 500 g for 2 min and the supernatant discarded. The remaining pellet was resuspended in terminal differentiation medium (SFDMII) and plated as described in section 2.1.4.

4.2.1.3. Enzymatic Dissociation

Enzymatic dissociation is described in section 2.1.4.

4.2.1.4. Rock Inhibitor Addition

For each of the dissociation conditions 8 wells were plated, 4 with, and 4 without Rock inhibitor Y-27632 (10 µM).

4.2.1.5. Viable Cell Counts

Cell viability was measured by a Trypan Blue exclusion assay.

24 h after the cells from the dissociation experiments were plated down, cells were dissociated again using 0.5% trypsin in PBS (Ca^{2+} and Mg^{2+} free). The medium was removed from the wells to a 15 ml Falcon tube (Media from each well were transferred to separate Falcon tubes), 500 µl of the trypsin PBS mix was then added to each well and incubated at 37 ^{o}C for 5 min. As the cells has only been plated for 24 h and were previously in single cell suspensions, trypsin did not take long to remove cells from the coverslips.

The trypsin/PBS/cell suspension was transferred into the Falcon tube containing the original medium from each well. A further 500 µl of PBS was added to each well and transferred to the appropriate Falcon tube.

Each Falcon tube now contained the living and dead cells from one well. These tubes were spun down at 500 g for 5 min. The supernatants were discarded and the pellets resuspended in 200 µl PBS. 200 µl 0.4 % Trypan Blue was added to this solution to give a 400 µl cell suspension in 0.2 % Trypan Blue. This suspension was incubated for 3 min to allow uptake of the stain by dead cells.

10 µl of each sample was added to a haemocytometer and the total number of cells with or without the blue stain counted in 4 separate regions. From this number, a percentage cell survival was calculated for each well. In order to prevent cell death during this procedure, the whole process was staggered with regards to the wells so that counting could occur within 5 min of Trypan Blue addition.

4.2.2. Immunohistochemical Analysis of β-III-Tubulin Expression

4.2.2.1. Paraformaldehyde

Stocks of 20% w/w paraformaldehyde (PFA) in PBS (Ca^{2+} and Mg^{2+} free, Gibco, Cat No. 14200-059) were prepared in advance and stored until use. PFA was dissolved in PBS through addition of NaOH until the powder went into solution. HCl was used to bring the solution pH back to 7.8 before PFA stocks were aliquoted at 500 µl and stored at -20 ^{o}C.

4.2.2.2. Blocking Mix

For 15 ml blocking mix, 750 µl FCS and 7.5 µl Triton X-100 (0.05% after dilution) were added to 14.25 ml PBS.

4.2.2.3. Immunostaining

Immunohistochemistry (IHVC) was performed using the monoclonal antibody anti-β-III-tubulin (Sigma) produced in rabbit and an anti-rabbit secondary antibody raised in goat (Sigma, Cat No. R9380).

Cells plated on glass coverslips, as described in section 2.1.4. were fixed for immunohistochemical staining in 0.5 ml 4 % PFA in PBS (Ca^{2+} and Mg^{2+} free). Coverslips were washed 3 times in 0.5 ml PBS before being incubated in 4% PFA for 10 min at room temperature. The PFA/PBS mixture was removed and the coverslips

were then incubated in 0.5 ml fresh PBS (no PFA) for 5 min. This wash step was repeated 3 times.

The PBS was removed and 0.5ml blocking mix added to the well. This was incubated at room temperature for 1 h. The blocking medium was removed and 0.5 ml of the primary antibody (anti-β-III-tubulin: 1:200 in blocking mix) was added to the well. The primary antibody was incubated at 4 ^{o}C overnight.

The primary antibody was then removed and the cells washed again 3 times for 5 min each time in PBS.

0.5 ml of the secondary antibody (goat anti-rabbit, 1:200 in blocking mix) was then added to the well and incubated at room temperature for 1 h. Aluminium foil was used after addition of the secondary antibody to prevent degradation of the fluorescent signal by exposure to light.

A further 3 washes with PBS were carried out and 0.5 ml Hoechst (Sigma, Cat. No. 33258 1:10000 of 5 mg/ml stock in PBS) was added to the well and incubated for 10 min. This was followed by a single 5 min wash in PBS before the glass coverslip was removed from the well gently, so as not to lose any cells, and was mounted on a glass microscope slide using Clearmount IHC mounting solution (Invitrogen, Cat. No. 00-8010). Stained coverslips were viewed and photographed using a fluorescent Leitz microscope.

4.2.3. Functional Analysis of hESC- and Primary Tissue-Derived Neurons

The whole-cell patch clamp and Ca^{2+} imaging techniques used in this chapter are described fully in sections 2.2.1.4. and 2.2.3. of Chapter 2: General Methods,

respectively. Individual agonist/antagonist application protocols are discussed in the results text and highlighted in the corresponding figures.

4.2.3.1. Solutions

ECS: as described in section 2.2.1.1.

50 mM KCl ECS: as per standard ECS, but with 50 mM KCl and 90 mM NaCl

Ca^{2+} Free ECS: as per standard ECS, but with no added $CaCl_2$ and 1 mM EGTA supplement

ICS: as described in section 2.2.1.2.

4.2.3.2. hESC-Derived Neurons

hESC-derived neurons were plated down as described in section 2.1.4. Functional analysis of cells began at 1 day PPD. Cells were maintained in culture for a maximum of 7 week The results were obtained from cells plated from multiple neurosphere preparations.

4.2.3.3. Human Fetal Primary Neurons

WGE was extracted from human fetal brain as described in section 2.1.5. hWGE-derived neurons were used for functional characterisation after 24 h PPD and within 2 days *in vitro* (DIV)

4.2.3.4. Postnatal Mouse Primary Neurons

WGE was extracted from neonatal mouse brain as described in section 2.1.7. mWGE-derived neurons were used for functional characterisation after 24 h PPD and within 2 days *in vitro* (DIV)

4.2.4. Statistical Analysis

Comparisons of variability across multiple data-sets were carried out using one way analysis of variance (ANOVA) followed by the *post-hoc* Tukey-Kramer multiple comparison test. Data-sets from hESC-derived neurons were compared first, followed by analysis of all data-sets. Prism4 was used for all statistical analysis.

Tukey-Kramer was chosen for multiple comparison testing as it is associated with a reduced rate of type I errors (false positives) and allows all possible pairwise comparisons (Ludbrook, 1991). The Kramer extension of the *post-hoc* Tukey test was used to correct for variation in the size of individual data-sets.

Data recorded regarding properties about which population distribution would be of interest (current amplitudes, threshold and V_m values) have been displayed as box-and-whisker plots in order to display a more accurate representation of the distribution of values that is seen using bar graphs with standard error of the mean. These charts were plotted in Prism4.

4.3. Results

4.3.1. hESC-Derived Neurosphere Plating Efficiency is Improved by Enzymatic Dissociation and Inhibition of ROCK by Y-27632

The generation of neurospheres, as detailed in section 2.1.3. of Chapter 2: General Methods, provided neuronal precursors which could be plated as single cells and further differentiated into mature neurons (Joannides *et al.*, 2007a). This process of dissociation and plating as single cells can be damaging to cells, resulting in a loss of both quality and quantity of neurons in these cultures.

In order to test the impact of enzymatic, compared to mechanical or chemical dissociation, cell suspensions were made from day 32 neurospheres using each of these methods (see section 4.2.1.). Figure 4.1 shows the increased viability observed with dissociation using both chemical and enzymatic against mechanical. In both chemical and enzymatic dissociation, the addition of 10 µM ROCK inhibitor increased cell viability. This effect was not seen in mechanical dissociation where viability was already greatly reduced. The highest mean viability obtained was using the enzymatic dissociation in the presence of ROCK inhibitor, at 76.5% cell survival. This method was used for all subsequent neurosphere plate-downs.

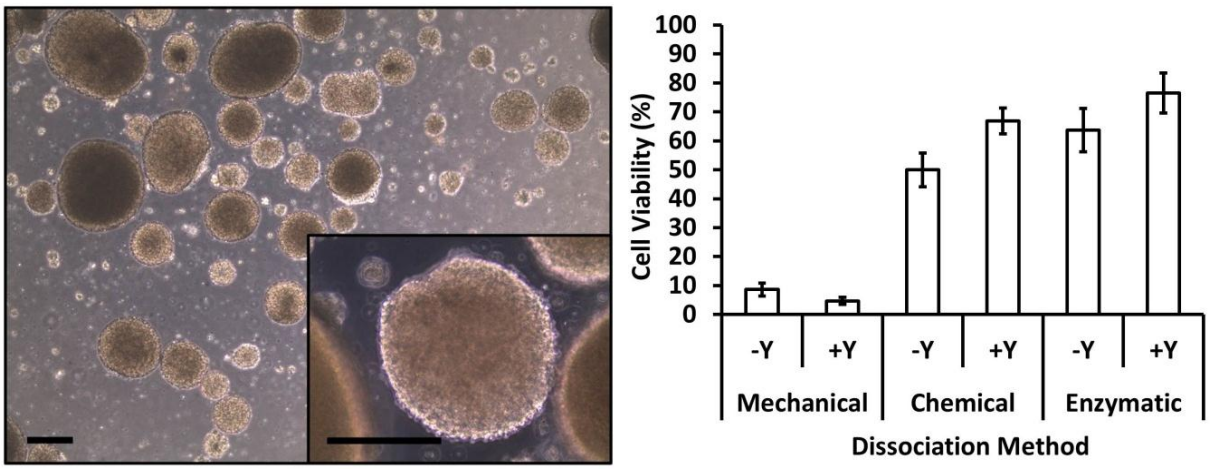

Figure 4.1. Enzymatic dissociation of neurospheres with ROCK inhibitor, Y-27632, increases viability of single cell cultures: Dissociation of neurospheres using various methods with or without ROCK inhibitor Y-27632 (Y). Left side, brightfield image of neurospheres (Scale bar: 300 µm). Right side graph indicates mean cell viabilities for each condition (for each condition *n* = 4, error bars represent SEM).

4.3.2. hESC Neurosphere Differentiation Protocol Produces Cells With Neuronal Characteristics

Previous work within our lab has shown that the differentiation procedure outlined in section 2.1.3. and 2.1.4. produces cells which express proteins associated with neuronal maturation, such as β-III tubulin and MAP2, as well as glutamate and

GABA receptors (Joannides *et al.*, 2007a). In order to assess the successful production of neurons from hESCs, the expression of β-III tubulin was investigated during terminal differentiation. Figure 4.2 shows that at PPD 3 a high proportion of these cells express the neuronal marker β-III tubulin. The close association of cells and the morphological characteristic of cells crossing and overlying one another prevented effective cell counts being made regarding percentage of cells expressing β-III tubulin. However, it is noticeable that in those regions where no cell nuclei are apparent (as measured with Hoechst), there is also no apparent expression of β-III tubulin suggesting that non-neuronal differentiation was minimal during terminal differentiation. The images also serve to highlight the tendency of these cells after several weeks PPD to form 3 dimensional sphere-like structures with large, protruding, multi-axon extensions. This 'clumping' of cells results in technical difficulties with whole-cell patch clamp, Ca^{2+} imaging and immunohistochemistry.

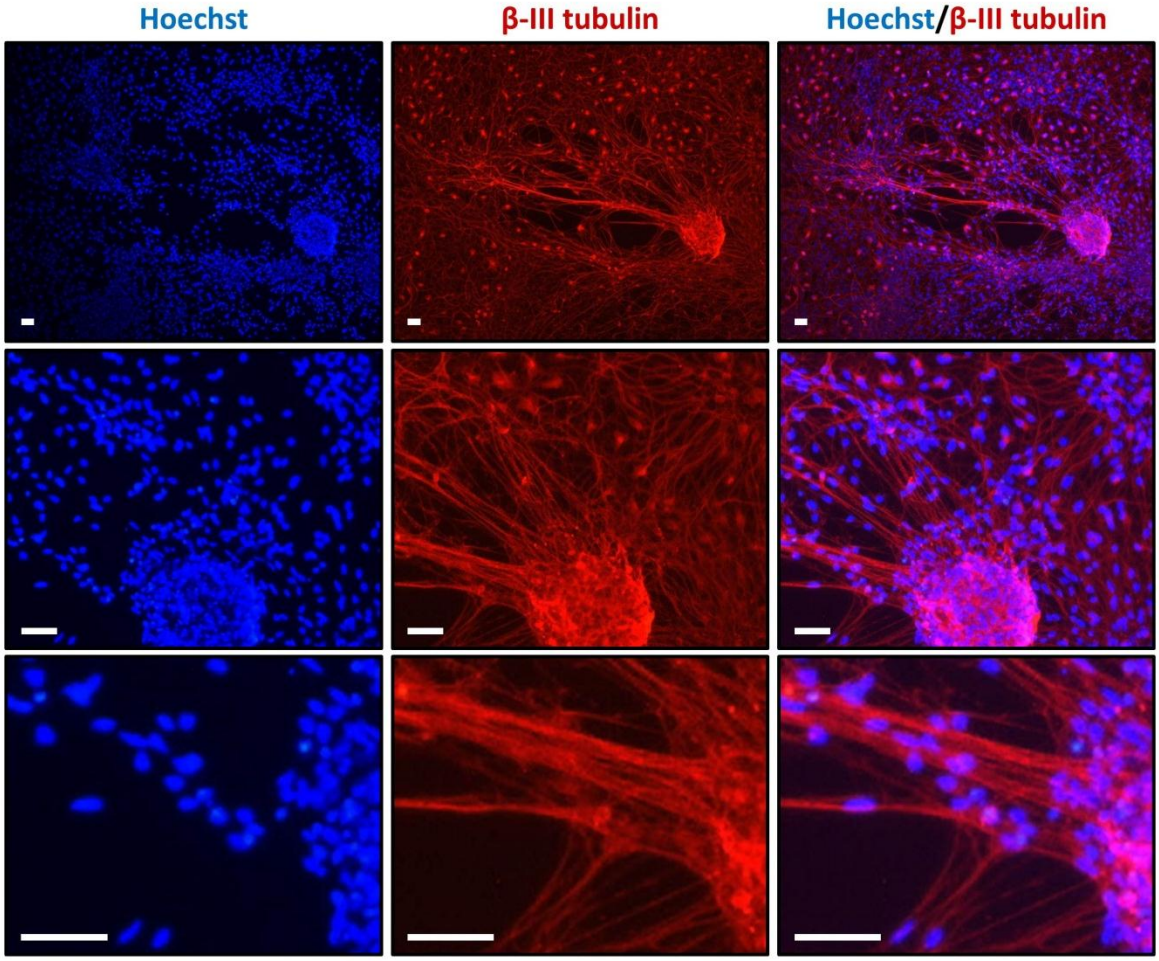

Figure 4.2. hESC-derived neurons express β-III tubulin protein: Anti-β-III tubulin (red, middle images) was used to stain the neuronal marker β-III tubulin in hESC-derived neurons at PPD week 3. Hoechst nuclear stain (blue, left images) was used to identify the nuclei. A merged image for each magnification is shown (right image). Progressively increased magnifications are shown to highlight expression distribution and morphology (top to bottom). Scale bars (white) indicate 50 µm.

It is not practical to label neuronal cells for whole cell patch clamp experiments. Although it is possible to transfect cells with GFP-tagged markers for neuronal expression and then selectively patch-clamp only those cells, the procedure of transfection, coupled with unknown effects of overexpression of GFP in these cells means this option was not utilised for the study of functional development in these cells. In place of a direct marker of neurons, selection of cells for attempted patch-clamp was made using morphological features. Only cells with a small (8-12 µm) soma, with long, branching axonal extensions (indicated in Figure 4.3) were chosen

and these were the most common cell type present. Other cell types present in smaller numbers and exhibited morphological features consistent with epithelial and glial cells. These were avoided for patch clamp and Ca^{2+} imaging experiments.

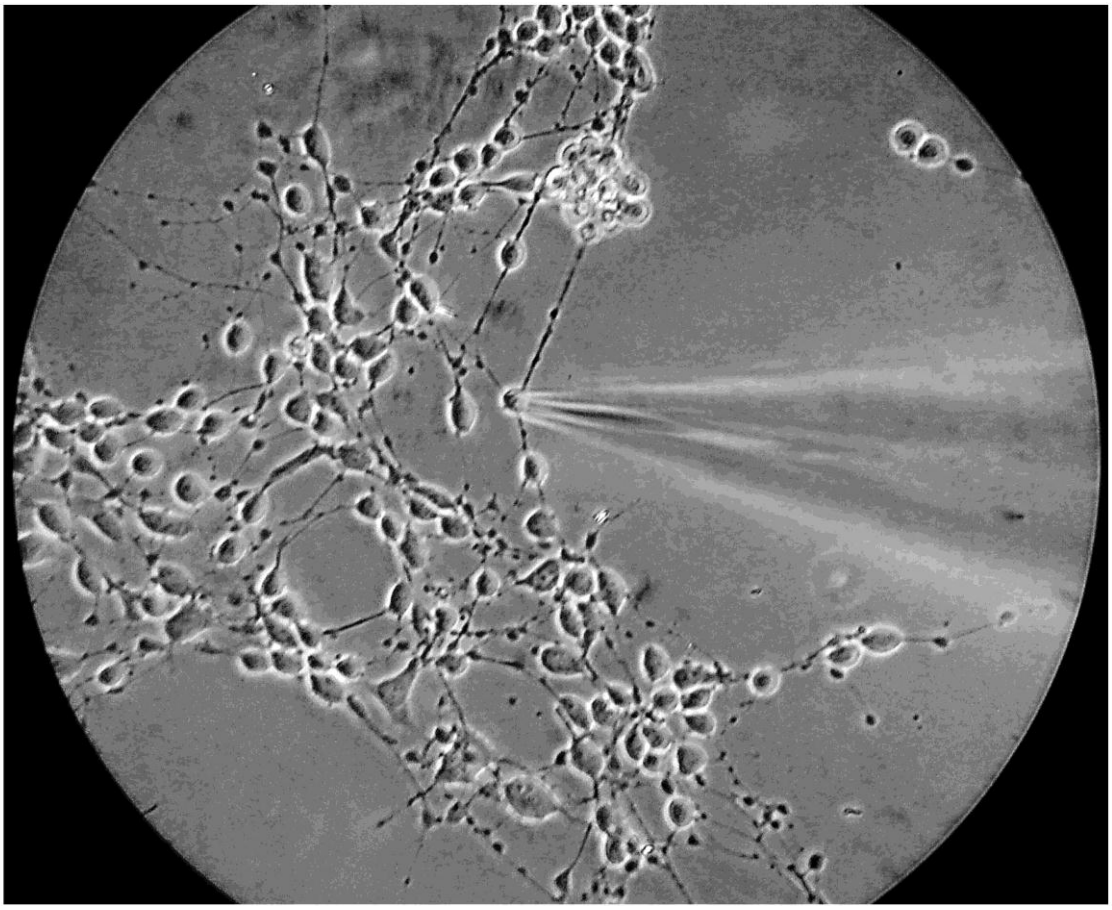

Figure 4.3. hESC-derived neurons display neuronal morphological features: Image of hESC-derived neurons at PPD week 1 with patch clamp pipette approaching a cell for whole-cell patch clamp. Image highlights the typical morphology of hESC-derived neurons and the preferred distribution for whole-cell patch clamp. Image recorded on an LG U990 compact cameraphone.

4.3.3. Functional Characterisation of hESC-Derived Neurons

Standard whole-cell patch-clamp and Ca^{2+} imaging techniques were employed to measure the functional development of hESC-derived neurons during the terminal differentiation stage PPD. Measurements of K^+, Na^+ and Ca^{2+} channel activities were made throughout the terminal differentiation at weeks 1, 2, 3 and 4+. Weeks 4, 5 and 6 were incorporated into the category of week 4+ as the progressive 'clumping'

of cells during the terminal differentiation phase resulted in low success rates of patch-clamp attempts. The ability of cells to fire spontaneous and induced action potentials was also recorded, along with the resting membrane potential. These characteristics were compared with measurements taken from hWGE- and mWGE-derived neurons. For the experiments in this chapter, hWGE-derived neurons (from fetuses all aged between 6 and 12 weeks post-conception) and mWGE-derived neurons (from postnatal day 1 mice) were all used within 2 DIV.

4.3.3.1. Cell Capacitance

Cell capacitance gives a measure of the cell membrane surface area. This was measured during whole-cell capacitance correction upon successful whole-cell access. The mean capacitance values for hESC-derived neurons show little variation during the terminal differentiation protocol (Figure 4.4). Mean values of 11.08, 12.05, 7.13 and 11.57 pF were recorded for weeks 1, 2, 3 and 4+, respectively. For fetal hWGE-derived neurons and neonatal mWGE-derived neurons, the mean capacitance values were 9.92 and 7.50 pF, respectively. Separate one way ANOVA tests were carried out on the data from only the hESC-derived neurons, and then from all data sets. In both cases ANOVA indicated no significant variation across the data sets.

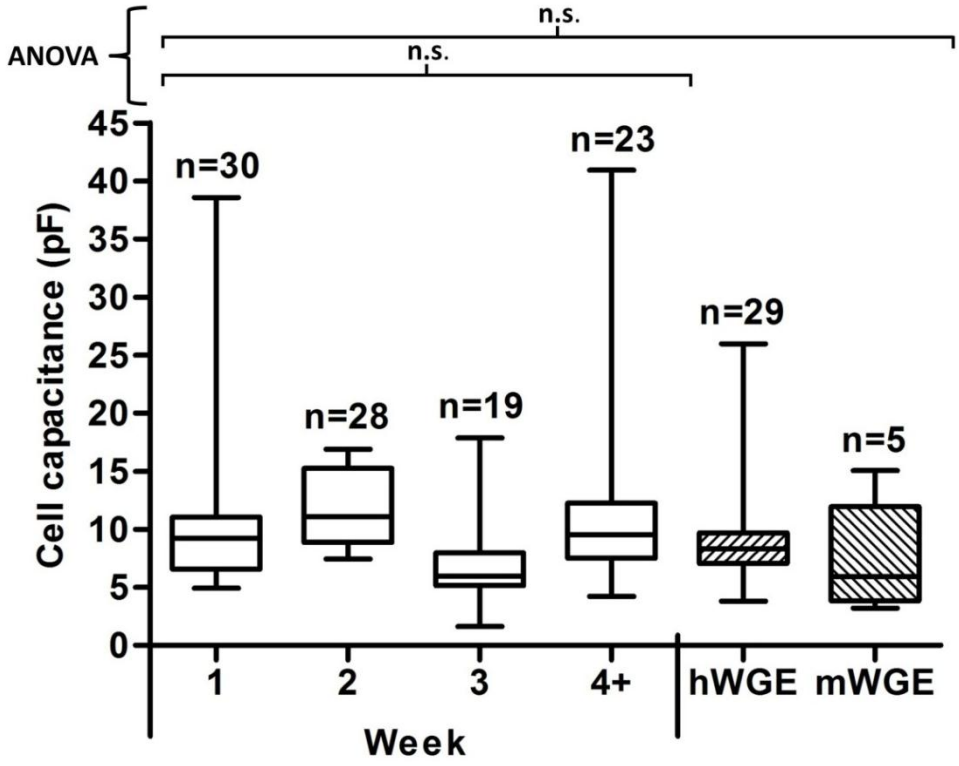

Figure 4.4. Cell capacitance development in hESC-derived neurons compared with primary neurons: The recorded capacitance (pF) for each cell during terminal differentiation of hESC-derived neurons was recorded. Box plots of the data are show here alongside those of data obtained from hWGE- and mWGE-derived neurons. ANOVA and *post-hoc* Tukey-Kramer tests were applied. ANOVA results indicated (n.s. indicates non-significance).

4.3.3.2. Voltage-Gated Ion Channel Development

Measurement of voltage-gated channel activity was carried out using the voltage-step protocol in the standard whole-cell patch clamp configuration outlined in section 2.2.1.4. K^+ currents were recorded in the presence and absence of extracellular Na^+ and were confirmed using 20 mM TEA block. Na^+ currents were recorded in the presence and absence of 20 mM TEA to reduce the effect of outward K^+ channel activity and were confirmed by their removal in the absence of extracellular Na^+ (NMDG-Cl equimolar replacement of NaCl in the ECS).

Figure 4.5 to Figure 4.10 show example traces indicative of those observed in the majority of cells from the stage/cell type indicated.

In all cell stages/types, K^+ currents, when activated, rose quickly and reached a stable plateau which was maintained for the duration of the voltage step. The I-V plot, showing the mean current at the plateau phase against the voltage, shows that there is little or no outward current at voltages more negative than -50 mV. The voltage-dependent mean outward plateau begins to be activated as the voltages become more positive peaking and often plateauing at approximately 40 mV. Voltage-activated K^+ currents were recorded in all cell types and at all cell stages.

In contrast, voltage-activated Na^+ currents were not measured in all cells. Figure 4.5 shows example traces recorded from a hESC-derived neuron at 1 week PPD and the current-voltage (I-V) plot generated from that recording. The example trace, indicative of those observed in the majority of cells at week 1, shows that there is no voltage-activated inward current in these cells. Cells measured later in the differentiation protocol displayed voltage-gated Na^+ channel activity. Figure 4.6 shows an example of a week 2 hESC-derived neuron displaying voltage-activated Na^+ currents. The shape of the current in these traces is indicative of those recorded in all neurons displaying voltage-activated Na^+ currents. Upon voltage-activation, there was a large inward current which was fast-activating and fast-inactivating. The I-V for this current, plotting the peak negative current density against the voltage, shows that little or no current is present at voltages more negative than -40 mV. More positive voltages elicit a larger current as the threshold voltage for the voltage-gated Na^+ channels is reached. The peak negative current is between approximately -30 to -20 mV and begins to reduce in subsequent sweeps.

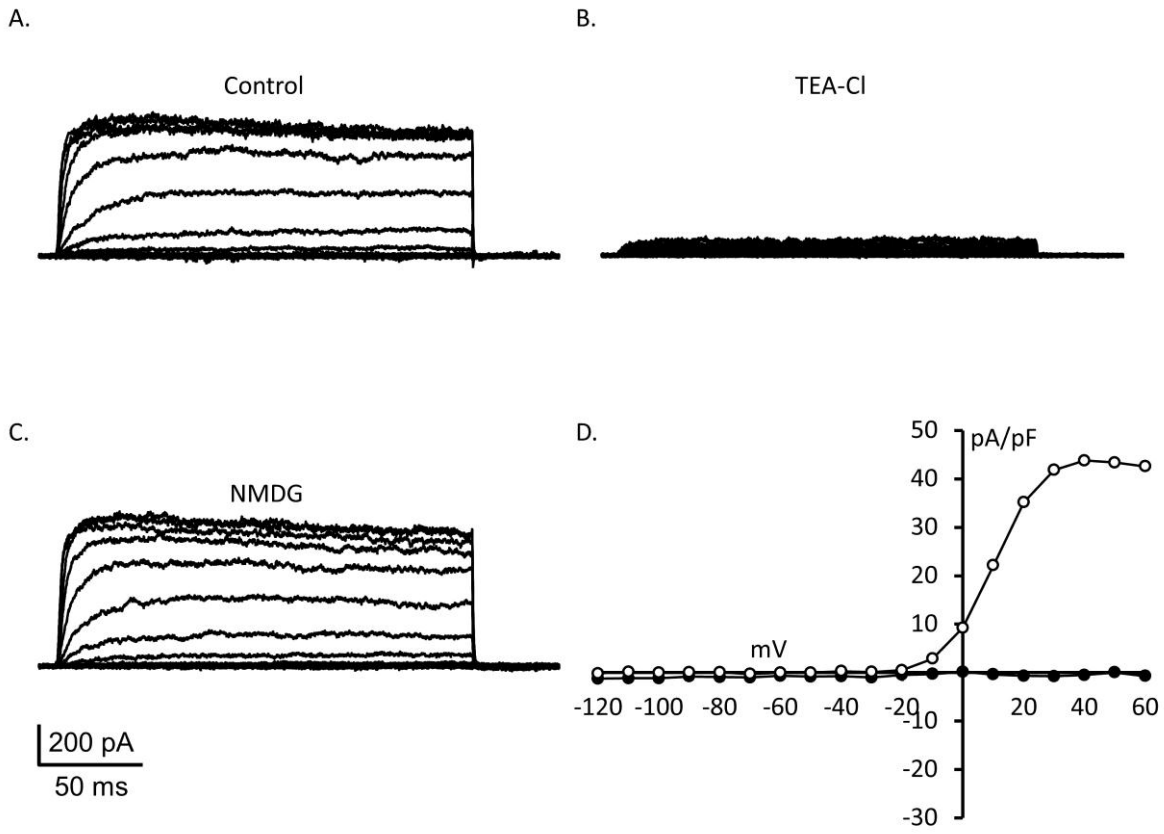

Figure 4.5. Voltage-activated currents in week 1 hESC-derived neurons: Example traces showing the currents elicited by a voltage-step protocol are shown (A, B and C). A. Voltage-activated currents in control (ECS) solution. B. Voltage-activated currents in the presence of 20 mM TEA-Cl. C. Voltage-activated currents during the replacement of extracellular Na^+ with NMDG. D. The current density-voltage curves for the mean outward plateau (open circles) and minimum inward peak (filled circles).

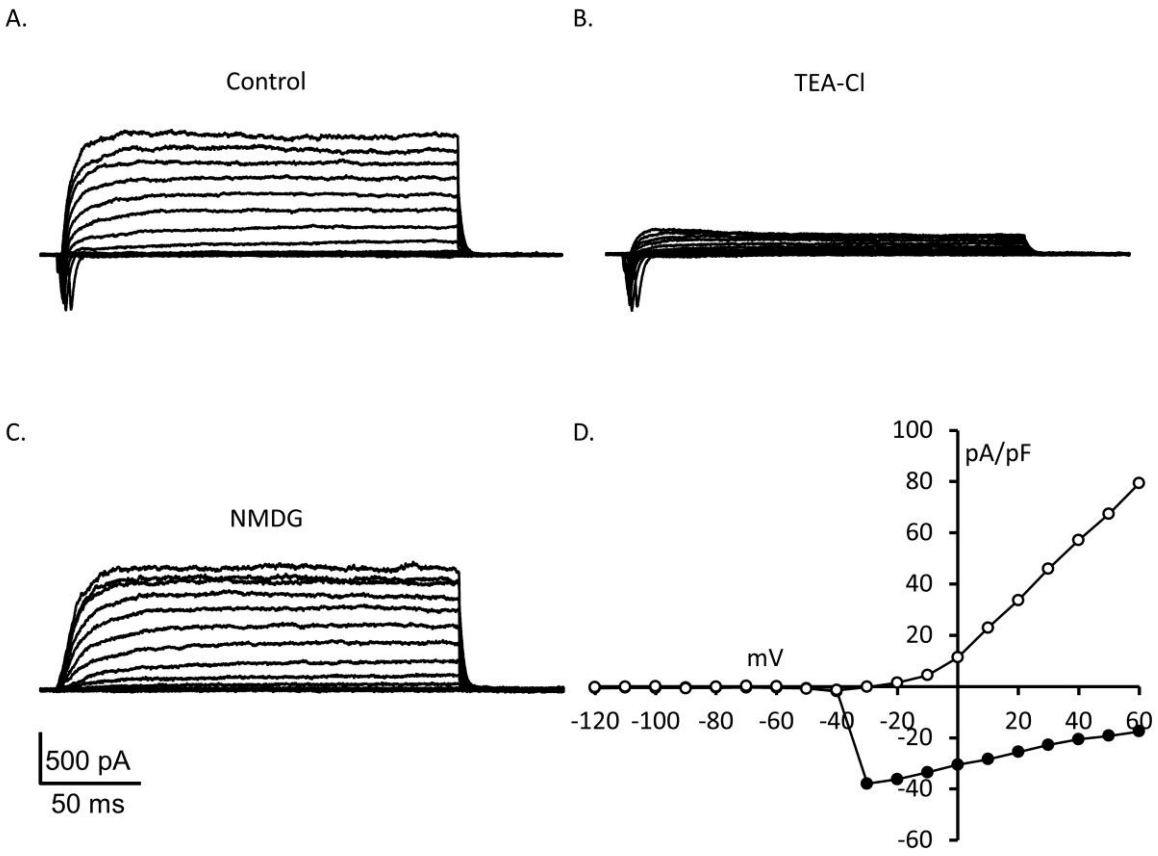

Figure 4.6 Voltage-activated currents in week 2 hESC-derived neurons: Example traces showing the currents elicited by a voltage-step protocol are shown (A, B and C). A. Voltage-activated currents in control (ECS) solution. B. Voltage-activated currents in the presence of 20 mM TEA-Cl. C. Voltage-activated currents during the replacement of extracellular Na^+ with NMDG. D. The current density-voltage curves for the mean outward plateau (open circles) and minimum inward peak (filled circles).

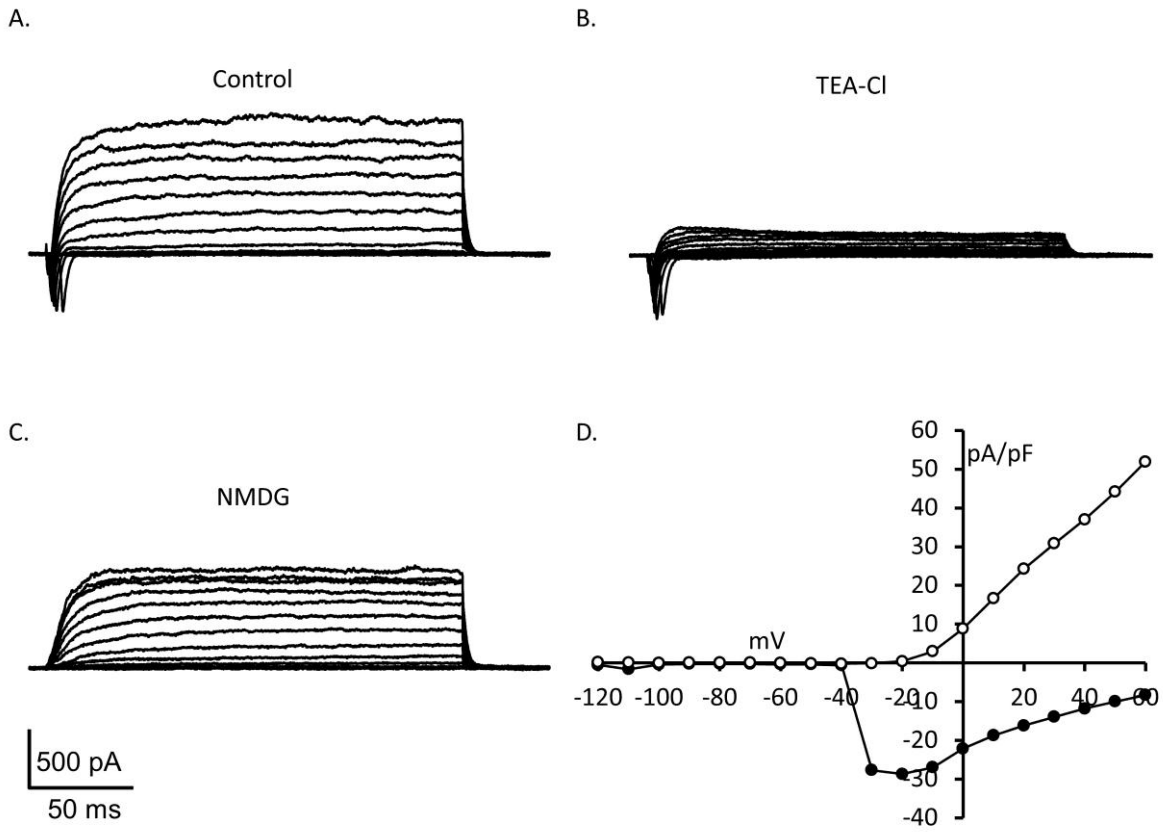

Figure 4.7 Voltage-activated currents in week 3 hESC-derived neurons: Example traces showing the currents elicited by a voltage-step protocol are shown (A, B and C). A. Voltage-activated currents in control (ECS) solution. B. Voltage-activated currents in the presence of 20 mM TEA-Cl. C. Voltage-activated currents during the replacement of extracellular Na^+ with NMDG. D. The current density-voltage curves for the mean outward plateau (open circles) and minimum inward peak (filled circles).

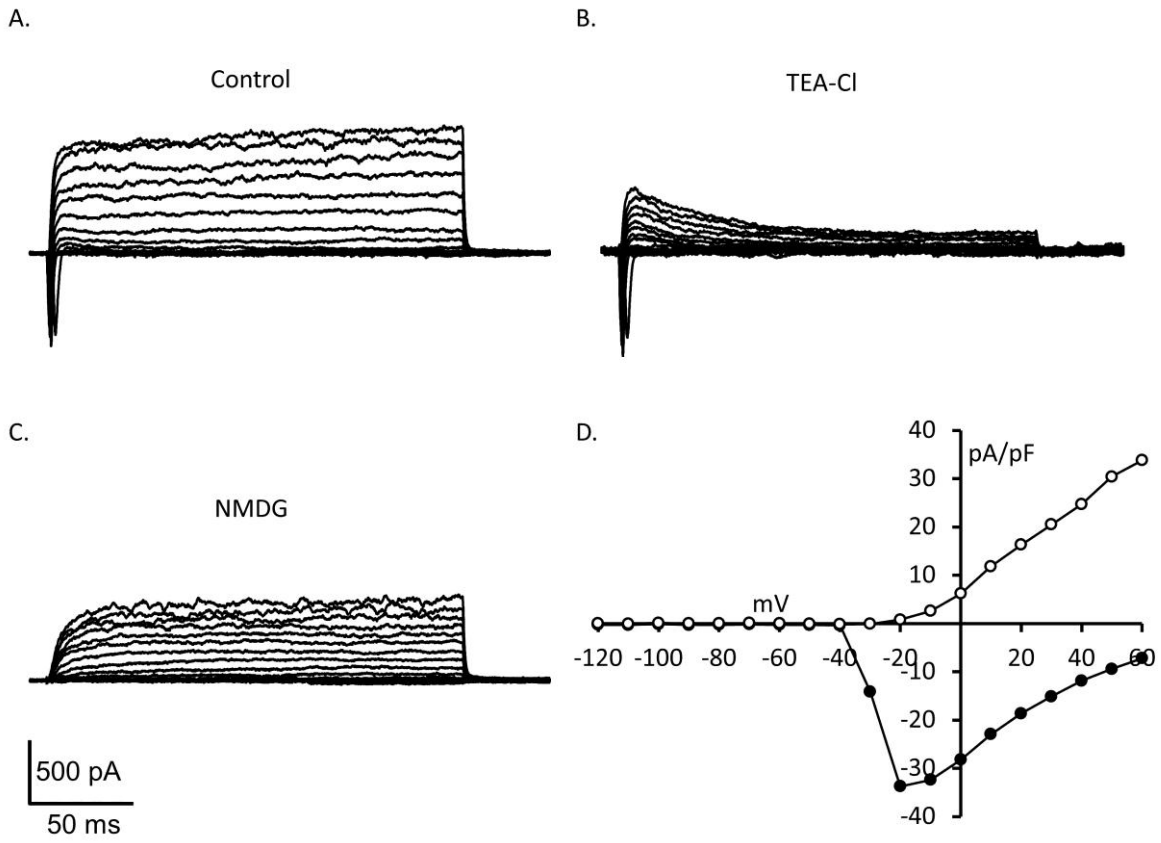

Figure 4.8 Voltage-activated currents in week 4+ hESC-derived neurons: Example traces showing the currents elicited by a voltage-step protocol are shown (A, B and C). A. Voltage-activated currents in control (ECS) solution. B. Voltage-activated currents in the presence of 20 mM TEA-Cl. C. Voltage-activated currents during the replacement of extracellular Na^+ with NMDG. D. The current density-voltage curves for the mean outward plateau (open circles) and minimum inward peak (filled circles).

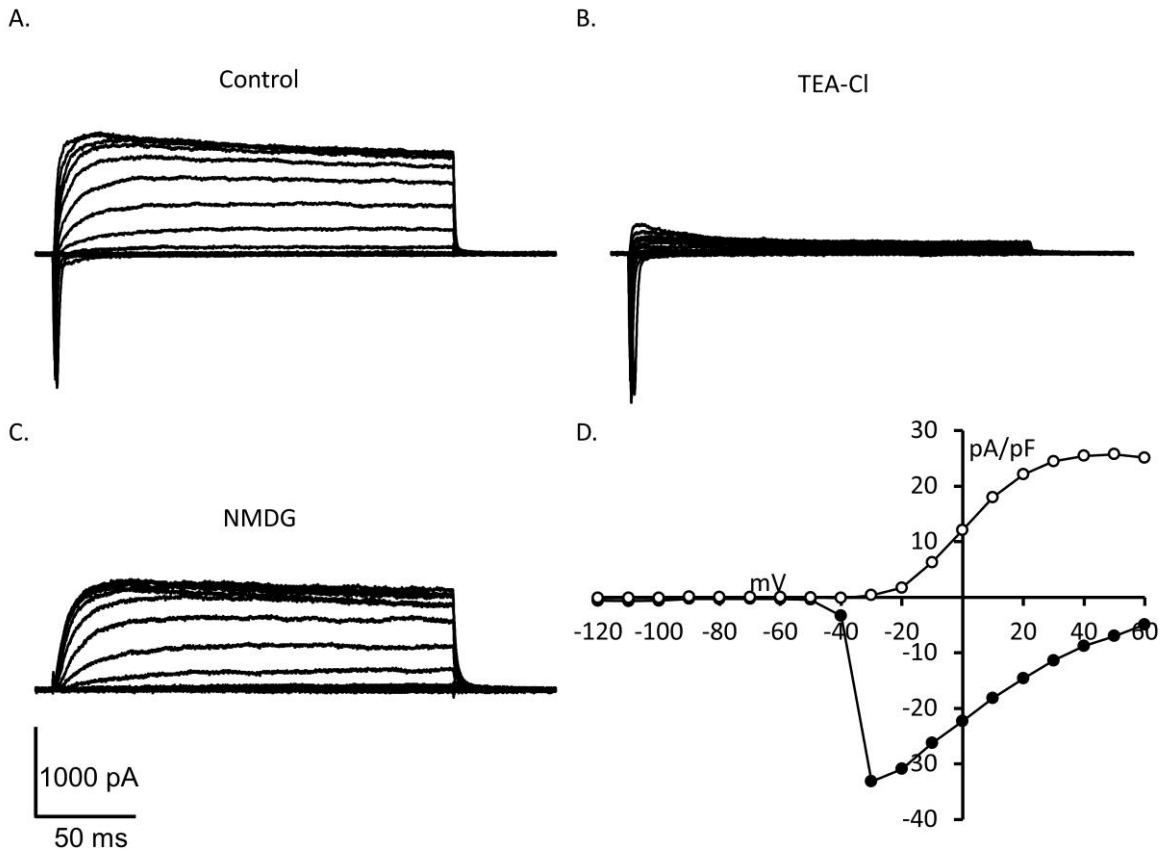

Figure 4.9 Voltage-activated currents in hWGE-derived neurons: Example traces showing the currents elicited by a voltage-step protocol are shown (A, B and C). A. Voltage-activated currents in control (ECS) solution. B. Voltage-activated currents in the presence of 20 mM TEA-Cl. C. Voltage-activated currents during the replacement of extracellular Na^+ with NMDG. D. The current density-voltage curves for the mean outward plateau (open circles) and minimum inward peak (filled circles).

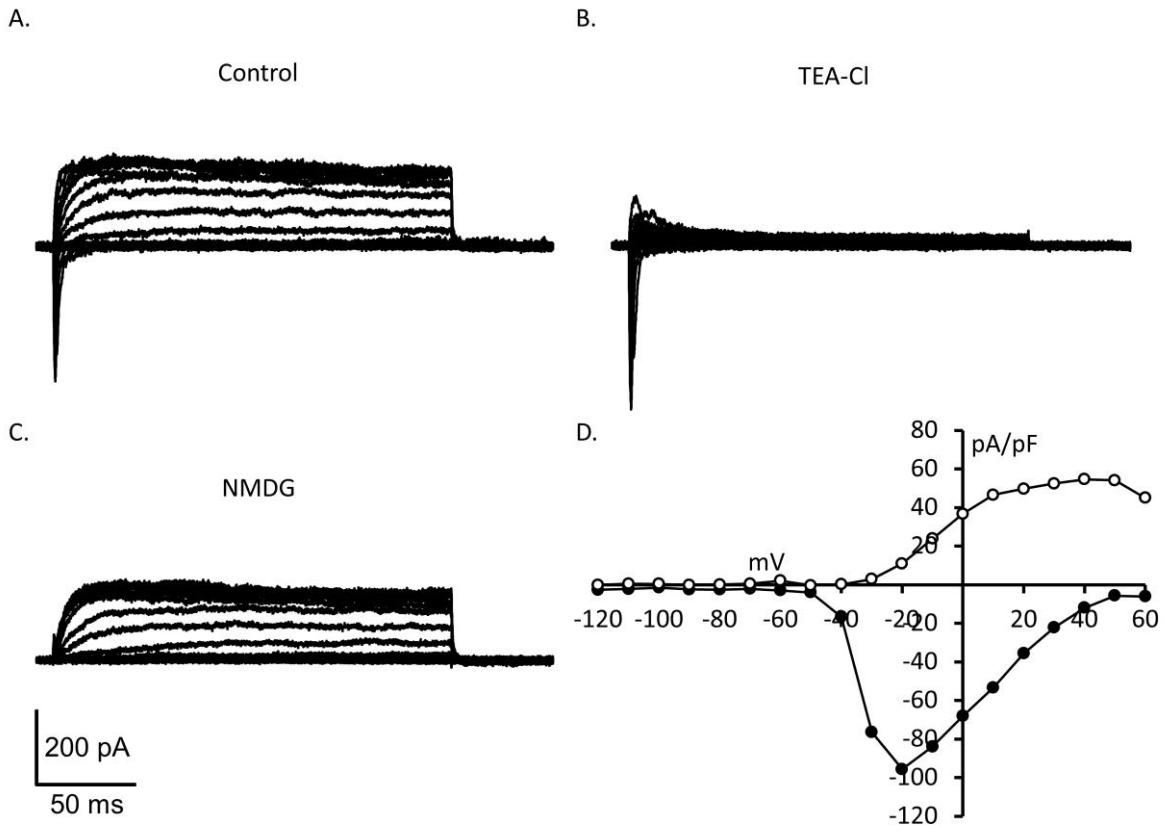

Figure 4.10 Voltage-activated currents in mWGE-derived neurons: Example traces showing the currents elicited by a voltage-step protocol are shown (A, B and C). A. Voltage-activated currents in control (ECS) solution. B. Voltage-activated currents in the presence of 20 mM TEA-Cl. C. Voltage-activated currents during the replacement of extracellular Na^+ with NMDG. D. The current density-voltage curves for the mean outward plateau (open circles) and minimum inward peak (filled circles).

4.3.3.3. K^+ Current Amplitude Development

The amplitude of K^+ currents was recorded over the terminal differentiation phase and compared with K^+ current amplitudes recorded from hWGE and mWGE-derived neurons. Figure 4.11 shows the observed mean, upper and lower quartiles and range of K^+ current amplitudes recorded in these cells. During the terminal differentiation phase the values rise from week 1 to week 2 and then remain relatively stable throughout. A large amount of variation is seen at all stages. The

measured mean amplitudes for both hWGE- and mWGE-derived neurons are lower than those of the hESC-derived neurons past week 1. mWGE-derived neurons show a substantially lower mean value suggesting that these cells have a lower expression of K^+ channels. Ranges of approximately 100 pA/pF for mean values of 47.90, 75.89, 76.64 and 60.84 pA/pF were recorded for PPD weeks 1, 2, 3 and 4+, respectively.

Separate one way ANOVA tests were carried out on the data, firstly from only the hESC-derived neurons, and then from all data sets. In both cases ANOVA indicated significant variation across the data sets (ANOVA: hESC-derived neurons: $P < 0.01$, all data sets: $P < 0.001$). A *post-hoc* Tukey-Kramer multiple comparison test confirmed that there was significant difference between several pairs of the data sets.

The mean amplitude for voltage-gated K^+ currents was significantly smaller in hESC-derived neurons of 1 week PPD than in those of 2 weeks PPD (Tukey-Kramer: week 1 vs. week 2: $P < 0.01$). Similarly there was a significant difference between week 1 and week 3 K^+ amplitudes (Tukey-Kramer: week 1 vs. week 3: $P < 0.01$). No significant difference was observed between the remaining data-sets within the hESC-derived neurons, however, significant differences were observed between week 2 vs. hWGE-derived neurons (Tukey-Kramer: week 2 vs. hWGE: $P < 0.01$), week 3 vs. hWGE-derievd neurons (Tukey-Kramer: week 3 vs. hWGE: $P < 0.01$) and between week 3 vs. mWGE-derived neurons (Tukey-Kramer: week 3 vs. mWGE: $P < 0.01$).

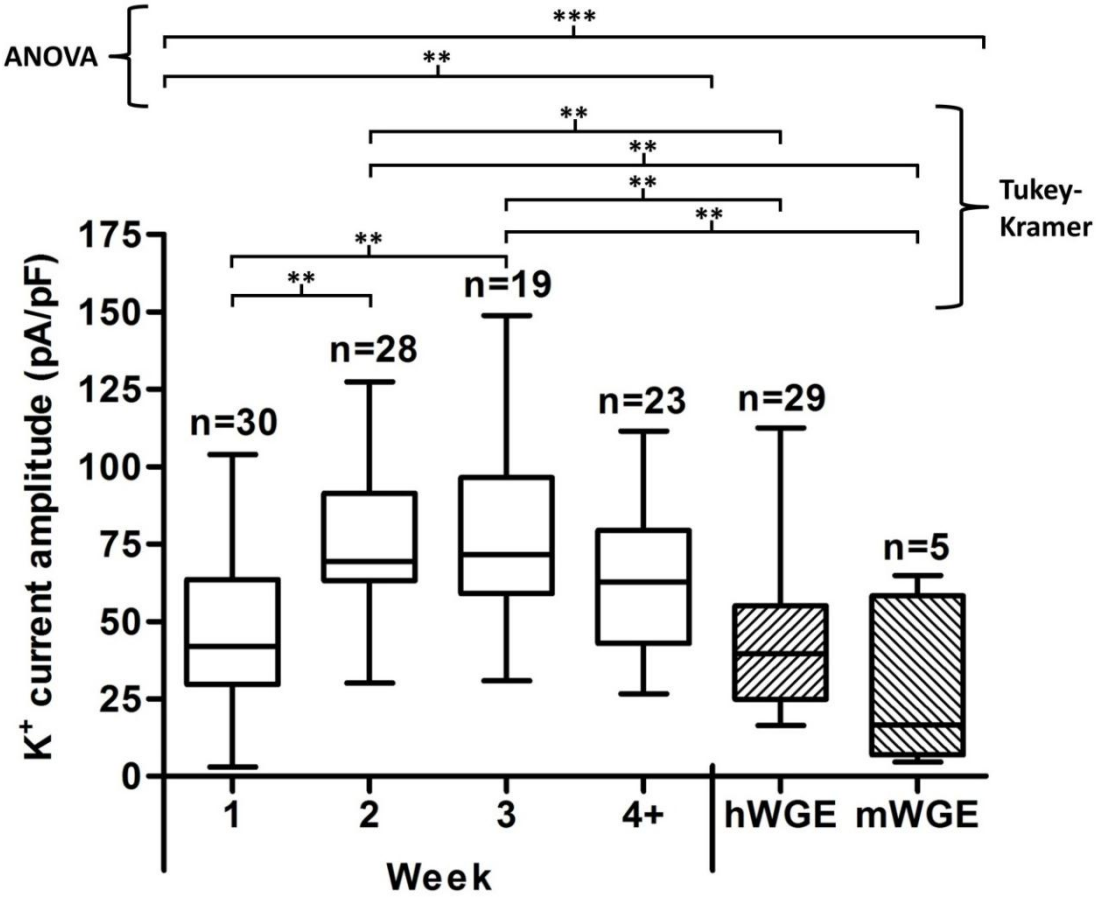

Figure 4.11. K^+ current amplitude in hESC-derived neurons compared to primary neurons: Average K^+ current amplitudes (pA/pF) for each week PPD and for hWGE and mWGE are shown (Boxes represent upper and lower quartiles, vertical bars represent range, numbers indicated above bars). ANOVA and *post-hoc* Tukey-Kramer tests were applied as indicated (horizontal bars, ** = $P < 0.01$, *** = $P < 0.001$). Non-significant Tukey-Kramer results are not-shown.

4.3.3.4. Na^+ Current Amplitude Development

As with the ontogeny of K^+ currents in hESC, the ontogeny of Na^+ current amplitudes was also measured in the same cells during the same period. Figure 4.12 shows the observed mean, upper and lower quartiles and range of Na^+ current amplitudes recorded in hESC-, hWGE- and mWGE-derived neurons. In hESC-derived neurons, Na^+ current amplitude does not significantly change during the terminal differentiation phase. The variation and mean values observed in these cells are

similar in value to those observed in hWGE-derived cells. mWGE-derived neurons show a much greater Na^+ amplitude than both hESC- and hWGE-derive neurons.

As before, separate one way ANOVA tests were carried out on the data, firstly from only the hESC-derived neurons, and then from all data sets. ANOVA indicated significant variation across all of the data sets but not across only the hESC-derived neurons (ANOVA: hESC-derived neurons: n.s., all data sets: $P < 0.001$). A *post-hoc* Tukey-Kramer multiple comparison test confirmed that there was significant difference between several pairs of the data sets. The mean values for each stage/cell type were -30.27, -41.04, -28.57, -20.76, -25.42 and -123.3 pA/pF PPD week 1, 2, 3, 4, hWGE- and mWGE-derived neurons, respectively.

The mean amplitude for voltage-gated Na^+ currents was significantly smaller for each of the hESC-derived neuronal stages and the hWGE-derive neuronal data compared with the mWGE-derived neuronal data (Tukey-Kramer: $P < 0.001$ for mWGE vs. all other data sets).

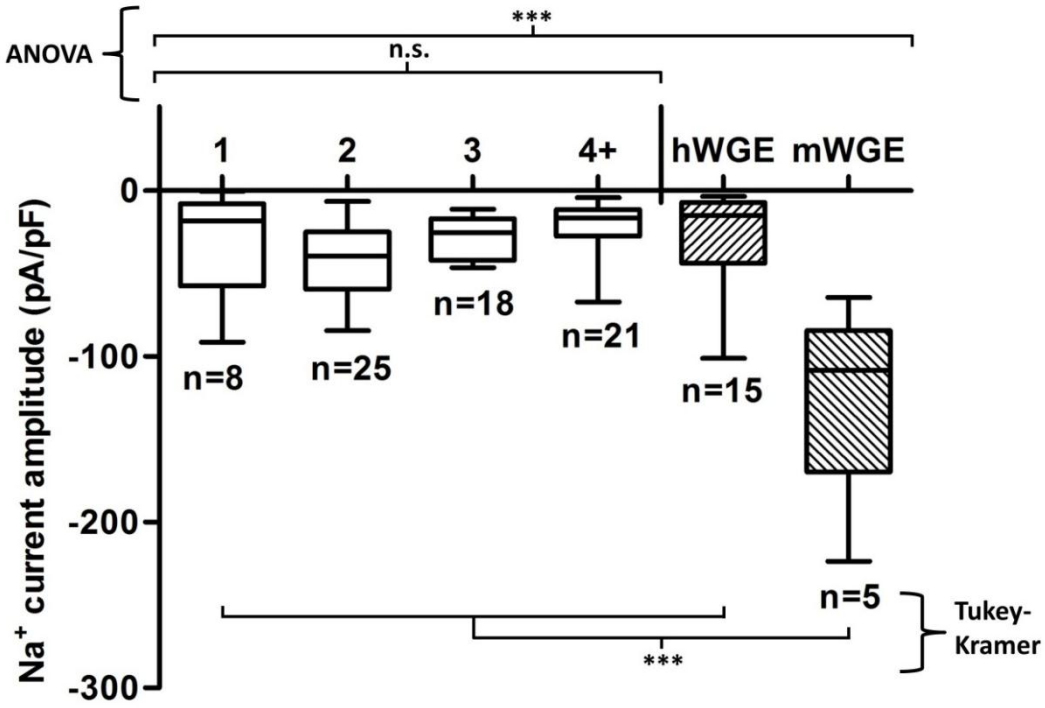

Figure 4.12 Na^+ current amplitudes in hESC-derived neurons compared to primary neurons: Average Na^+ current amplitude (pA/pF) for each week PPD and for hWGE and mWGE are shown (Boxes represent upper and lower quartiles, vertical bars represent the range, numbers indicated below bars). ANOVA and *post-hoc* Tukey-Kramer tests were applied as indicated (** = $P < 0.01$, *** = $P < 0.001$). Non-significant Tukey-Kramer results are not-shown. Significant differences between pairs are indicated by horizontal bars, where these comparisons are equal they have been grouped for visual clarity.

4.3.3.5. Percentage of Cells Displaying Na^+ Channel Activity

Unlike voltage-gated K^+ channel activity, voltage-gated Na^+ channel activity was not observed ubiquitously. As these channels serve to act as markers of excitatory membranes, the percentage of cells displaying their activity was recorded in hESC-neurons during the terminal differentiation phase and in hWGE- and mWGE-derived neurons (Figure 4.13). It is evident that the number of cells displaying voltage-gated Na^+ channel activity in hESC-derived neurons increases dramatically from week 1 to week 2. There was a substantial rise from approximately 27% (8/30) to 90% (25/28). The high percentage of cells displaying voltage-gated Na^+ channel activity was

sustained for the remainder of the terminal differentiation phase. Approximately 52% of hWGE-derived neurons and 100% of mWGE-derived neurons displayed voltage-gated Na^+ channel activity.

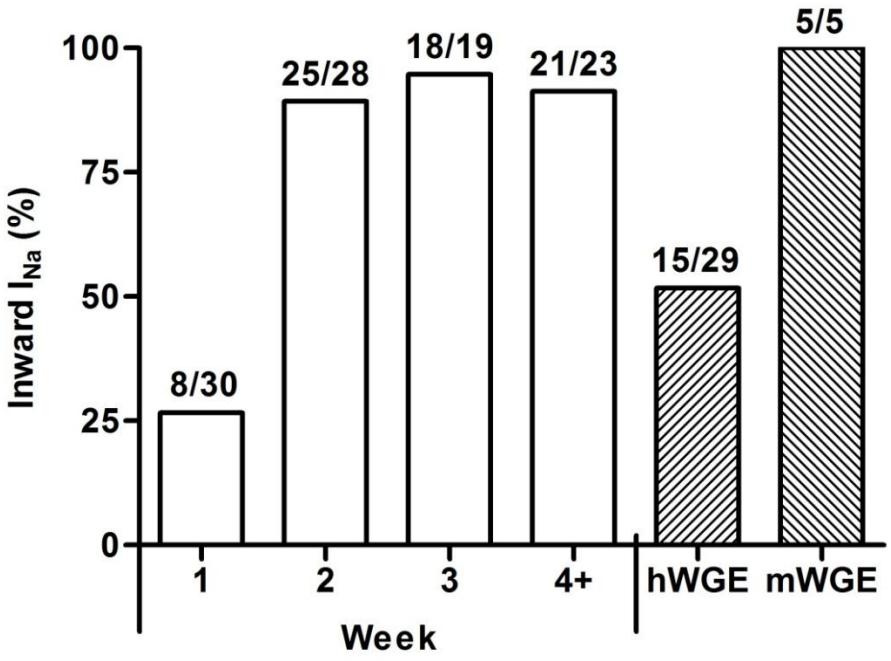

Figure 4.13. Percentage of cells with voltage-gated Na^+ channels in hESC-derived neurons compared with primary neurons: The percentage of cells displaying voltage-gated Na^+ channel activity using the voltage-step protocol are shown for hESC-derived neurons for each week PPD and for hWGE and mWGE (numbers are given above each bar).

4.3.3.6. Percentage of Cells Displaying Ca^{2+} Channel Activity

Measuring Ca^{2+} channel activity in neurons is often carried out using intracellular replacement of K^+ (with Cs^+), to block outward K^+ currents, and extracellular Ca^{2+} replacement (with Ba^{2+}), which amplify Ca^{2+} channel current recordings. This experimental set-up requires separate experiments to be performed for the analysis of Ca^{2+} channel activity. As several parameters were already being recorded for each cell during the terminal differentiation protocol it would have been difficult to

carry out Ca^{2+} current analysis on the same cell preparations using electrophysiology. Therefore, it was decided to employ the less laborious method of Ca^{2+} imaging to measure Ca^{2+} channel activity. This method also provides selectivity for Ca^{2+} current activity and therefore allows the use of standard solutions without antagonists or ionic replacements to reduce the effects of other channel activity. Figure 4.14 shows an example recording from a Ca^{2+} imaging experiment where a PPD week 3 hESC-derived neuron, loaded with 6 µM Fura-2, was exposed to extracellular application of 50 mM K^+. The observed rise in the ratio of fluorescence emission at 540 nm when excited alternately at both 380 nm and 340 nm is indicative of influx of Ca^{2+} through voltage-gated Ca^{2+} channels upon membrane depolarisation induced by the increased extracellular K^+ concentration.

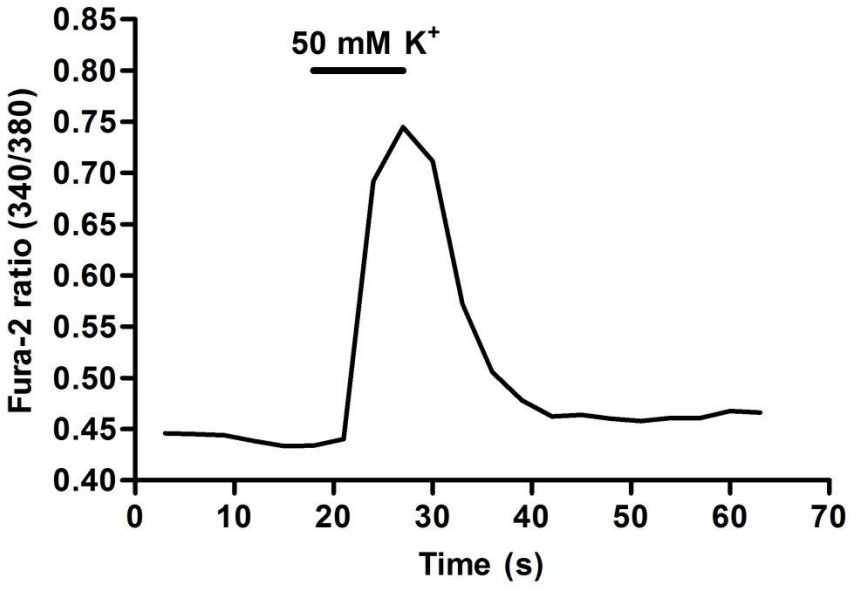

Figure 4.14. Measurement of voltage-gated Ca^{2+} channels in hESC-derived neurons: Fura-2 was used to measure cytosolic free Ca^{2+} changes in a week 3 PPD cell. Extracellular application of 50 mM K^+ (indicated by the black bar) was used to depolarise the membrane and bring the membrane potential above the activation threshold for voltage-gated Ca^{2+} channels.

As with voltage-gated Na^+ channel activity, voltage-gated Ca^{2+} channel activity was not observed in all cells. The percentage of cells displaying Ca^{2+} channel activity was recorded in hESC-neurons during the terminal differentiation phase and in hWGE- and mWGE-derived neurons (Figure 4.15). The percentage of cells displaying voltage-gated Ca^{2+} channel activity in hESC-derived neurons rose considerably from PPD week 1 to week 2. At week 1, approximately 15% (5/33) of these cells display voltage-gated Ca^{2+} channel activity. By week 2, this percentage had risen to around 91% (20/22). This high percentage was maintained throughout the remainder of the terminal differentiation phase. Approximately 60% (26/43) of hWGE-derived and 87% (89/102) of mWGE-derived neurons showed voltage-gated Ca^{2+} channel activity.

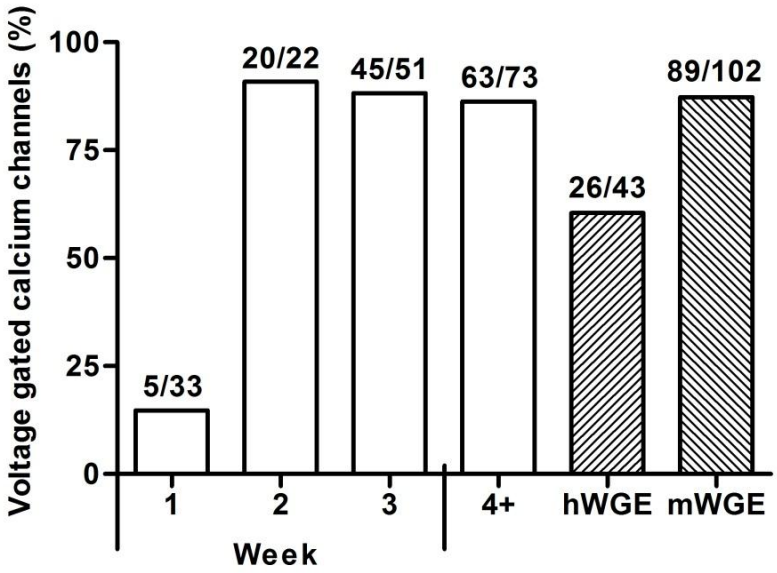

Figure 4.15. Percentage of cells with voltage-gated Ca^{2+} channels in hESC-derived neurons compared with primary neurons: The percentage of cells displaying a rise in the Fura-2 (380/340 nM) ratio upon extracellular application of 50 mM K^+ are shown for hESC-derived neurons for each week PPD and for hWGE and mWGE (numbers are given above each bar).

4.3.3.7. Measurement of Induced-Action Potentials

Voltage-gated K^+ channels and, more specifically, Na^+ and Ca^{2+} channels are associated with excitability within cellular membranes. This excitability takes the form of action potentials. In order to assess the neuronal properties of hESC-, hWGE- and mWGE-derived neurons the ability to fire action potentials was investigated. Figure 4.16 shows an example recording from a PPD week 3 hESC-derived neuron during a current-step protocol designed to induce an action potential-like response. A single sweep is also shown which highlights the characteristic shape of an iAP during current-step stimulation.

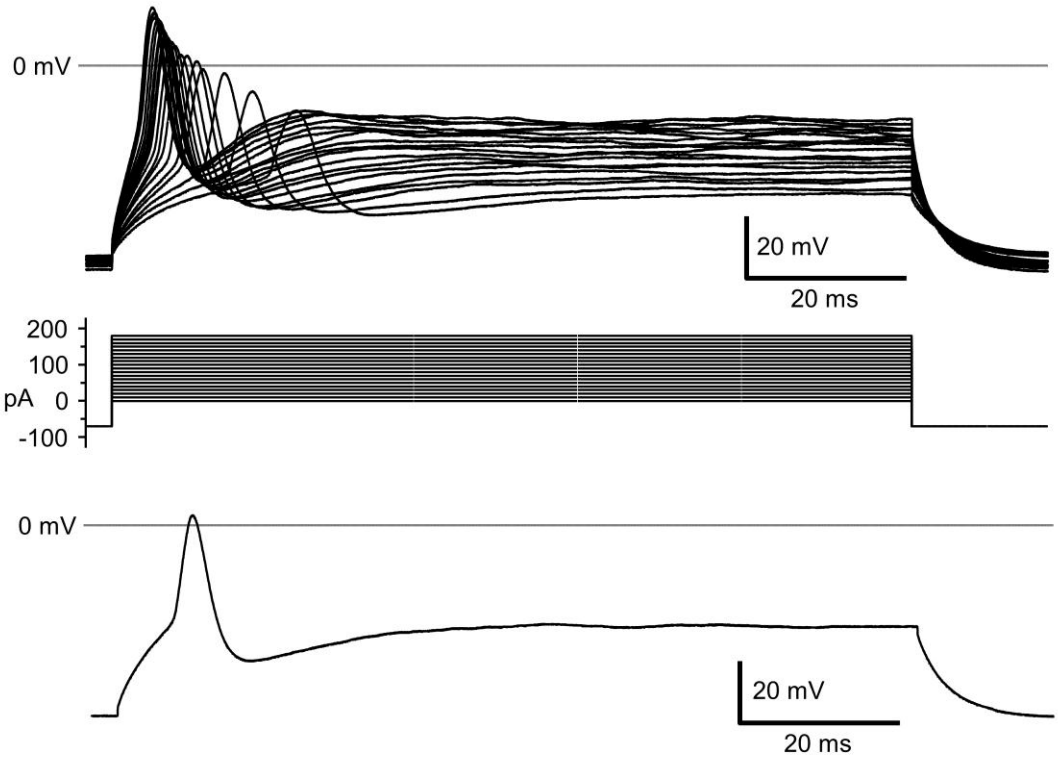

Figure 4.16. Induced action potentials in hESC-derived neurons: An example from a PPD week 3 cell. The top trace shows the current-step protocol used to elicit an action potential in this cell. The bottom trace shows the first sweep which induced an action potential.

Exemplar iAPs for each of the terminal differentiation weeks and for the hWGE- and mWGE-derived neurons are shown in Figure 4.17.

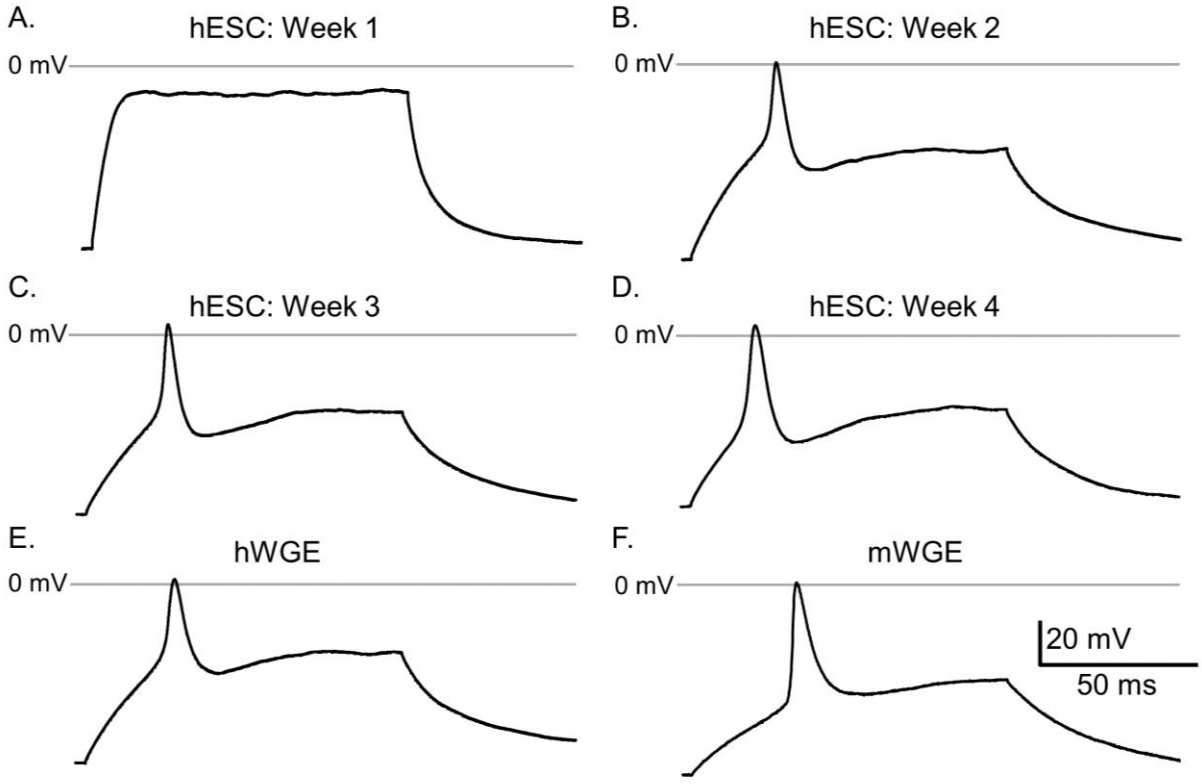

Figure 4.17. Induced action potentials in hESC-, hWGE- and mWGE-derived neurons: An example iAP is shown from one cell from each week of the terminal differentiation protocol and for the hWGE- and mWGE-derived neurons.

4.3.3.8. Percentage of Cells Displaying Induced-Action Potentials

The percentage of hESC-, hWGE- and mWGE-derived neurons which displayed iAPs upon current step stimulation was recorded (Figure 4.18). As with both Na^+ and Ca^{2+} channel ontogenesis, the percentage of hESC-derived neurons which display iAPs was relatively low at 35% (7/20) at 1 week PPD. The percentage then rose sharply by week 2, reaching approximately 89% (25/28). This high percentage was maintained throughout the remainder of the terminal differentiation phase. The percentage of hWGE-derived neurons with iAPs was approximately 41% (12/29), and in mWGE-derived neurons was 100% (5/5).

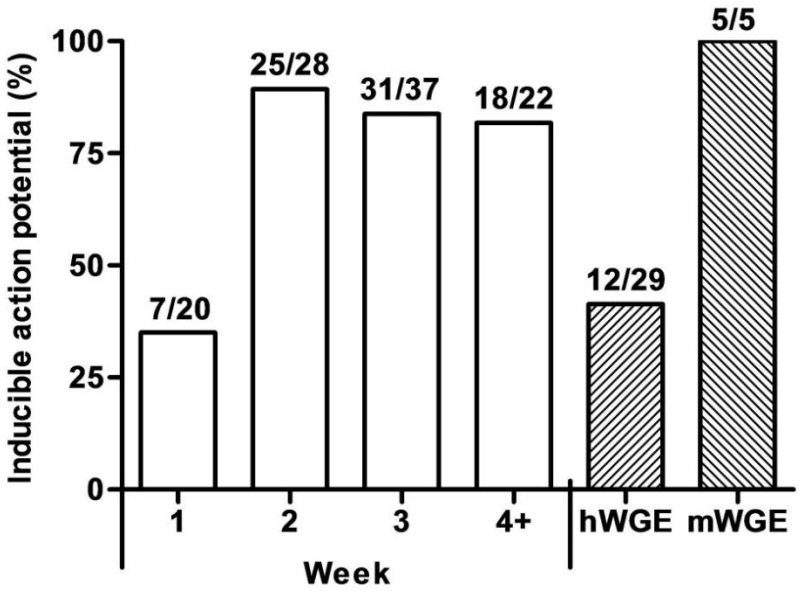

Figure 4.18. Percentage of cells with inducible action potentials in hESC-derived neurons compared to primary neurons: The percentage of cells displaying iAPs using the current-step protocol are shown for hESC-derived neurons for each week PPD and for hWGE and mWGE (number of observations are given above each bar).

4.3.3.9. Action Potential Threshold Development

When an action potential is induced, the membrane potential must exceed the action potential threshold value. This value, along with a measure of the resting membrane potential of the cell, provides an indication of the cell's readiness to fire an action potential and the amplitude of stimulus required. The action potential threshold for iAPs was measured in hESC-, hWGE- and mWGE-derived neurons. Figure 4.19 shows an example iAP recorded in a PPD week 3 hESC-derived neuron. It also shows a plot of the derivative of the original plot. This derivative plots the rate of change in membrane potential with respect to time (dV/dt) against the voltage (mV). This plot highlights regions where large changes in the membrane potential occur (such as during threshold activation). Using this method, it is possible to measure more accurately the threshold values.

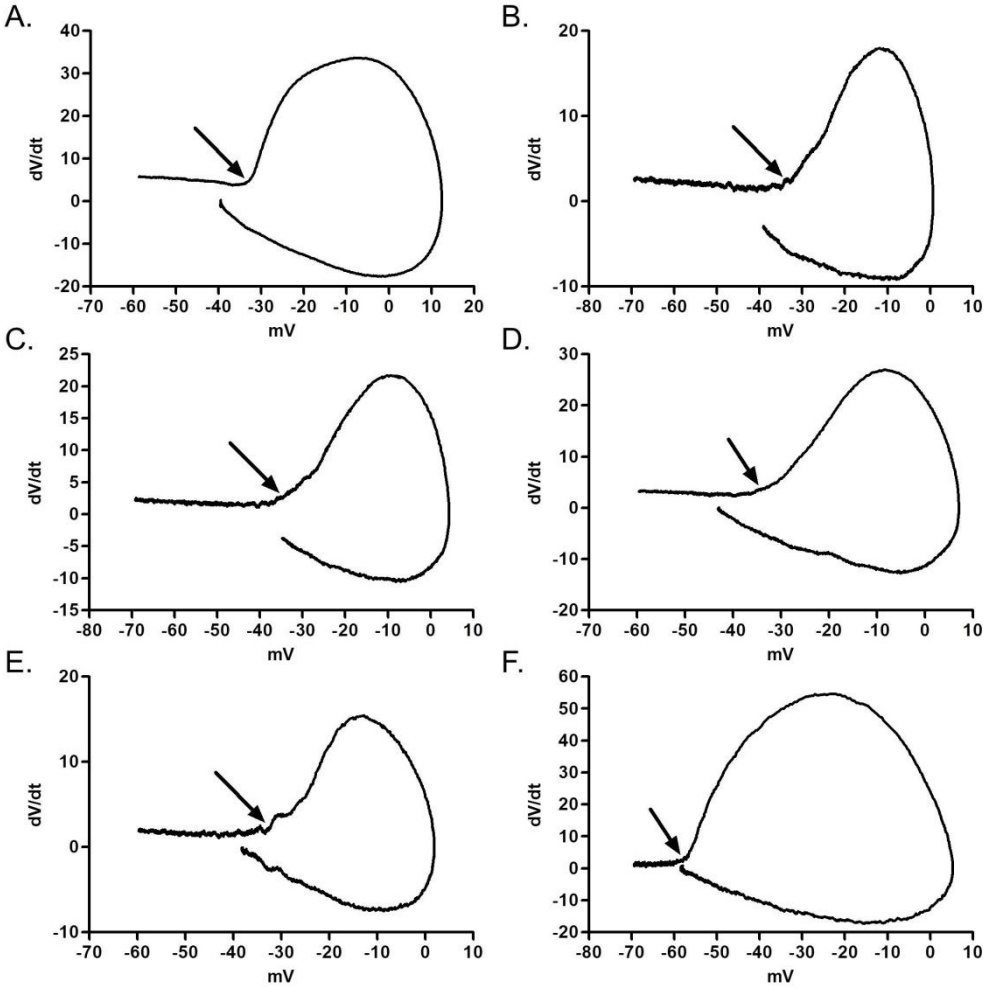

Figure 4.19. Measurement of iAP threshold values: For each cell, the iAP threshold was measured. iAP thresholds were visualised by plotting the derivative (dV/dt) of the original against the membrane voltage (mV). The threshold value was taken as the membrane voltage at which the plot begins to rise sharply (indicated by the arrows). iAP threshold plots are shown for one cell from each week of the terminal differentiation protocol.

Figure 4.20 displays the measured iAP threshold values for hESC-, hWGE- and mWGE-derived neurons. The threshold values are very similar for all PPD weeks during the terminal differentiation phase for the hESC-derived neurons. Most strikingly, the iAP threshold value for mWGE is significantly more negative than that recorded for the other cell types. The mean values recorded were -32.52, -33.58, -31.20 and -34.33 mV for post plate-down weeks 1, 2, 3 and 4+, respectively. The

mean iAP thresholds for fetal hWGE- and post-natal mWGE-derived neurons were -27.32 and -52.50 mV, respectively.

As before, separate one way ANOVA tests were carried out on the data, firstly from only the hESC-derived neurons, and then from all data sets. ANOVA indicated significant variation across all of the data sets but not across only the hESC-derived neurons (ANOVA: hESC-derived neurons: n.s., all data sets: $P < 0.001$). A *post-hoc* Tukey-Kramer multiple comparison test confirmed that there was significant difference between several pairs of the data sets.

The mean iAP threshold was significantly less negative for each of the hESC-derived neuronal stages and the hWGE-derive neuronal data compared with the mWGE-derived neuronal data (Tukey-Kramer: $P < 0.001$ for mWGE vs. all other data sets).

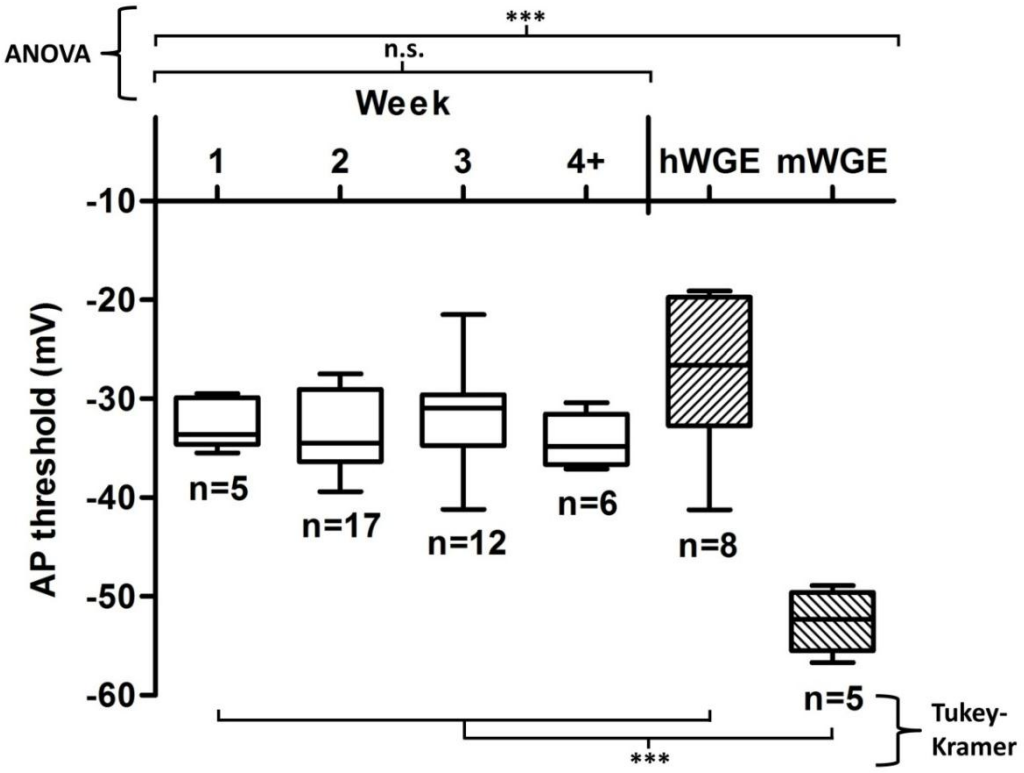

Figure 4.20. iAP threshold values in hESC-derived neurons compared with primary neurons: The average iAP threshold values for each week PPD and for hWGE and mWGE are shown (Boxes represent upper and lower quartiles, vertical bars represent the range, number of observations indicated below bars). ANOVA and *post-hoc* Tukey-Kramer tests were applied as indicated (** = $P < 0.01$, *** = $P < 0.001$). Non-significant Tukey-Kramer results are not-shown. Significant differences between pairs are indicated by horizontal bars, where these comparisons are equal they have been grouped for visual clarity.

4.3.3.10. Resting Membrane Potential Development

V_m was recorded for hESC-, hWGE- and mWGE-derived neurons. Figure 4.21 shows the V_m values for each cell type and for the stages of terminal differentiation for hESC-derived neurons. As was observed for the threshold values, the mean V_m for all weeks PPD in hESC-derived neurons are similar at approximately -30 mV. hWGE-derived neurons displayed a mean V_m which was a similar value to the hESC-derived cells. The mean V_m of mWGE-derived neurons was significantly more negative than all other cell types.

Separate one way ANOVA tests were carried out on the data, firstly from only the hESC-derived neurons, and then from all data sets. ANOVA indicated significant variation across all of the data sets but not across only the hESC-derived neurons (ANOVA: hESC-derived neurons: n.s., all data sets: $P < 0.001$). A *post-hoc* Tukey-Kramer multiple comparison test confirmed that there was significant difference between several pairs of the data sets. The mean V_m was significantly less negative for each of the hESC-derived neuronal stages and the hWGE-derive neuronal data compared with the mWGE-derived neuronal data (Tukey-Kramer: $P < 0.001$ for mWGE vs. all other data sets).

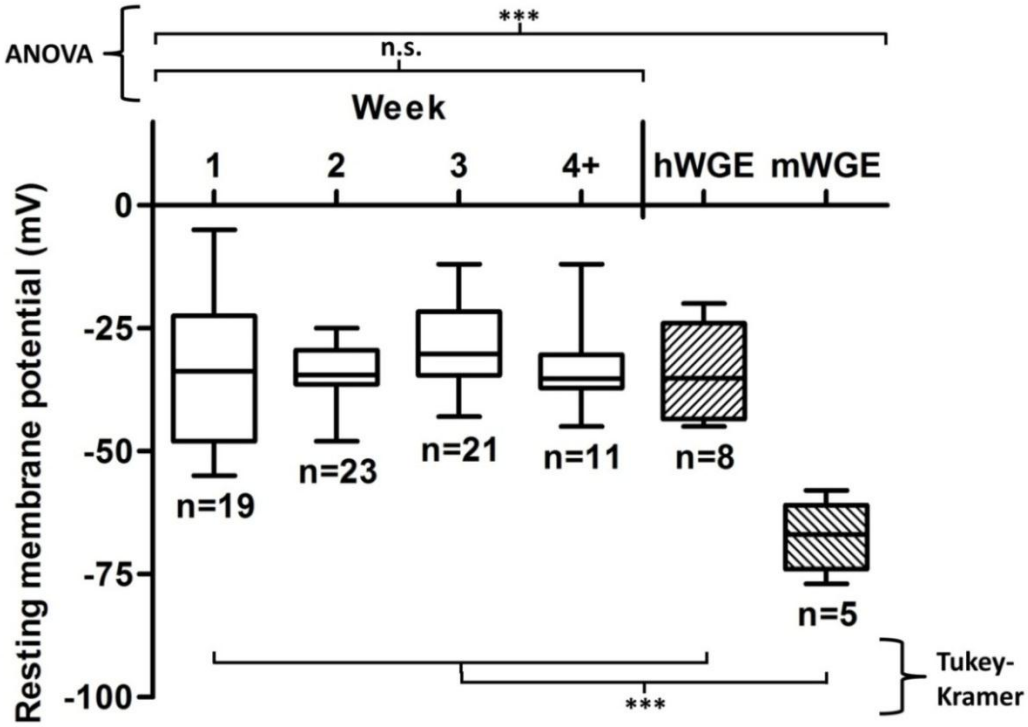

Figure 4.21. Resting membrane potential in hESC-derived neurons compared with primary neurons: The average V_m for each week PPD and for hWGE and mWGE are shown (boxes represent upper and lower quartiles, vertical bars represent the range, number of observations indicated below bars). ANOVA and *post-hoc* Tukey-Kramer tests were applied as indicated (*** = P < 0.001). Non-significant Tukey-Kramer results are not-shown. Significant differences between pairs are indicated by horizontal bars, where these comparisons are equal they have been grouped for visual clarity.

4.3.3.11. Measurement of Spontaneous Activity

Spontaneous action potentials (sAPs) were not recorded in any of the hESC-derived neurons at any stage of the terminal differentiation (74 cells examined). In both hWGE and mWGE, multiple cells displayed spontaneous electrical activity in the form of sAPs. Figure 4.22 shows an exemplar trace from an hWGE-derived neuron. Spontaneous activity was only observed in 2 of the 8 hWGE-derived neurons examined.

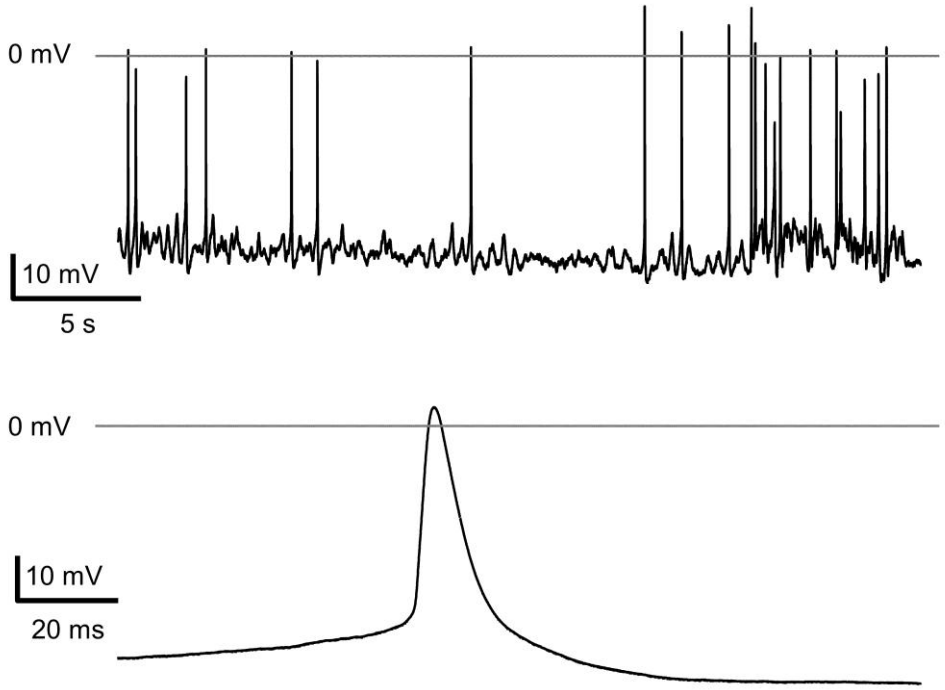

Figure 4.22. Spontaneous action potentials in hWGE neurons: Spontaneous action potentials recorded in zero current (I=0) using the Gap free protocol in neurons from hWGE. No stimulus was applied to elicit action potentials. Top trace: Section of trace showing multiple spontaneous events. Bottom trace: a single spontaneous action potential showing the characteristic shape of these events.

Figure 4.23 shows a recorded trace from an mWGE-derived neuron. Spontaneous activity was observed in all of the 5 mWGE-derived neurons examined.

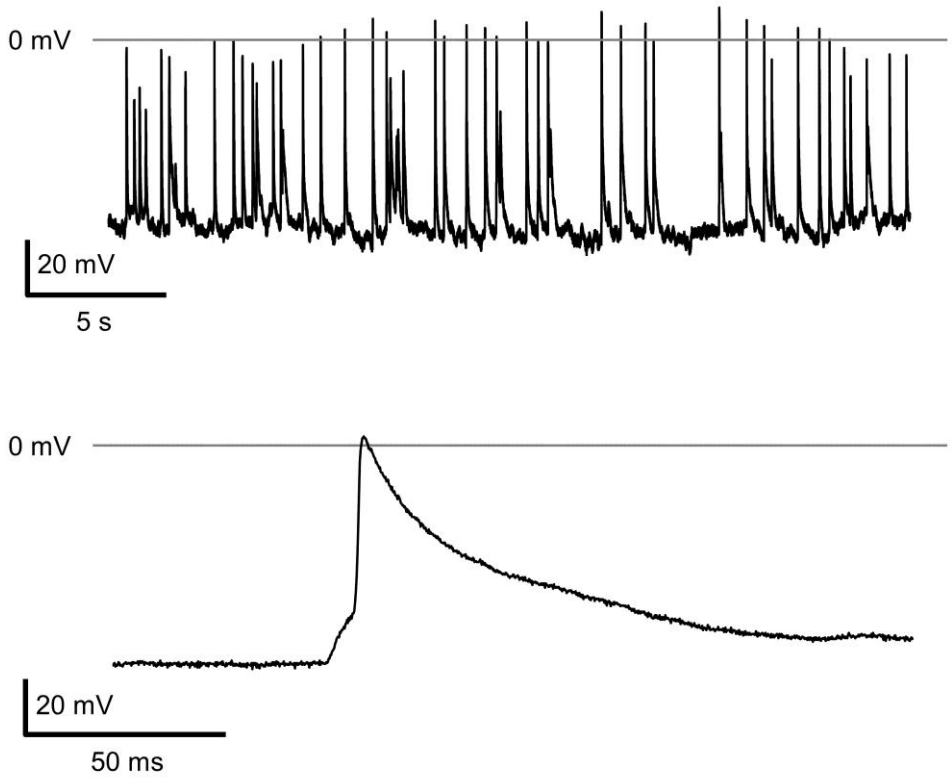

Figure 4.23. Spontaneous action potentials in mWGE neurons: Spontaneous action potentials recorded in zero current (I=0) using the Gap free protocol in neurons from mWGE. No stimulus was applied to elicit action potentials. Top trace: Section of trace showing multiple spontaneous events. Bottom trace: a single spontaneous action potential showing the characteristic shape of these events.

4.4. Conclusions

To say that stem cells have differentiated into neurons requires that the cells display, at the very least, basic neuronal functions *in vitro*. That these cells express neuronal markers and display neuronal morphology is not enough to consider them as mature or functionally active neurons. It is well documented that neuronal excitability and the cross-communication between neuronal cells and populations is necessary to both development and maintenance of neuronal function *in vivo* (Spitzer, 2006).

With the aim of investigating the development of functional characteristics in hESC-derived neuronal populations, several aspects were considered. It was necessary to treat the cells in a consistent way to allow both complimentary and comparative analysis across labs and with other work being carried out in the same lab.

In order to provide neurons which are amenable to whole-cell patch-clamp techniques it is necessary to produce single-cell cultures. Furthermore, by separating the cells and dissociating the neurosphere there is an increase in the accessibility for each cell to the medium and a reduction in cell-to-cell contact-mediated growth inhibition (Svendsen *et al.*, 1998). Mechanical dissociation of neurospheres has been shown to damage cells and provide a low level of cell survival for plating. It has been suggested that chemical dissociation using alkaline conditions can improve this viability (Sen *et al.*, 2004). Similarly, enzymatic dissociation with trypsin appears to be too harsh on cells in neurospheres and results in high levels of cell death. As such, less vigorous enzymes such as Accutase are often used in neurosphere dissociation to obtain satisfactory cell viability (Wachs *et al.*, 2003; Joannides *et al.*, 2007b).

During dissociation, Rho-kinase upregulation mediated via the Rho-associated protein kinase p160ROCK (ROCK) promotes anoikis, a form of apoptosis triggered by loss of contact with neighbouring cells and the extracellular matrix (Koyanagi *et al.*, 2008). The addition of Y-27632, a selective inhibitor of ROCK, to dissociated neurosphere preparations and other models of mechanical neuronal injury, reduces apoptosis and promotes cell survival (Dergham *et al.*, 2002; Xu *et al.*, 2008; Rodrigues *et al.*, 2011).

The addition of the ROCK inhibitor Y-27632 provided an increase in the viability of plated cells (Figure 4.1) and has now become standard procedure within the lab. Previously the use of Accutase was already established as the standard method of dissociation and this procedure was also shown here to achieve increased plate-down viability.

With any tissue culture procedure, especially stem-cell based tissue culture work, it is important to consider the implications of user-dependent. As such, it was important that the cells produced for the experiments in this thesis were of as consistent quality as those used elsewhere. For this purpose, the IHC staining of terminally differentiated cells with anti-β-III tubulin (Figure 4.2) along with images showing morphological characteristics (Figure 4.3) were used as an indication that these cells were similar in appearance and lineage to the standard hESC-derived neuronal cultures. Furthermore, this provides further evidence that the differentiation procedure was producing viable neuronal tissue.

The functional development of hESC-derived neurons was investigated with respect to key physiological properties. The measurements obtained from fetal hWGE and post-natal mWGE provides comparative data from two key stages of development. Access to regular primary fetal hWGE tissue is relatively rare but provides precious human cells from an early developmental stage. It is less likely, certainly within our lab, to be able to obtain post-natal neuronal tissue from human subjects. As a substitute for this, postnatal mouse (postnatal day 1) pups were used to obtain neurons from mWGE. These cells provided comparative data from a more mature stage of neuronal development.

The functional activities of voltage-gated K^+, Na^+ and Ca^{2+} channels were measured in hESC-derived neurons at PPD weeks 1, 2, 3 and 4+. The same characterisation process was also performed on fetal-derived hWGE (obtained from fetuses aborted between gestational weeks 6 and 12 within 2 DIV) and post-natal mWGE (post-natal day 1 within 2 DIV). These tissues were obtained in accordance with local and national guidelines. In all cell types, the capacitance, voltage-gated channel activity, V_m, ability to fire iAPs and sAPs and the iAP threshold were measured.

Figure 4.5 to Figure 4.8 show typical recordings of voltage-gated K^+ and Na^+ channel activity in hESC-derived neurons and those recorded from hWGE- and mWGE-derived neurons. The characteristic trace and I-V shape is similar to those seen in recordings from primary neurons, and cells heterologously expressing delayed rectifier voltage-gated K^+ channels and voltage-gated Na^+ channels (Zhou *et al.*, 1998; Castle *et al.*, 2001; Schaarschmidt *et al.*, 2009).

The recorded outward voltage-activated currents were confirmed as K^+ currents through blockade with 20 mM TEA-Cl. A high variation of K^+ current amplitude was observed at all weeks PPD (Figure 4.11). That primary tissue-derived neurons had significantly lower K^+ channel amplitudes than week 2 and 3 hESC-derived neurons suggests that hESC-derived neurons may be at a different stage developmentally from these primary cells. However, there was no observed significant difference between the K^+ current amplitudes at week 4 and those recorded from hWGE- and mWGE-derived neurons, suggesting that, by the later stages of terminal differentiation, hESC-derived neurons are similar to their primary counterparts with respect to their K^+ channel dennsity. It has been observed in embryonic mouse brain that developing neurons, migrating from the ventricular zone (VZ), through

the intermediate zone (IZ), towards the cortical plate (CP), show a reduction in voltage-gated K^+ current amplitude during development (Picken Bahrey & Moody, 2003b). This would suggest that the hESC-derived neurons may be at an earlier developmental stage than the hWGE- and mWGE-derived neurons during the middle stages (weeks 2 and 3) of terminal differentiation.

Voltage-gated Na^+ currents, typical of all stages of terminal differentiation in hESC-derived neurons and in hWGE- and mWGE-derived neurons, were recorded and confirmed as Na^+ current if they were absent upon replacement of extracellular NaCl with NMDG-Cl. hESC-derived neurons displayed voltage-gated Na^+ currents that were similar in amplitude to fetal hWGE-derived neurons and smaller than post-natal mWGE-derived neurons (Figure 4.12). This suggests that hESC-derived neurons are at a developmental stage which is closer to fetal than post-natal neurons with respect to their Na^+ channel activity. It has been shown previously that neurons exiting the cell cycle in the VZ, and subsequently migrating to the IZ show an increase in voltage-gated Na^+ current amplitude (Picken Bahrey & Moody, 2003a) suggesting that hESC- and fetal hWGE-derived neurons are developmentally less mature than neonatal mWGE-derived neurons regarding their Na^+ channel activity.

All cell types and stages exhibited voltage-gated K^+ channel activity. Only a proportion of the cells displayed voltage-gated Na^+ channel activity. As voltage-gated Na^+ channels are a requirement for the induction of an action potential, the percentage of cells showing voltage-gated Na^+ channel provides an indication of the proportion of cells within a population that are excitable. In hESC-derived neurons, the percentage of cells expressing functional voltage-gated Na^+ channels rose

sharply from PPD week 1 to week 2 (approx. 27% in week 1 to 89% in week 2, as shown in Figure 4.13). This high percentage was maintained for weeks 3 and 4+ at approx. 95 % and 91%, respectively. In fetal hWGE-derived neurons, approx. 52 % cells displayed voltage-gated Na^+ channel activity compared to 100% in post-natal mWGE-derived cells. That the percentage of hESC-derived neurons displaying voltage-gated Na^+ channel activity reaches a similar level to post-natal mWGE-derived neurons and is greater during the later weeks of terminal differentiation than fetal hWGE-derived neurons suggest that, with respect to the number of cells that have the potential to fire action potentials, these cells are differentiating into a more homogenous population with a more mature population phenotype than the fetal hWGE-derived neurons.

Voltage-gated Ca^{2+} channels were shown to be active in all of the cell populations studied. Figure 4.14 shows an example Ca^{2+} imaging trace from a cell exhibiting voltage-gated Ca^{2+} channel activity during membrane elicited by depolarisation induced by extracellular application of 50 mM KCl. The percentage of cells displaying such voltage-gated Ca^{2+} channel activity was comparable to that of voltage-gated Na^+ channels. Initially, in the first week of terminal differentiation, a relatively low proportion of the hESC-derived neurons displayed voltage-gated Ca^{2+} channel activity (14.7 %). By week 2, this percentage had risen to 90.9% and this was maintained throughout the remaining weeks (88.2% and 86.3% for week 3 and 4+, respectively). The percentage of cells showing voltage-gated Ca^{2+} channel activity was 60.5% in of fetal hWGE and 87.2% in post-natal mWGE. As with the Na^+ channel results, this suggests that these hESC-derived neurons are differentiating towards a more mature and homogeneous population phenotype. The presence of

voltage-gated Ca^{2+} channels is important for both the formation and function of synapses between neighbouring neurons (Iwasaki *et al.*, 2000) and for regulation of neuronal development (Bootman *et al.*, 2001; Greer & Greenberg, 2008).

The ability of a neuron to fire an action potential relies on the expression of voltage-gated Na^+ channels. In all cells recorded, only those with demonstrable voltage-gated Na^+ currents measured in voltage clamp were able to display iAPs in current clamp. However, functional expression of voltage-gated Na^+ channels did not guarantee iAP capability. In hESC-derived neurons at 1 week PPD only 35% of cells were capable of iAPs.

As with the percentage of cells displaying voltage-gated Na^+ and Ca^{2+} channel activity, the pattern of iAP ability during terminal differentiation of hESC-derived neurons suggests a change during differentiation from a more fetal population phenotype to a more post-natal phenotype.

The current-step protocol for measuring iAPs (as outlined in section 2.2.2.5.) uses current injection to bring the membrane potential of the cell to approximately -80 mV before inducing APs with a current step. This hyperpolarisation removes voltage-inactivation of the Na^+ channels and allows an action potential to be induced upon current stepping. Without this, the membrane potential may be depolarised enough that Na^+ channels are inactivated making iAPs unlikely.

For an AP to occur across a membrane V_m must be negative enough to remove steady-state inhibition of voltage-gated Na^+ currents. In order to assess the spontaneous excitability of the neuronal populations further, the iAP threshold, V_m and sAP generation within these populations were recorded.

Successful iAP generation was determined as an alteration of current-step induced increase of membrane potential above the standard curve seen in a non-excitatory cell which takes the membrane potential sharply and transiently above 0 mv, followed by a rapid repolarisation to a baseline potential determined by the current step size. It is possible to predict the iAP threshold from the recorded trace of membrane potential (mV) plotted against time. However, it becomes easier to predict the correct threshold value if the derivative (change in membrane potential divided by change in time from the previous value, dV/dt) is plotted against the membrane potential (mV) for each data point as shown in Figure 4.20 (Sekerli *et al.*, 2004).

The patterns observed for both mean iAP threshold and mean V_m values in these cells suggest that the hESC-derived cells are not developing, with respect to their iAP threshold and V_m values, past a stage more similar to fetal hWGE- than post-natal mWGE-derived neurons. The V_m values observed in both hESC- and hWGE-derived neurons was considerably more positive than that of mature neurons suggesting that these cells remain in a more immature stage than the post-natal mWGE-derived neurons. That the iAP values are relatively less negative in the hESC- and hWGE-derived neurons than the mWGE-derived neurons suggests that these cells are fundamentally different in their electrical excitability. A reduction in action potential threshold during development has been proposed for some neuronal populations (Gao & Ziskind-Conhaim, 1998; Picken Bahrey & Moody, 2003b).

As mentioned, the iAP protocol produced an artificial hyperpolarised 'resting' membrane potential through current injection. This was used to uncover the potential for AP induction. For a measure of the actual electrical activity within a

cellular population it is important to measure the spontaneous activity at the physiological V_m. For this purpose, recordings of cells in the zero current injection (I=0) mode of the current clamp was carried out for 90 s in order to establish the presence or absence of spontaneous electrical events. In all hESC-derived neurons at all stages of terminal differentiation there was no observable spontaneous activity (0/74). Spontaneous activity was observed in both hWGE- (2/8) and mWGE-derived neurons (5/5). It is, perhaps, understandable that no spontaneous activity was observed in the hESC-derived neurons as the mean V_m value was so depolarised that it is possible there was complete steady-state inactivation of the voltage-gated Na^+ channels in these cells, thus preventing AP induction. However, there was no significant difference between the V_m and iAP values of hESC- and hWGE-derived neurons and yet spontaneous activity was measured in some hWGE-derived neurons. This suggests that the relatively depolarised mean V_m and iAP threshold values are not entirely responsible for the apparent lack of spontaneous activity. This lack could be indicative of an inability of the hESC-derived neurons to form functional synapses, or that they are still developmentally more immature than the fetal hWGE-derived neurons. It could also reflect differences in the Na^+ channel subtypes expressed in these cells, resulting in different functional characteristics.

Several physiologically relevant functional characteristics have been observed in hESC-derived neurons undergoing terminal differentiation *in vitro*. These have been compared to results obtained for fetal hWGE- and post-natal mWGE-derived neurons providing a relatively immature and mature population of striatal cells, respectively. The amplitude of currents carried by voltage-gated K^+ and Na^+ channels, the percentage of cells showing voltage-gated Na^+ and Ca^{2+}, the

percentage of cells displaying iAPs, the iAP threshold, V_m and spontaneous activity within these cells was recorded. For visual purposes Figure 4.24 displays the key patterns of the findings.

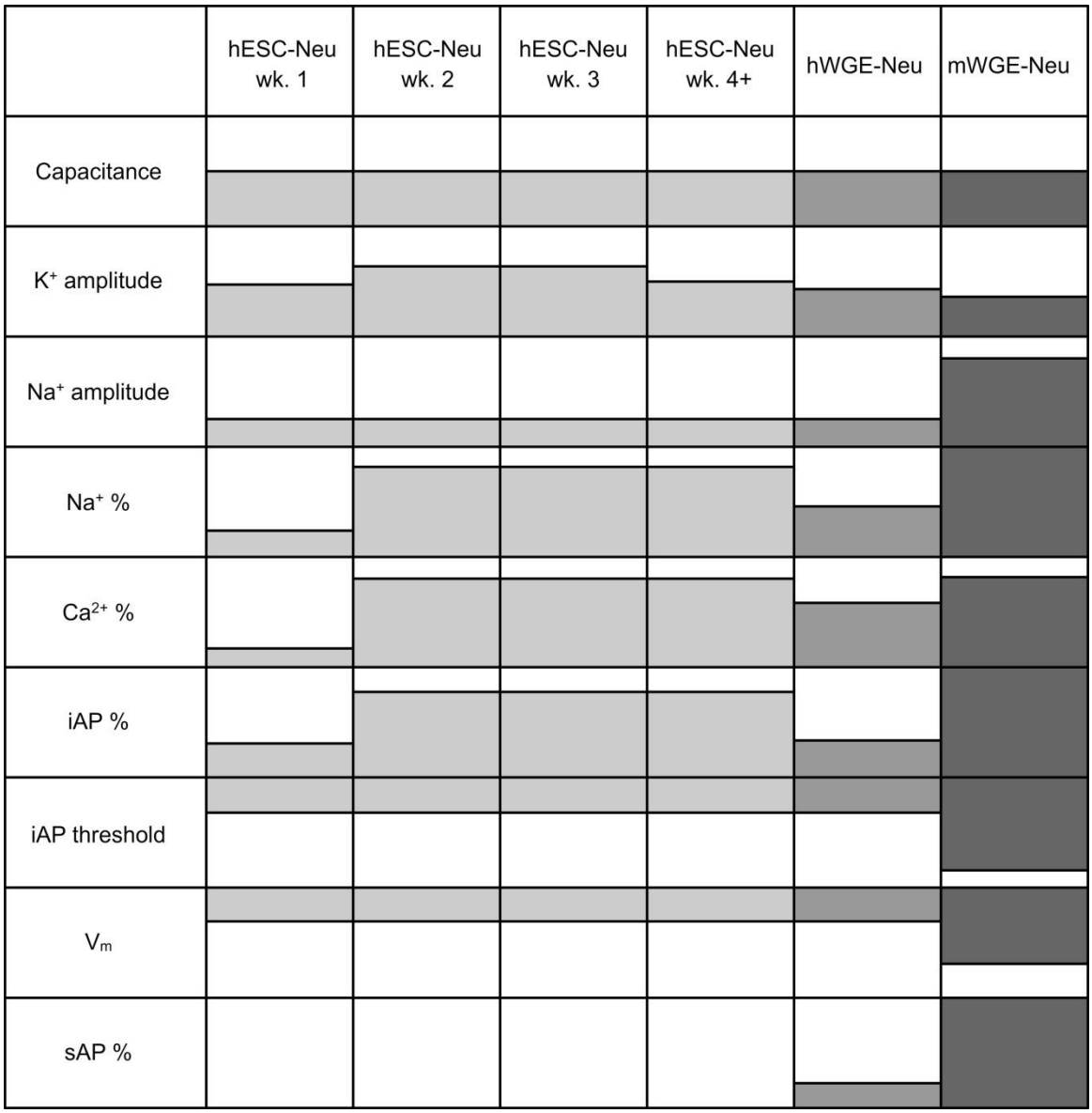

Figure 4.24. Visual representation of functional characterisation of hESC-, hWGE- and mWGE-derived neurons: For each of the key findings, the general pattern of values across the cell types/stages is illustrated. Actual values are not used, this image is intended as an aid for comparisons between cells.

In summary, it is apparent that the terminal differentiation of hESC-derived neurons is accompanied by an alteration in the functional electrical characteristics of the cells. Voltage-gated Na^+ channel activity was apparent in a higher percentage of cells as they differentiate. Similarly, a higher proportion of cells displayed voltage-gated Ca^{2+} channel activity from week 1 to week 2 PPD. This increase in the voltage-gated channel activity is mirrored by an increase in the percentage of cells able to fire an AP upon current injection (iAPs). Conversely, it is apparent that the iAP threshold, V_m and absence of spontaneous activity is not altered throughout. The relatively depolarised V_m and iAP threshold values suggest a more immature phenotype, and the lack of sAPs suggest that electrical signalling is not occurring in these populations. That such a key component of neuronal development is missing in these cells is indicative of an incomplete developmental environment. Unfortunately it is not obvious if the apparent lack of spontaneous activity is the result, the cause, or independent of the relatively depolarised resting membrane potential values, but it is likely the two are linked.

That the cells are increasing their potential for excitability, assayed as an increase in the percentage of cells displaying iAPs, mimics neuronal development *in vivo* and is promising for further development of the differentiation protocol (Gao & Ziskind-Conhaim, 1998; Picken Bahrey & Moody, 2003b). The hESC-derived neurons showed a greater similarity to fetal hWGE-derived neurons than to neonatal mWGE derived neurons with respect to the majority of measured functional characteristics. Significant differences between both hESC- and hWGE-derived neurons and mWGE-derived neurons were observed in their mean Na^+ current amplitude, iAP threshold and V_m values. This suggests that these cells are at a developmental stage more

similar to fetal neurons than neonatal neurons. However, there is an apparent similarity between the proportion of cells displaying Na^+ and Ca^{2+} channel activity and iAPs observed between hESC-derived neurons and mWGE-derived neurons which are not reflected in the hWGE-derived neuronal populations. It is interesting to note that the similarities between hESC- and hWGE-derived neurons are those factors which are based on measurements of channel properties (amplitudes and activation thresholds), whereas the similarities between hESC- and mWGE-derived neurons are in those characteristics which are population based (percentage of cells with a certain response). This may be indicative of variability in the populations of different cell types (neuronal and non-neuronal cells) between hESC-derived neurons and fetal hWGE-derived neurons. It is highly likely that the neurosphere and differentiation protocols produce a population of cells which is more homogeneously neuronal than is present in early fetal WGE. This relative homogeneity may be present in the more mature WGE of the postnatal mouse. Although these hESC-derived neuronal populations may be, like the mWGE-derived neurons, more homogeneous than the fetal hWGE-derived neurons they are apparently more immature in their neuronal development than these neonatal cells.

That the neuronal population present in fetal hWGE-derived neurons is capable of spontaneous activity suggests it is able to be influenced by electrical activity-induced differentiation. Similarly, the neonatal mWGE-derived neurons also display spontaneous activity. This mimics data observed in other studies (Spitzer, 2006) and highlights the importance of *in vitro* primary neuronal models of development as the gold-standard to which hESC-derived neuronal differentiation must be

compared. The apparent lack of spontaneous activity in the hESC-derived neurons suggests that activity-dependant effects on neuronal development are not currently involved in the differentiation of these cells. Furthermore, it suggests that the differentiation protocol used in this study requires further adaptation to stimulate differentiation which is more similar to that occurring *in vivo*.

Suggested adaptations may be focused on the stimulation of neurotransmitter receptors, transient $[Ca^{2+}]_i$ induction, electrical stimulation via electrodes during culture or modifications of the extracellular ionic concentrations to alter membrane properties. Studies into the effects of co-culture of neurons with embryonic mouse glial populations have indicated an increase in spontaneous activity in hESC-derived neuronal populations (Johnson *et al.*, 2007). Similar results have now been replicated within our lab suggesting a link between glial conditioned media and the development of spontaneous activity. Further work is required to discover the causal factor in this increase in activity. Periods of increased extracellular K^+ concentrations during adult rat hippocampal neuronal precursor cell culture increase neurogenesis and improve *in vitro* neuronal fate determination (Deisseroth *et al.*, 2004). Similarly, mild electrical stimulation of mESCs improved neuronal differentiation suggesting that this is not entirely a synapse-dependent effect (Yamada *et al.*, 2007).

The utilisation of a differentiation protocol for hESCs which reduces non-human products and uses chemically defined ingredients provides the potential for the production of therapeutic grade material for transplantation. It also provides hESC-derived populations which have been differentiated in more consistent environments. The control of media content offered by using serum replacements

and feeder-free cultures provides an alternative to the more widely used methods of using non-human feeder cells for stem cell cultures, and animal products such as FBS in their subsequent differentiation protocols.

The production of chemically-defined protocols for producing hESC-derived neurons which are similar in nature to clinically relevant neuronal populations will provide a therapeutic tool for the potential treatment of neurodegenerative conditions. The work in this chapter highlights the need for a greater understanding of the functional characteristics of these developing neurons, both *in vivo* and *in vitro* and a need for greater control of electrical signalling during terminal differentiation.

Chapter 5. GABAergic Signalling in hESC-Derived and Primary Neurons

5.1. Introduction

The use of human primary tissue in studies of development and disease modelling provides two distinct advantages over animal tissue and hESC-derived tissue. Firstly, the tissue is derived from human cells making it more clinically relevant than that obtained from animal sources. Secondly, primary human tissue has undergone a degree of differentiation within the developing fetus and, as such, is more developmentally appropriate than current stem-cell models. The disadvantages of human primary tissue are largely due to the lack of availability and the ethical issues associated with its use. However, tissue obtained from abortions is, although under strict government guidelines and patient cooperation, available in certain circumstances for use in basic research.

5.1.1. GABA

GABA is one of the major neurotransmitters in the brain. Acting through stimulation of its receptors, $GABA_A$Rs and $GABA_B$Rs, it is vital for proper brain development and function {}. It is worth noting that $GABA_C$ receptors are mentioned in many papers. However, since 2008, they have been reclassified as a subtype of $GABA_A$Rs and are now referred to as ρ1-3 (Olsen & Sieghart, 2008).

5.1.2. $GABA_A$ Receptors ($GABA_A$Rs)

These ligand-gated, ionotropic receptors open a Cl^- selective anion pore upon activation through GABA binding. As pentameric transmembrane receptors, they consist of 5 transmembrane subunits. There are multiple subtypes of these subunits which can combine to form multiple heteromers. At present the accepted subtypes

are as follows; α 1-6, β 1-3, γ 1-3, ρ 1-3 , δ, ε, π, θ(Olsen & Sieghart, 2008). The degree to which these subtypes can combine is not yet fully known. If randomised heteromeric subunit composition was observed, there would be many thousands of possible permutations. However, it has been shown that this is highly unlikely and that there may be as few as 26 possible combinations endogenously expressed. Each of the combinations of subunits present specific pharmacological profiles and responses to agonists and antagonists. In the human brain, the $(\alpha1)_2(\beta2)_2(\gamma2)$ subtype is the most common (Olsen & Sieghart, 2008).

5.1.3. $GABA_B$ Receptors ($GABA_BRs$)

Unlike $GABA_ARs$, $GABA_BRs$ are metabotropic G-protein-coupled receptors. Acting through a signalling cascade involving adenylyl cyclase and cAMP, these receptors mediate and modulate both K^+ and Ca^{2+}channels (Birnbaumer, 1990; Cooke, 1999). Other than some links with pain, behaviour and some possible developmental roles, the endogenous function of $GABA_BRs$ have not been clearly established (Olsen & Sieghart, 2008).

5.1.4. Role of GABA in Neuronal Development

Whilst the function of GABA in the adult brain as an inhibitor of neuronal excitability is well established, more recent observations have provided evidence for a developmental role of this neurotransmitter. When GABA binds to $GABA_ARs$ a Cl^- channel is opened. The electrical response to this increase in Cl^- conductance is determined by the gradient of Cl^- across the plasma membrane and Vm. If $[Cl^-]_i$ is high enough (resulting in an E_{Cl} value less negative than V_m), then Cl^- will leave the cell down its electrochemical gradient, depolarising the cell and increasing its excitability – this is GABA acting as an excitatory neurotransmitter. Conversely, if

$[Cl^-]_i$ is low enough (resulting in an E_{Cl} value more negative than V_m), then GABA binding to $GABA_A$Rs will result in Cl^- influx, hyperpolarisation and a decrease in excitability – this is GABA behaving as an inhibitory neurotransmitter (Chavas & Marty, 2003).

The discovery that, in immature, prenatal and early postnatal rodent neurons, GABA is excitatory has led to an increase in research into this mechanism and its consequences. It was initially shown that the response was dependent on $[Cl^-]_i$ (Owens *et al.*, 1996) through the use of gramicidin perforated patch clamp, which allows electrical access to the cell without disturbing the endogenous intracellular Cl^- concentration (Marty & Finkelstein, 1975; Horn *et al.*, 1988). Studies went on to show that immature prenatal and early postnatal neurons show differential expression of two Cl^- transporters, Na-K-2Cl co-transporter 1 (NKCC1) and K-Cl co-transporter 2 (KCC2), when compared with mature adult neurons (Ben-Ari, 2002; Yamada *et al.*, 2004). In physiological conditions, NKCC1 transports Cl^- into the cell using the Na^+ electrochemical gradient and co-transports K^+ as a means to maintain electro-neutrality. KCC2 transports Cl^- out of the cell by harnessing the K^+ electrochemical gradient. NKCC1 is highly expressed in immature neurons and is down-regulated during development. KCC2 shows the opposite trend, with low or zero expression early on, and an increase in expression during neuronal maturation. The differential expression of both of these transporters during development is believed to control $[Cl^-]_i$ and as a consequence, determines the electrical response to GABA application (See model in Figure 5.1 (Owens *et al.*, 1996; Yamada *et al.*, 2004). If the shift of V_m towards E_{Cl} during $GABA_A$R activation exceeds the threshold for voltage-gated Ca^{2+} channel activation then the resulting influx in $[Ca^{2+}]_i$ can be

measured using standard Ca^{2+} imaging techniques (Figure 5.1). In this chapter, such an excitatory response to GABA activity was measured indirectly as a GABA-evoked, depolarisation-mediated activation of voltage-gated Ca^{2+} channels. Conversely, an inhibitory response to GABA is defined throughout this chapter as a lack of such GABA-evoked Ca^{2+} influx in physiological $[Cl^-]_o$ in cells which did demonstrate Ca^{2+} responses to both 50 mM KCl and GABA in non-physiological, low $[Cl^-]_o$ solutions.

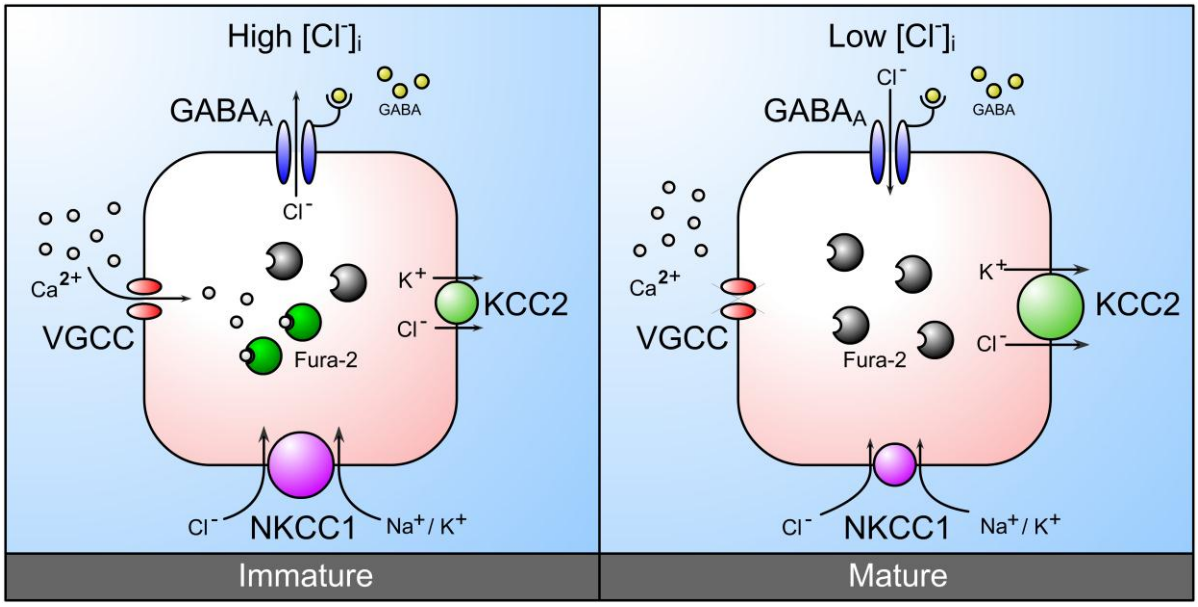

Figure 5.1: Model of GABAergic Signalling in Developing Neurons: Diagram showing the resulting ionic movement upon GABA binding to $GABA_A$Rs in cells with an immature (high $[Cl^-]_I$) or a mature (low $[Cl^-]_I$) phenotype and the associated change in Fura-2 fluorescence activation as a result of Ca^{2+} influx through voltage-gated Ca^{2+} channels.

This striking 'double-action' of GABA appears to have a role in a wide variety of developmental processes; it has so far been linked with cell proliferation (Fiszman *et al.*, 1999), differentiation (Tozuka *et al.*, 2005), integration of synapses (Ge, 2006), migration (Behar *et al.*, 2000) and adult neuronal function (Fritschy & Mohler, 1995). Furthermore, it has also been shown that this effect is not only apparent in immature cells of the earlier stages of development, but is also present

in immature precursor cells which reside in the adult nervous system (Carleton *et al.*, 2003).

The knowledge that voltage-gated Ca^{2+} channels are activated through GABA-mediated depolarisation suggests that GABA can indirectly affecti Ca^{2+}-dependent gene expression. Ca^{2+} transients have been associated with developmental cues and through this action it has been suggested that GABA modulates enzyme function, neurite outgrowth and transmitter release (Obrietan & Vandenpol, 1995; Owens *et al.*, 1996; Fiszman *et al.*, 1999).

5.1.4.1. Proliferation

The link between GABA-mediated excitation and an effect on cell proliferation has been shown in a variety of neuronal cell types (LoTurco *et al.*, 1995; Fiszman *et al.*, 1999; Haydar *et al.*, 2000; Nguyen *et al.*, 2003; Represa & Ben-Ari, 2005). However, the observations are contradictory, and while proliferation is induced by GABA in some populations, in others it is inhibited (Fiszman *et al.*, 1999; Nguyen *et al.*, 2003). The induction of cell proliferation is a less well understood effect of GABA and whether it induces proliferation in immature cells and inhibits it in more developed precursors has yet to be investigated.

5.1.4.2. Migration

The effects of GABA on neuronal migration are varied and often contradictory. Observations that GABA promotes motility (Behar *et al.*, 1998), accelerates migration and also acts as a migration inhibitor (Varju *et al.*, 2001) suggest that there are many other factors which also contribute to the GABA response. It has been suggested that GABA may mediate migration by altering the volume of the

cell, a factor often associated with cell migration (Habela *et al.*, 2009). As GABA opens a Cl^- channel, the resulting ionic imbalance may result in obligatory water movement to compensate for the change in osmolarity. Indeed a reduction in cell volume upon sustained opening of GABA-gated Cl^- channels in glioma cells has been demonstrated (Habela *et al.*, 2009). As this would only happen in cells in which E_{Cl} is less negative than V_m, this observation suggests only immature neuronal cells would be affected. It is interesting to note that volume dynamics also play a role in cell division and, therefore, proliferation (Represa & Ben-Ari, 2005).

5.1.4.3. Differentiation

GABA induces or increases differentiation in neuronal progenitor populations. Blocking GABARs in those same cells reduces differentiation. This suggests GABA plays an important role in neuronal maturation (Tozuka *et al.*, 2005; Parga *et al.*, 2007). Parga and colleagues have shown that treatment of mesencephalic precursor neurospheres with the $GABA_A$ antagonist bicuculline increases the number of dopaminergic (DA) neurons *in vitro*, they went on to show that this was directly due to increased DA neuron differentiation (Parga *et al.*, 2007). Cancedda and colleagues showed that excitatory GABA activity is essential for correct morphological maturation *in vivo* by carrying out *in utero* transfection of KCC2 in fetal rat cortical neurons at a developmental stage where endogenous KCC2 is not normally expressed. They reported no significant difference in migration, but correct morphological maturation was lost. Overexpressing an inwardly rectifying K^+ channel in a separate set of experiments, to mimic the loss of depolarisation upon GABA application seen with the KCC2 expression experiments, showed that this effect was the result of the loss of GABA-dependent depolarisation, lending further

weight to the theory that it is GABA excitation that results in changes to gene expression and function (Cancedda *et al.*, 2007).

5.1.4.4. Integration

It is becoming more apparent that neuronal activity itself induces the process of neurogenesis and synaptic integration, allowing the developing circuitry to self-regulate and produce the required complex signalling pathways that are necessary for proper bodily function and behaviour (Kempermann & Gage, 1999; Fuchs & Gould, 2000; Ming *et al.*, 2001; Doetsch & Hen, 2005). Shaoyu Ge and colleagues showed that newborn dentate gyrus granule cells are activated by tonic (non-synaptic) GABA inputs, and are then integrated into functional circuits via phasic (synaptic) GABA and glutamate inputs *in vivo.* By knocking down NKCC1 translation using short hairpin RNA (shRNA) they were able to reduce $[Cl^-]_i$ and, therefore generate GABA-mediated hyperpolarisation. This led to 'marked defects in their synapse formation and dendritic development *in vivo*' characterised by reduced dendritic length, branch number and complexity (Ge, 2006).

5.1.5. Ontogeny of Excitatory/Inhibitory Responses to GABA

The development of the GABA response is dependent on $[Cl^-]_i$, which is dependent on NKCC1 and KCC2 expression. Developmentally, the downregulation of NKCC1 and complementary upregulation of KCC2, correlating with the switch from excitatory to inhibitory GABA responses, has been shown to occur between 3-8 days in vitro (DIV) in cerebellar granule cells from post-natal day rat. Glutamatergic responses were shown to remain similar through this period (Rego *et al.*, 2001). The increase in KCC2 expression may even be triggered by activity relating to synaptic integration. This phenomenon can be observed across multiple species and

neuronal subtypes and it is now seen as a general rule that immature neurons respond to GABA with excitation and mature neurons by inhibition (Ben-Ari, 2002). Rego and colleagues reported that 100% of cerebellar granule cells taken from postnatal day 6 Wistar rats were excitatory upon application of GABA, this dropped to 0% over the next 8 DIV (Rego *et al.*, 2001). Similarly, Ganguly and co-workers reported that 100% of E18 rat hippocampal neurons were excitatory upon application of GABA even after 3-4 DIV, a number which dropped to 0 by 18 DIV. They went further to show that it was the action of GABA that itself promoted this switch, as blockers of GABA activity delayed the change towards inhibitory responses. They also showed that applications of GABA modulated the expression levels of KCC2 (Ganguly *et al.*, 2001). However, no information is currently available about the phenomenon in human neural development.

5.1.6. GABAergic Signalling During Stem Cell Differentiation

This information, suggesting that GABA plays a part in all the key areas of neuronal development, suggest that more work is required not only to understand the developmental processes that are occurring within maturing neuronal networks, but also to provide information that may be useful in producing new developmental protocols for the production of differentiated mature neurons from hESCs or IPS cells *in vitro*. To be able to exploit naturally occurring developmental cues is already the accepted goal of many hESC differentiation protocols. The use of neurotrophic factors such as BDNF and GDNF in differentiation experiments is now commonplace. The evidence so far suggests that *in vitro* modification of endogenous GABAergic activity in developing neuronal populations produces measurable effects on the physical and functional characteristics of those neurons.

Much more work is needed to characterise these effects and harness them for possible clinical benefit. One particularly important observation, which underlines this potential benefit, is that neuronal trauma *in vivo* promotes down-regulation of KCC2 and subsequently switches GABA responses in the damaged neuronal tissue from inhibitory to excitatory (Rivera *et al.*, 2005). It is hypothesised that this is to both induce neurogenesis in these areas and to promote synaptic integration which will potentially promote repair in the traumatised region (Ben-Ari, 2002; Rivera *et al.*, 2005). Should the mechanism for recruitment and integration of functionally developed neurons to the site of damaged neuronal tissue be already in place, it follows that understanding and exploiting this may lead to improved tissue transplantation treatment of neurodegenerative conditions.

5.1.7. Aims of Chapter

In order to investigate GABAergic signalling within fetal neuroprogenitor populations, and to apply knowledge gained from research into other stem-cell sources, GABAergic signalling in fetal hWGE-derived neurons was investigated. Particular attention was be paid to Ca^{2+} mobilisation as an indirect effect of $GABA_AR$ activation as this has been shown to directly affect cellular properties. Modulation of GABAergic signalling was investigated in an attempt to identify potential tools for further research. Where possible, evidence of GABAergic signalling and modification of this signalling were investigated in hESC- and neonatal mWGE-derived neurons also.

5.2. Non-Standard Methods

5.2.1. Solutions

ECS: as described in section 2.2.1.1.

50 mM KCl ECS: as per standard ECS, but with 50 mM KCl and 90 mM NaCl

Low Cl^- ECS: Equimolar replacement of NaCl with sodium-isothionate (Sigma)

Mixtures of ECS and Low Cl^- ECS were made as described in the relevant text.

ICS: as described in section 2.2.1.2.

5.2.2. Gramicidin-Perforated Patch Clamp

Gramicidin-perforated patch clamp was performed as was whole-cell patch clamp (2.2.2.), with the follow exceptions, as per previously published methodology (Ebihara *et al.*, 1995).

A modified intracellular solution containing 150 mm KCl and 10 mm Hepes buffered to pH 7.2 using NaOH, supplemented with gramicidin (Sigma, stock 100 mg/ml in ethanol, pipette solution concentration: 100 μg/ml) was sonicated (XL2020 , Qsonicator, CT, USA) until the precipitate (gramicidin) was no longer macroscopically visible.

Upon effective GΩ seal formation, the pipette was left in place (without applied pressure) to allow gramicidin incorporation into the cell membrane. The access resistance was continually measured using the on-line seal-test (Clampex). When this value dropped to less than 20 MΩ (within 40 min of seal formation) and remained stable for a period of 5 min, experimental protocols were applied.

GABA applications were made during voltage-step protocols as described in the relevant text.

5.2.3. Reagents

N-Methyl-D-aspartic acid (NMDA): Sigma, stocks of 100 mM in H_2O

γ-Aminobutyric acid (GABA): Sigma, stocks of 300 mM in H_2O

α-Amino-3-hydroxy-5-methylisoxazole-4-propionic acid hydrate (AMPA): Sigma, stocks of 10 mM in H_2O

Kainic acid monohydrate (Kainate): Sigma, stocks of 10 mM in H_2O

L-Glutamic acid (L-Glu): Sigma, stocks of 100 mM in H_2O

Picrotoxin: Sigma, stocks of 50 mM in ethanol

3-(Aminosulfonyl)-5-(butylamino)-4-phenoxybenzoic acid (Bumetanide): Sigma, stocks of 20 mM in ethanol

1,3-Dihydro-1-[2-hydroxy-5-(trifluoromethyl)phenyl]-5-(trifluoromethyl)-2H-benzimidazol-2-one (NS 1619): Sigma, stocks of 10 mM in ethanol

5.3. Results

5.3.1. MTOP-Derived Tissue is Functionally Similar to STOP-Derived Tissue

Functional analysis of MTOP- and STOP-derived tissue was carried out to determine whether there were measurable differences in key physiological readouts between tissue sources. Ca^{2+} imaging was used to assess the effect, on intracellular Ca^{2+}, of external application of a depolarising 50 mM K^+ solution and of several known neuronal agonists, namely NMDA, GABA, AMPA, kainate and L-glutamic acids.

Figure 5.2 shows example Ca^{2+} imaging recordings from MTOP- (A.) and STOP-derived neurons (B.). The mean fluorescence ratio increase as a percentage of baseline is shown (C.) for each agonist.

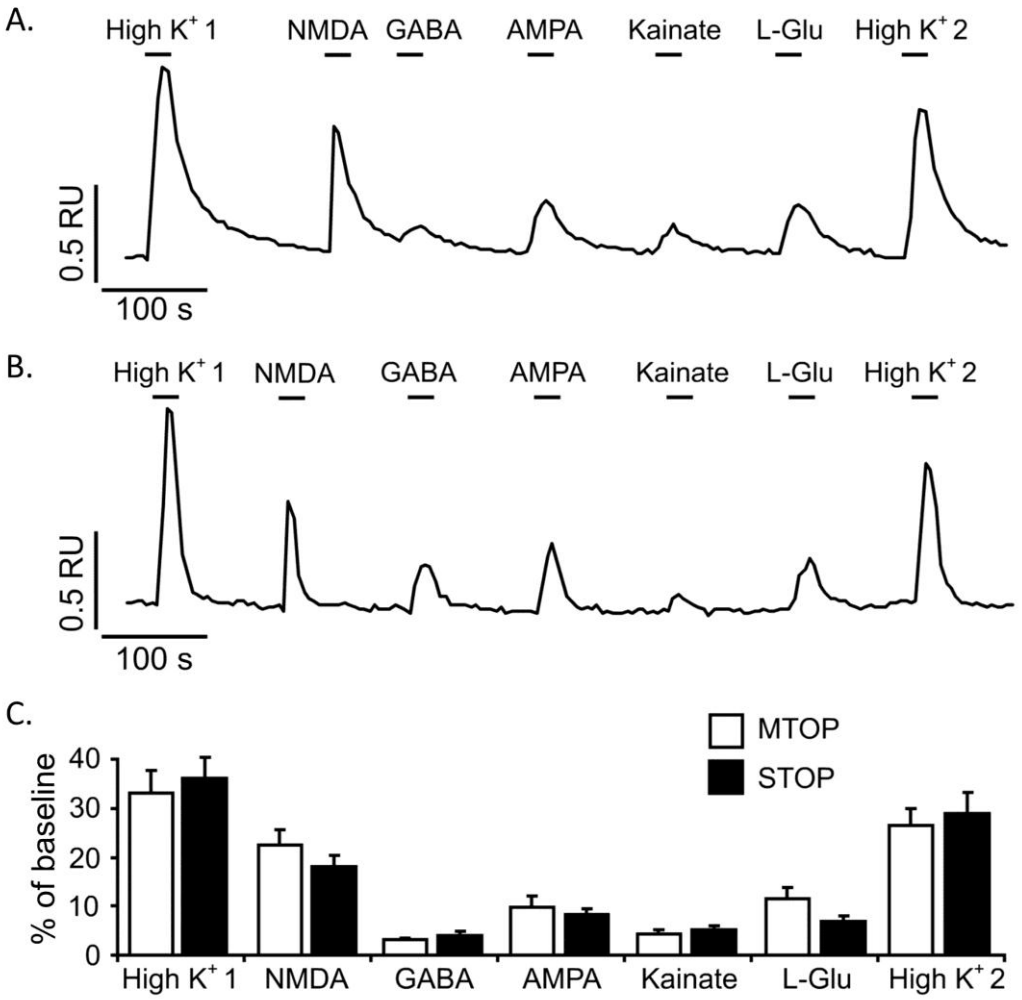

Figure 5.2. MTOP-derived hWGE cells *in vitro* display similar functional characteristics as STOP-derived hWGE cells *in vitro*: Rises in intracellular Ca^{2+} in exemplar, individual cells derived from MTOP (A.) and STOP (B.) fetal hWGE tissue during brief applications of depolarizing 50 mM K^+ solutions (high K^+ 1 and high K^+ 2), 50 µM GABA, 50 µM kainate, 50 µM α-amino-3-hydroxyl-5-methyl-4-isoxazole-propionate (AMPA), 50 µM N-methyl-D-aspartic acid (NMDA), and 100 µM L-glutamic acid (L-Glu) as indicated (black bars). Relative $[Ca^{2+}]_i$ is plotted as relative units (R.U.) versus time to allow comparison. C. Mean rises in $[Ca^{2+}]_i$ in response to each agonist and high K^+ solutions plotted as percentage increase in fluorescence above baseline (*n* = 230 MTOP, *n* = 88 STOP, error bars represent SEM). Reproduced from (Kelly *et al.*, 2011).

5.3.2. hWGE-Derived Neurons Display Functional Ionotropic GABA Receptors

Extracellular application of GABA during whole-cell patch-clamp of hWGE-derived neurons elicited an inward current (indicating outward Cl^- movement) which was dependent on GABA concentration. The current elicited was composed of a fast activating and slow inactivating component typically taking 1-2 s to reach maximum amplitude before steadily declining to a plateau which was then maintained throughout the remaining GABA application (Figure 5.3.A.). This GABA-induced current was also observed in hESC-derived neurons, at week 3 PPD, and post-natal mWGE-derived neurons, at DIV 3. GABA-concentration dependence was observed in all cells. hWGE-, mWGE- and hESC-derived neurons gave EC_{50} values for GABA of 19.9 ± 1.19 µM, 7.18 ± 0.55 µM and 53.37 ± 7.17 µM, with Hill coefficients of 1.7, 1.6 and 1.3, respectively.

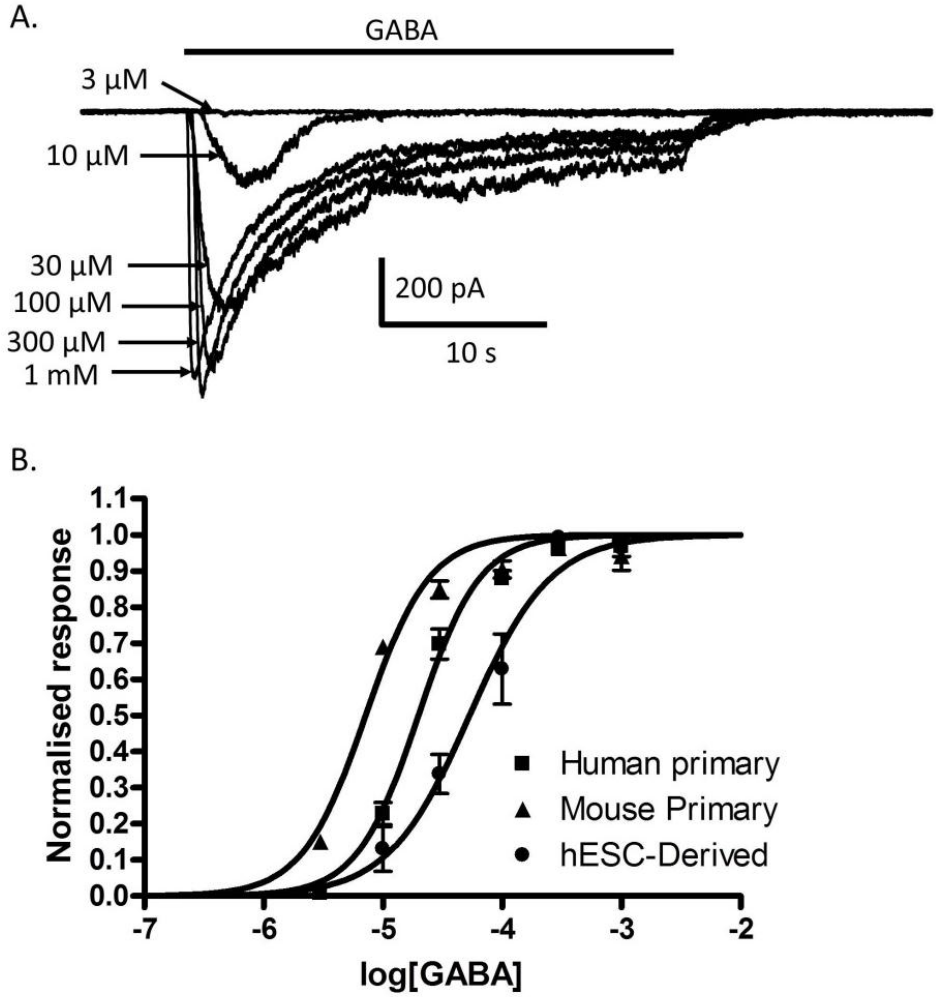

Figure 5.3. GABA-induced currents in primary and hESC-derived neurons are concentration dependent: Extracellular application of GABA at various concentrations resulted in inward currents. A. an example trace showing currents in a DIV 3 neuron from hWGE in response to indicated concentrations of GABA. B. Concentration-response curves fitted to data obtained from hWGE-, mWGE- (DIV 1) and hESC-derived (post plate-down week 3) neurons (all points; *n* = 5, error bars indicate SEM). EC_{50} values, hWGE: 19.9 µM, mWGE: 7.18 µM, hESC-Neu: 53.37 µM.

A voltage-step protocol (see section 2.2.2.4.) coupled with extracellular GABA application enables the reversal potential for GABA currents (E_{GABA}) in hWGE-derived neurons to be measured (Figure 5.4). GABA-induced currents (after leak subtraction) were shown to reverse at 3.8 mV. Due to the calculated junction potential (section 2.2.1.4.) for the solutions used in this experiment, this value is calculated to be 1.6 mV (3.8 mV - 2.2 mV).

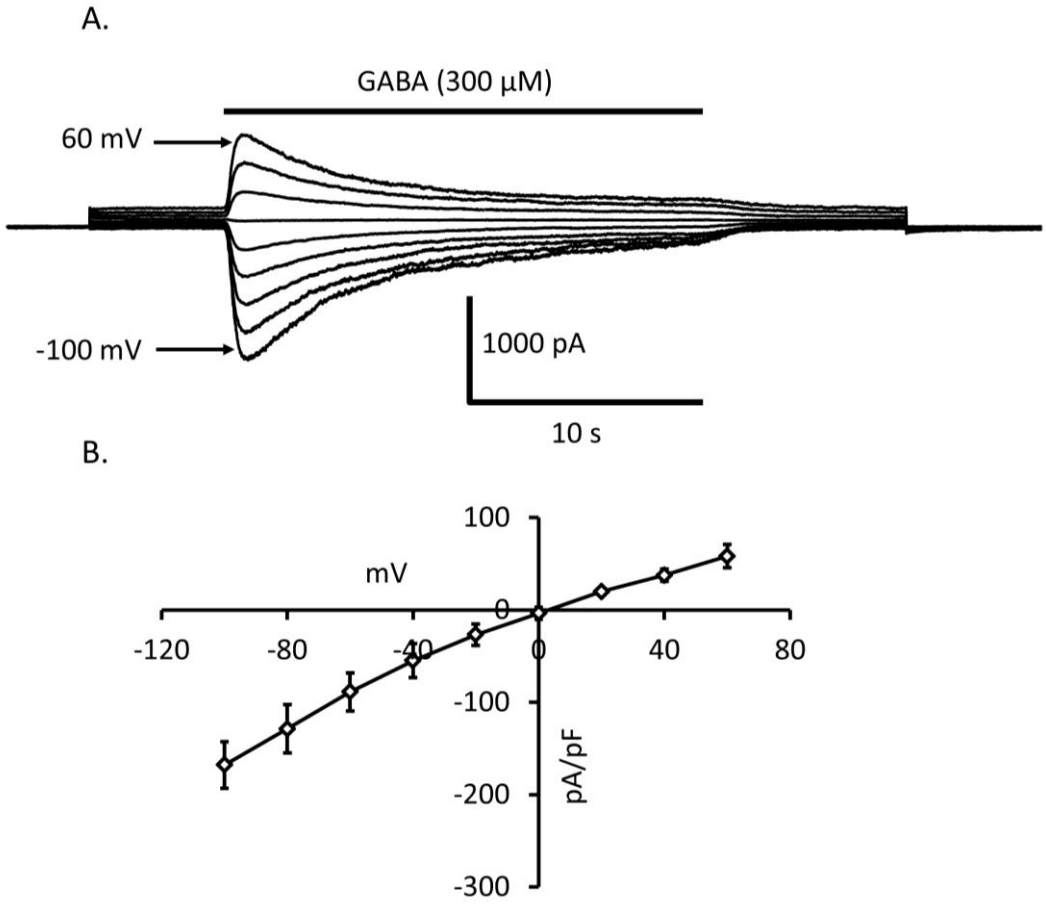

Figure 5.4. GABA-induced currents in hWGE-derived neurons at various voltages: Extracellular application of GABA (300 µM) during variable voltage steps (9 steps, first step -120 mV, final step 60 mV, step-step change 20 mV) resulted in currents of variable amplitude. A. an example trace from a DIV 3 hWGE-derived neuron, voltage steps and GABA application times are indicated. B. plot of the average leak-subtracted GABA-induced current for each voltage (*n* = 5, error bars indicate SEM).

Pre- and co-application of 50 µM picrotoxin reduced the mean peak GABA-induced current to approximately 25% of the control current (Figure 5.5). This effect was reversed after a wash period in the control ECS with a mean peak current of 99% of the initial response.

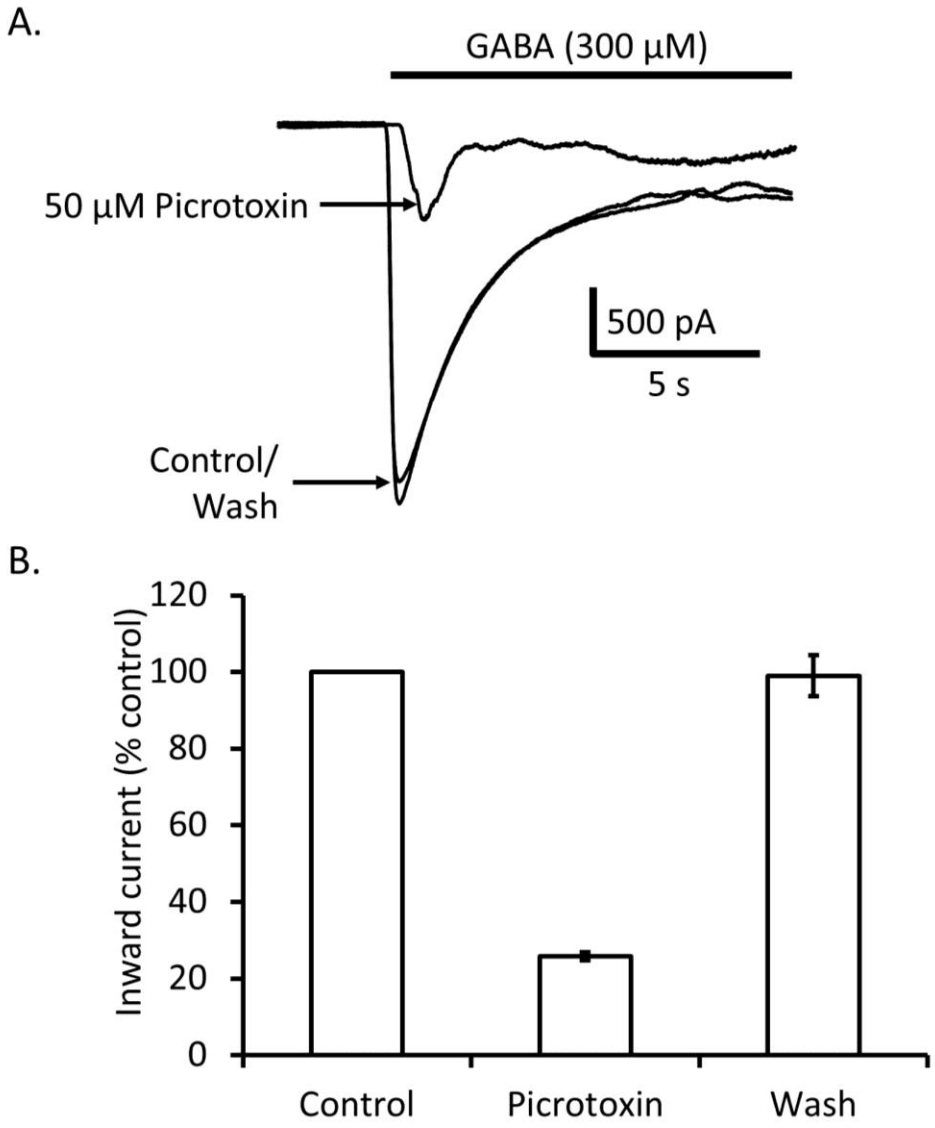

Figure 5.5. GABA-induced currents in hWGE-derived neurons are reduced by picrotoxin: Currents induced by extracellular application of 300 µM GABA were significantly reduced when 50 µM picrotoxin was pre- (90 s) and co-applied. A. An example trace from a DIV 2 hWGE-derived neuron showing the GABA induced current with or without picrotoxin as indicated. B. shows the average peak current as a percentage of that obtained in the control solution for the control, picrotoxin block and a 180 s wash in control solution *(n* = 3, error bars indicate SEM).

Ca^{2+} imaging was used to measure transient rises in intracellular free Ca^{2+} in hWGE-derived neurons during extracellular application of GABA (Figure 5.6). The effect of picrotoxin on GABA-induced currents was replicated using this protocol with a

reduction in the mean normalised fluorescence ratio increase to approximately 34% of the control. Again, this effect was reversed upon wash in control solution with a mean normalised fluorescence ratio increase of 77% of the control.

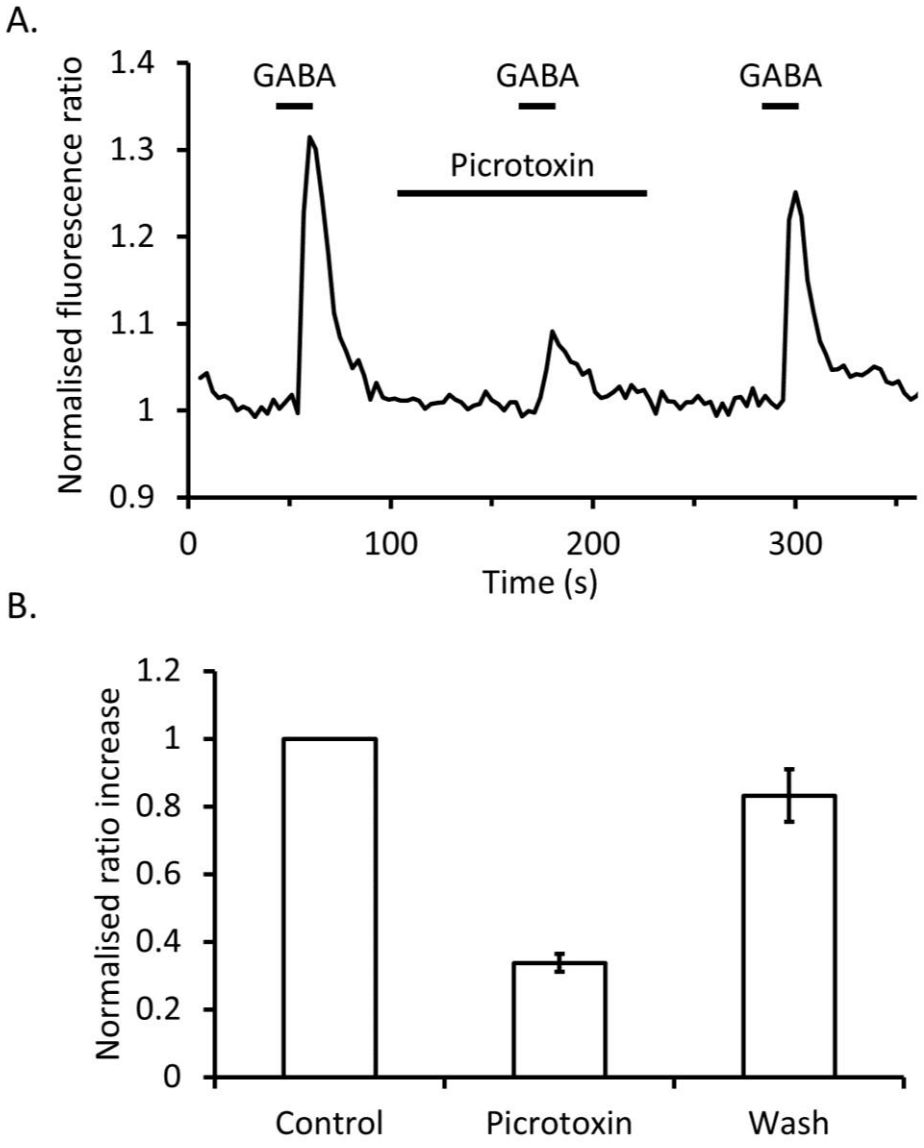

Figure 5.6 GABA-induced Ca^{2+} transients in hWGE-derived neurons are reduced by picrotoxin: Transient increases in intracellular Ca^{2+} upon extracellular application of 300 µM GABA were significantly reduced when 50 µM picrotoxin was pre- (60 s) and co-applied. A. An example trace from a DIV 2 hWGE-derived neuron showing the GABA induced Ca^{2+} transient with or without picrotoxin as indicated. B. shows the average peak Ca^{2+} transient amplitude as a percentage of that obtained in the control solution for the control, picrotoxin block and a 60 s wash in control solution *(n* = 25, error bars indicate SEM).

5.3.3. hWGE-Derived Neurons Display Both Inhibitory and Excitatory Responses to GABA

GABA-induced Ca^{2+} transients were not present in all cells at standard extracellular Cl^- concentrations. In all cells that displayed Ca^{2+} transients in response to a depolarising application of 50 mM KCl, confirming the presence of voltage-gated Ca^{2+} channels (required for the indirect measurement of excitatory GABA responses), GABA induced a transient rise in intracellular Ca^{2+} when applied in a low Cl^- solution. Figure 5.7 shows exemplar Ca^{2+} imaging recordings from separate cells displaying an excitatory (A.) and an inhibitory (B.) response to GABA in normal Cl^- solution. Upon repeated extracellular application of GABA, in sequentially reduced extracellular Cl^-, Ca^{2+} transients increased in 'excitatory' cells and appeared then increased in 'inhibitory' cells.

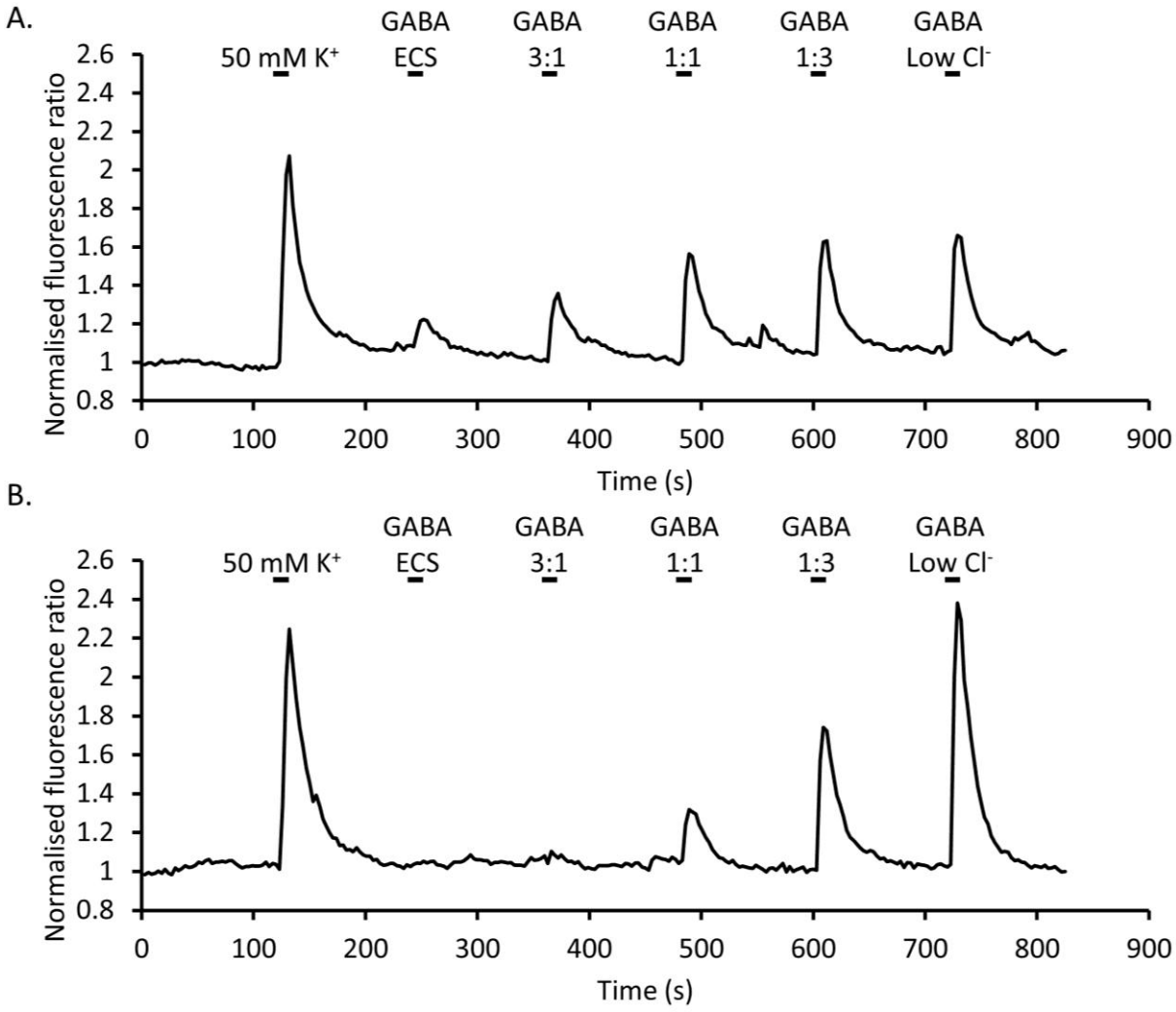

Figure 5.7. hWGE-derived neurons display either excitatory or inhibitory responses to GABA which are dependent on extracellular Cl^- concentration: GABA-induced Ca^{2+} transients were observed in all hWGE-derived neurons which displayed voltage-gated Ca^{2+} channel activity in response to 50 mM K^+ depolarisation. Cells either displayed 'excitatory' or 'inhibitory' responses to 300 µM GABA in physiological Cl^-. Excitatory responses (as in A.) were increased by reducing extracellular Cl^-. Inhibitory responses (as in B.) were changed to excitatory and then increased by reducing extracellular Cl^-. Cl^- concentrations: ECS (144.9mM), 1:3 (111.15 mM), 1:1 (77.4 mM), 3:1 (43.65 mM), Low Cl^- (9.9 mM).

The percentage of cells displaying an excitable response to extracellular GABA application was measured during *in vitro* culture of fetal hWGE-derived neurons. Recordings were made at three time-points after cells were plated (1-2, 6-7 and 14-16 DIV). Post-natal day 1 (DIV 1-2) mWGE-derived neurons were used as a

comparison. Approximately 88.9% of mWGE DIV 2 neurons displayed excitatory responses to GABA. In fetal hWGE-derived neurons 66.5%, 45.1% and 21.8% of cells displayed excitatory responses for DIV 1-2, 6-7 and 14-16, respectively.

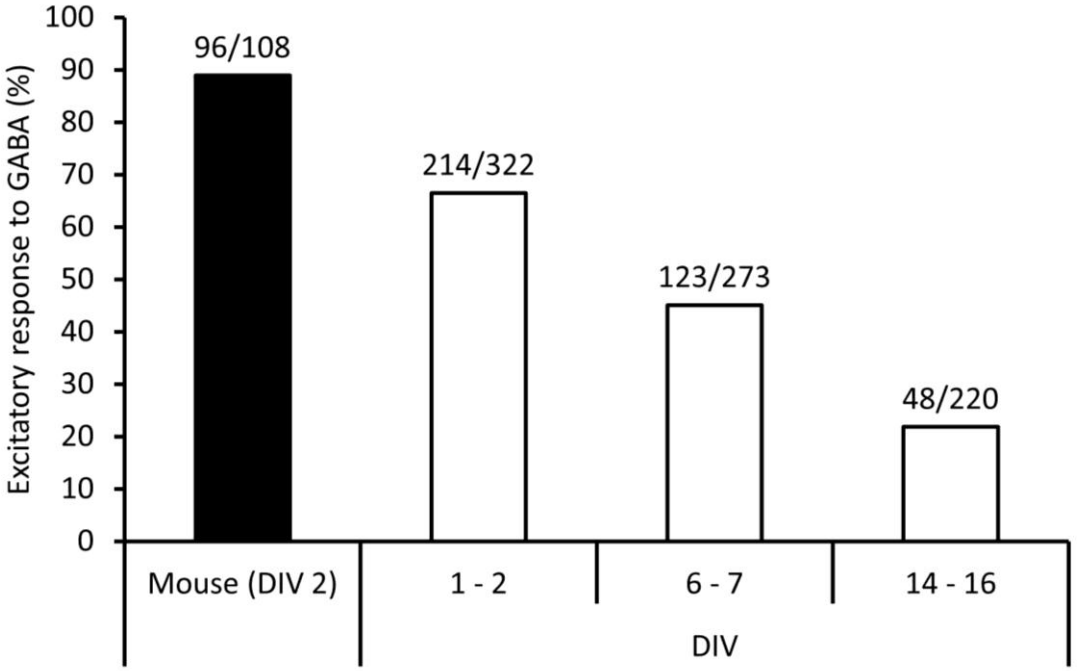

Figure 5.8. The percentage of hWGE-derived neurons with excitatory responses to GABA reduces during culture *in vitro*: The percentage of voltage-dependent Ca^{2+} channel expressing cells displaying a transient increase in Ca^{2+} in response to an external application of 300 µM GABA in physiological extracellular Cl^- is shown for mWGE-(black) and for hWGE-derived neurons which have been cultured *in vitro* for the indicated days (DIV). Percentages are based the number of observations as indicated above each bar.

5.3.4. Bumetanide Switches Excitatory GABA Responses to Inhibitory

The excitatory response to GABA is an indirect result of $GABA_AR$ activation-mediated efflux of Cl^-, subsequent depolarisation of V_m and corresponding activation of voltage-gate Ca^{2+} channels. Modulation of the intracellular Cl^- concentration, altering the Cl^- gradient and therefore movement upon GABA channel opening, should influence the resulting Cl^- movement. If the Cl^- concentration was reduced within the cell, the net movement of Cl^- would shift

towards movement into the cell. Bumetanide, an antagonist of the Cl^- transporter NKCC1 (which transports Cl^- into the cell), was pre- and co-applied with GABA during Ca^{2+} imaging of fetal hWGE, post-natal mWGE- and PPD week 3 hESC-derived neurons (Figure 5.9).

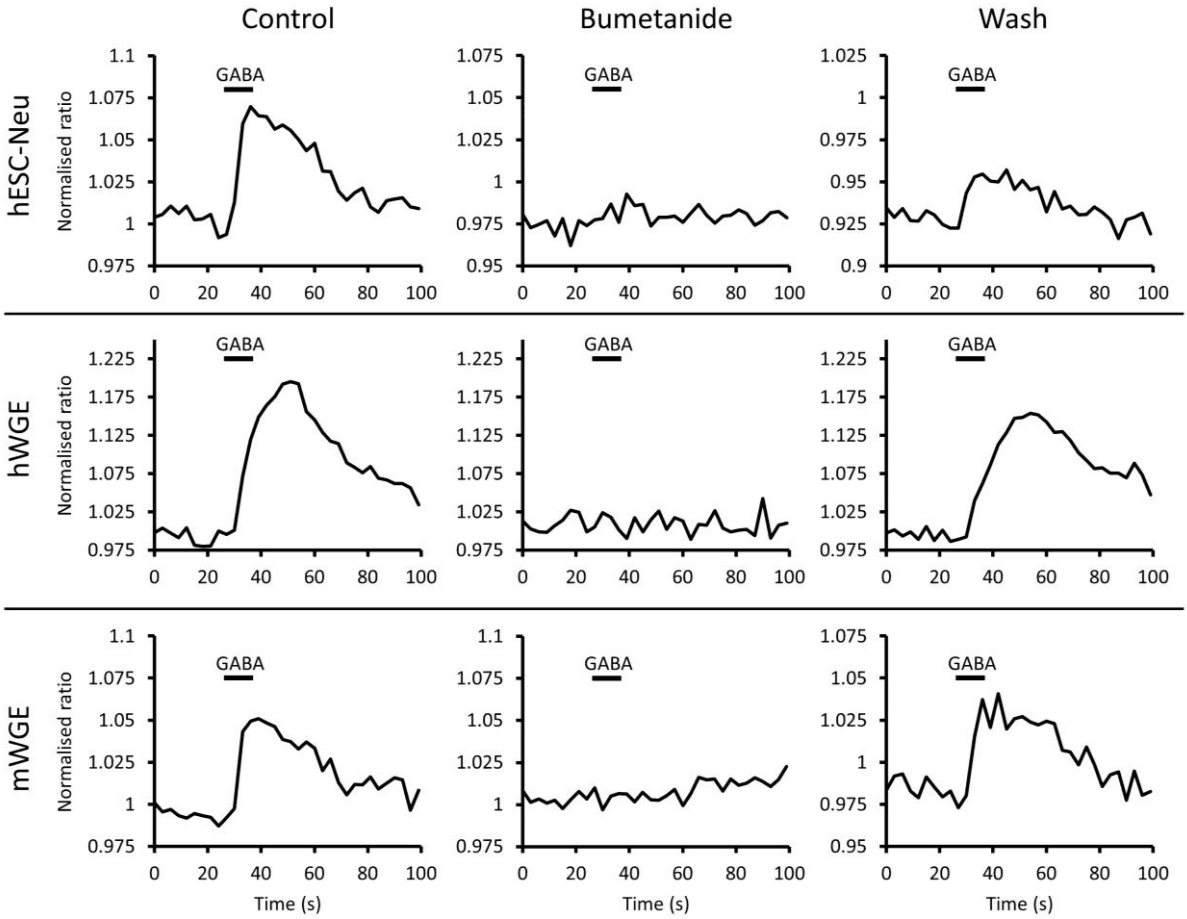

Figure 5.9. hWGE, mWGE and hESC-derived neuronal responses to GABA switch from excitatory to inhibitory in the presence of bumetanide: In cells which showed an excitatory Ca^{2+} response to 300 µM GABA (left graphs), responses were switched to inhibitory by extracellular pre-application of 20 µM bumetanide for 5 min (middle graphs). This effect was reversed by washing with the control solution for 5 min giving excitatory responses (right graphs). Example Ca^{2+} imaging traces displaying the effect of bumetanide on GABA excitation in hWGE- (top), mWGE (middle) and hESC-derived (bottom) neurons are shown.

In all three cell types, bumetanide resulted in the loss of excitatory responses in the majority of cells which showed excitatory responses during control GABA applications (examples shown in Figure 5.9, % shown in Figure 5.10).

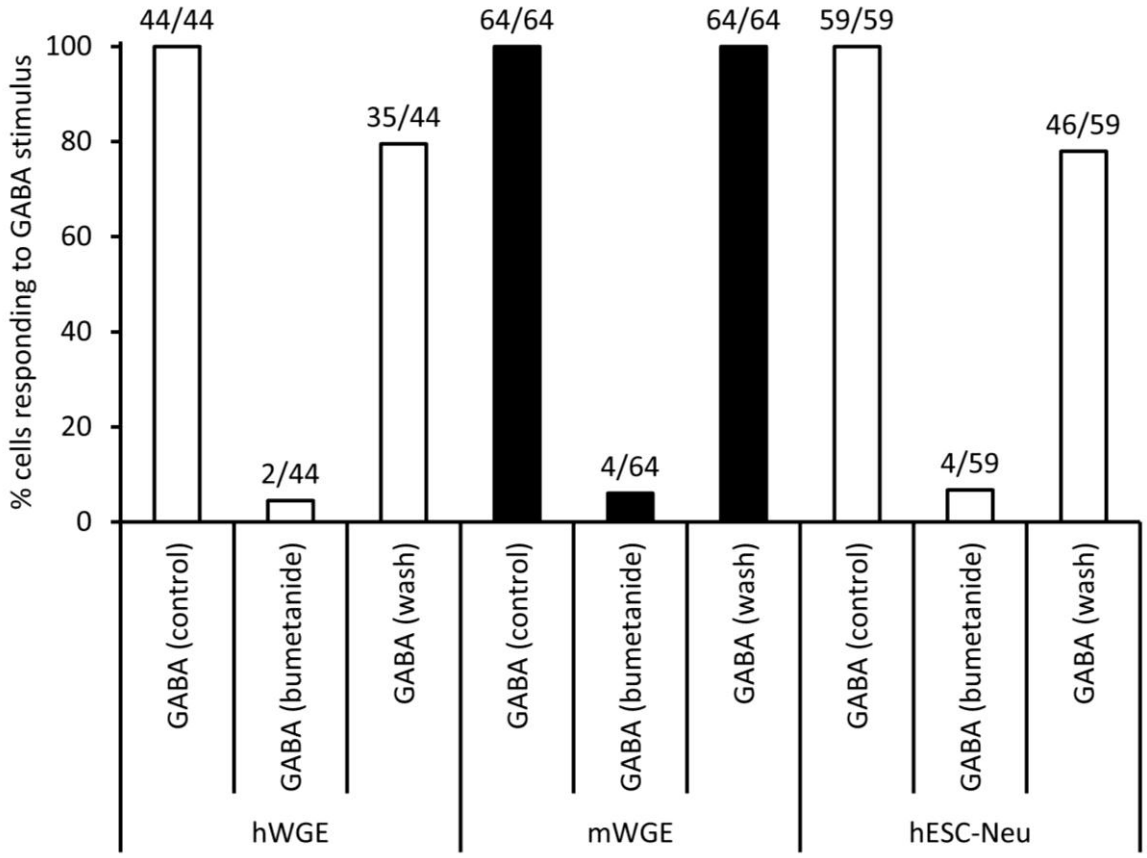

Figure 5.10. Percentage of cells which 'switch' from excitatory to inhibitory GABA responses in response to bumetanide application: The percentage of cells from hWGE-, mWGE and hESC-derived neurons that display an excitatory response to 300 µM GABA before, during and after pre- and co-application of 20 µM bumetanide as outlined in Figure 5.9.

The 'switching' of excitatory responses to inhibitory responses by bumetanide was investigated further using gramicidin-perforated patch-clamp. As gramicidin pores are impermeable to Cl^-, the intracellular Cl^- concentration remains unaffected by the ICS Cl^- concentration throughout the recording (Abe *et al.*, 1994). This allows the measurement of E_{GABA}, which can be used to predict $[Cl^-]_i$. Figure 5.11.A. shows the recording of E_{GABA} using GABA applications during a voltage-step protocol in a

gramicidin-perforated whole-cell recording before (control), during 20 µM bumetanide application (bumetanide) and after a wash period in control solution (wash). E_{GABA}, predicted from the plot of leak-subtracted peak GABA-induced currents at each voltage (B.) and is shown in C. The predicted $[Cl^-]_i$ concentration, calculated from the Nernst equation, is shown for each condition (D.).

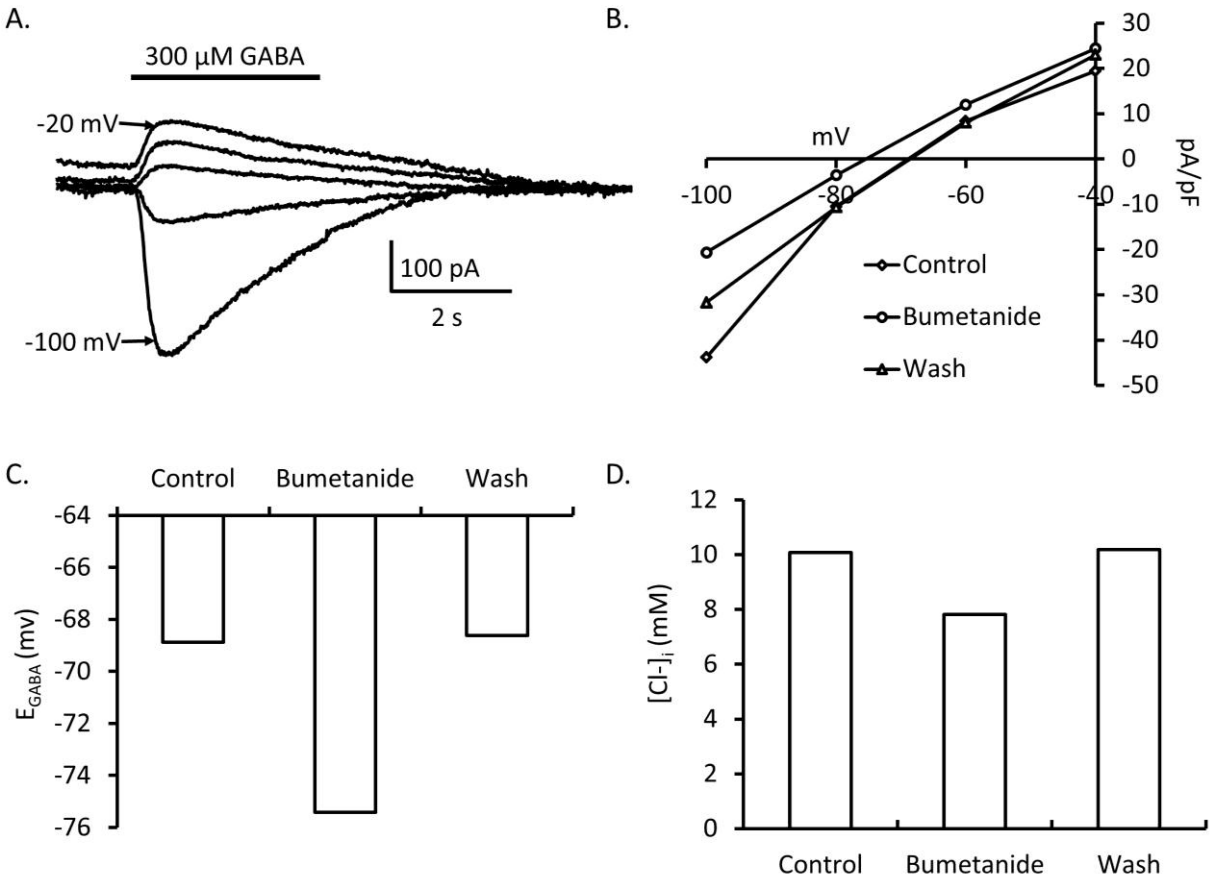

Figure 5.11. Extracellular bumetanide negatively shifts E_{GABA} in hWGE-derived neurons: Results from a single cell during gramicidin perforated patch-clamp. A. The currents recorded during 300 µM GABA applications at different voltages (indicated). B. Peak current density plotted against voltage in control solution, during application of 20 µM bumetanide (5 min pre-application) and after a 5 min wash in the control solution. C. Predicted E_{GABA} values (using the current-voltage plots in B.). D. Predicted intracellular concentrations before, during and after wash of bumetanide application (predicted using the Nernst equation).

5.3.5. NS1619 Switches Inhibitory GABA Responses to Excitatory

The large-conductance Ca^{2+}-activated K^+ (BK_{Ca}) channel activator NS1619 has been shown to hyperpolarise V_m in cultured cells (Olesen *et al.*, 1994). In fetal hWGE-derived neurons at DIV 14, NS1619 was shown to 'switch' responses to GABA from inhibitory to excitatory (Figure 5.12). In all fetal hWGE-derived neurons displaying inhibitory responses to GABA (that were also shown to have the potential for excitatory responses by applying GABA in low Cl^- solution), extracellular pre- and co-application of NS1619 with GABA resulted in excitatory responses, an effect which was shown to be reversible after washout with the control extracellular solution, whereupon inhibitory responses to GABA were again observed.

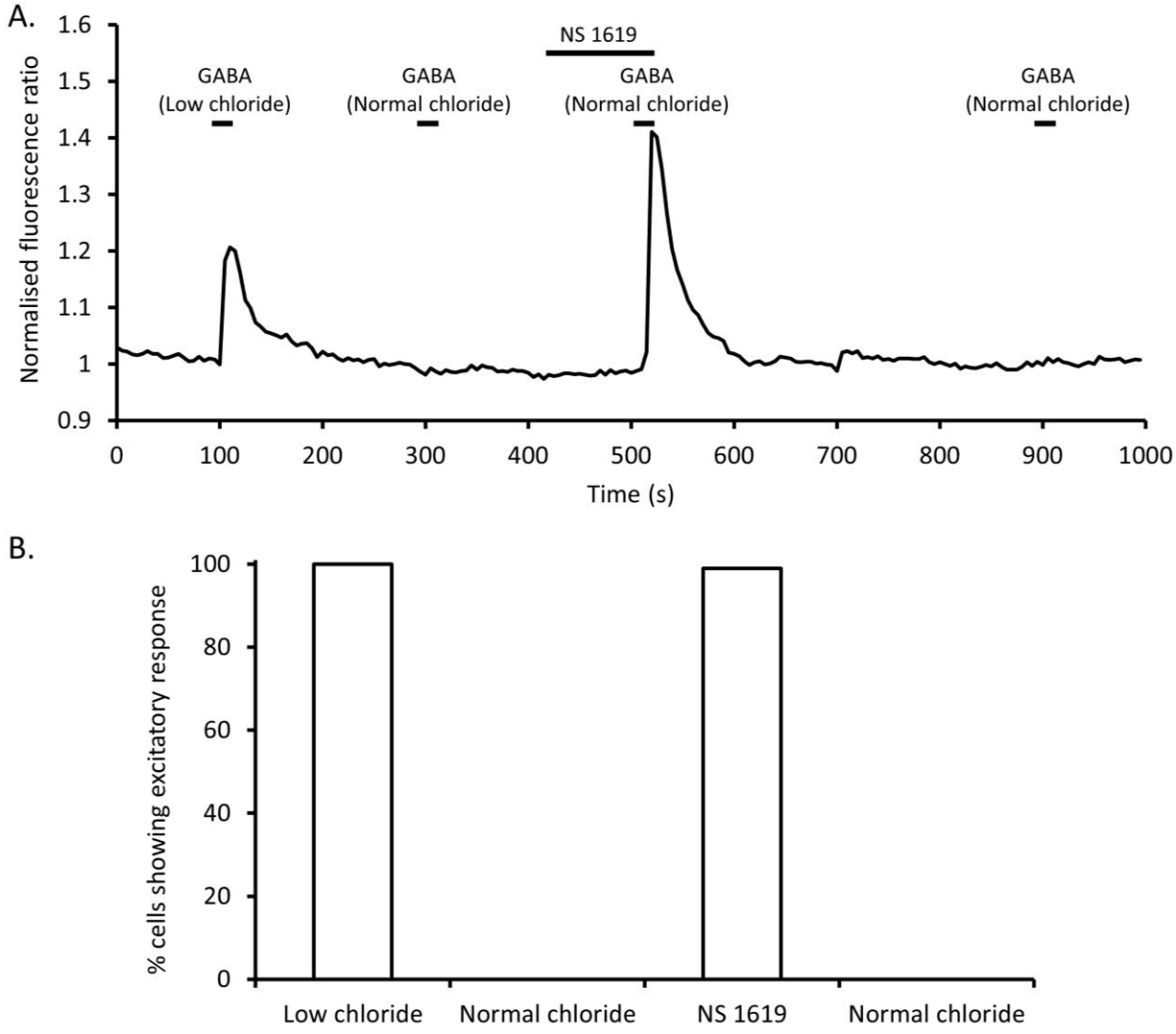

Figure 5.12. hWGE-derived neuronal responses to GABA switch from inhibitory to excitatory in the presence of NS1619: In cells which showed an inhibitory Ca^{2+} response to 300 µM GABA (left graphs), responses were switched to excitatory by extracellular pre-application of 10 µM NS1619 for 85 s (as indicated). This effect was reversed by washing with the control solution for 375 s giving inhibitory responses once again. A. An example Ca^{2+} imaging trace displaying the effect of NS1619 on GABA excitation in hWGE-derived neurons is shown. B. The percentage of cells from hWGE-derived neurons that display an excitatory response to 300 µM GABA before, during and after pre- and co-application of 10 µM NS1619 *(n* = 99).

5.4. Discussion

5.4.1. MTOP-Derived Tissue is Functionally Similar to STOP-Derived Tissue

That WGE tissue derived from MTOP behaved in a functionally similar manner to STOP-derived tissue suggests that there is no noticeable effect on the physiological function of WGE neurons derived from MTOP compared to STOP. This allowed MTOP-derived tissue to be used in further research into human neuronal development.

In Figure 5.2 responses of both MTOP- and STOP-derived tissue to various neuronal agonists can be seen. It is apparent from the example traces (A. and B.) that the responses to these agonists have a similar effect on intracellular Ca^{2+} in each case. Similarly the mean responses are very similar for both cells types.

The greater abundance of MTOP tissue compared to STOP tissue means that this work, published alongside other experimental data indicating the viability of MTOP is comparable to that in STOP-derived tissue, will hopefully allow for an increase in the availability of human fetal neurons for research and clinical use (Kelly *et al.*, 2011).

5.4.2. hWGE-Derived Neurons Display Functional Ionotropic GABA Receptors

GABA currents were measured in fetal hWGE-, post-natal mWGE and hESC-derived neurons *in vitro*. GABA was shown to alter intracellular Ca^{2+} in a $[Cl^-]_o$-dependent fashion. The effect of extracellular GABA on intracellular Ca^{2+} concentration was shown to be affected by two drugs, bumetanide and NS1619.

Recordings of currents induced by extracellular GABA application in fetal hWGE-, post-natal mWGE and hESC-derived neurons demonstrate that ionotropic GABA

receptors are present and functional in these cells (Figure 5.3). The concentration-response curves for these currents were plotted for each cell type providing EC_{50} values which are similar to those observed for $GABA_A$Rs in previous findings from neuronal populations. The EC_{50} values of 19.9 µM, 7.2 µM and 53.4 µM were predicted for hWGE-, mWGE- and hESC-derived neurons, respectively. These compare with values of 20 µM in post-natal day 1-14 in rat hypothalamus (Huang & Dillon, 2002), 111 µM in gestational week 5-8 human dorsal root ganglion (Valeyev *et al.*, 1999) and 11 µM in post-natal day 14 rat striatum (Olga A, 1998). Furthermore, the inward currents elicited by extracellular GABA (Figure 5.3) are characteristic in shape of these previously reported Cl^- selective $GABA_A$Rs. The calculated reversal potential for Cl^-, using the Nernst equation and the solutions used in the experiment, is -2.2 mV. In fetal hWGE-derived neurons, the predicted reversal for GABA-induced currents (after leak subtraction) was 1.6 mV (Figure 5.4), providing further weight to the suggestion that these channels are $GABA_A$Rs.

The selective $GABA_A$R antagonist, picrotoxin (PTX), was used to establish further the presence of these receptors in fetal hWGE-derived neurons. In whole-cell patch clamp, pre- and co-application of 50 µM PTX reversibly blocked mean peak GABA-induced currents by approximately 75% (Figure 5.5). This effect on $GABA_A$Rs was also measured indirectly as a 66% reduction in the transient intracellular Ca^{2+} rise resulting from GABA-induced Cl^- efflux-mediated membrane depolarisation (Figure 5.6).

That, unlike GABA currents, Ca^{2+} transients resulting from extracellular GABA applications were not observed in all cells, even those shown to have voltage-gated Ca^{2+} channels, suggested that, in some cells, $GABA_A$R-mediated Cl^- movement did

not result in depolarisation of the membrane potential past the activation threshold for voltage-gated Ca^{2+} channels. In order to test this idea, the extracellular concentration of Cl^- was reduced sequentially, altering the Cl^- equilibrium and forcing a greater depolarising shift upon $GABA_AR$ activation. This reduction in extracellular Cl^- bought about Ca^{2+} transients in cells which previously showed inhibitory responses in the control solution, and increased Ca^{2+} transient sizes in those cells which already displayed excitatory responses to GABA. This suggests that within the fetal hWGE-derived neuronal population there is heterogeneity within the population of cells where GABA is either excitatory, or inhibitory in response to $GABA_AR$ stimulation.

5.4.3. Development of GABAergic Signalling in hWGE-Derived Neurons

As the 'switch' of GABA responses from excitatory to inhibitory is implicated in neuronal development (Ben-Ari, 2002), the presence of inhibitory cells in relatively immature neuronal populations was further investigated. Measurements of cells displaying voltage-gated Ca^{2+} channel activity (in response to 50 mM K^+ depolarising stimulus) were made in response to GABA applications made in normal (144.9mM) and low (9.9 mM) extracellular solutions. The percentage of cells displaying excitatory responses was recorded at 3 PPD time points. Measurements at 1-2, 6-7 and 14-16 DIV were compared with those from post-natal day 1 mWGE-derived neurons at 2 DIV.

Previous results have shown that early (1-5 day) post-natal, and embryonic (E18) rat neurons display 100% excitatory GABA responses at 1-3 DIV and that these responses 'switch' during continued culture over approximately 14 days to 0% excitatory (Ganguly *et al.*, 2001; Rego *et al.*, 2001).

In fetal hWGE-derived neurons at 1-2 DIV only 66.46% of neurons displayed excitatory responses to GABA Figure 5.8. This value decreased during continued culture reaching 45% at DIV 6-7 and 22% by DIV 14-16. In post-natal day 1 mWGE-derived neurons 89% were shown to have excitatory responses to GABA.

That there is such a difference (66% vs. 89%) between human and mouse-derived neurons is interesting in that it highlights the potential for a variation in what is now considered a fundamental characteristic of neuronal development. In all cells displaying inhibitory responses, the presence of both $GABA_A$Rs and voltage-gated Ca^{2+} channels were confirmed through repeat application of GABA in a low Cl^- solution. This removed the potential for non-neuronal cells, or those without voltage-gated Ca^{2+} channels, from providing false negative results. It is also interesting to note that, unlike the results of previous studies on immature rat neurons, the percentage of excitatory responses was not reduced fully to 0% by DIV 16 in fetal hWGE-derived neurons.

5.4.4. Bumetanide Switches Excitatory GABA Responses to Inhibitory

In order to investigate the relationship between intracellular Cl^- concentrations and the observed excitatory or inhibitory responses to GABA, the effect of a selective blocker of NKCC1 (a transporter of Cl^-) on excitatory responses was measured. NKCC1 activity has been linked to GABA excitation/inhibition in a number of studies (Ben-Ari, 2002; Nabekura *et al.*, 2002; Palma *et al.*, 2006). The use of bumetanide for the modification of excitatory responses to inhibitory responses represents a potential tool for modulation of differentiation in hESCs.

In fetal hWGE-, post-natal mWGE- and hESC-derived neurons displaying excitatory responses to extracellular GABA application, bumetanide was shown to modulate the GABA response, 'switching' the response from excitatory to inhibitory (Figure 5.9) in the majority of cells (Figure 5.10). In fetal hWGE-derived neurons, bumetanide treatment resulted in loss of excitatory responses in approximately 95% (42/44) of cells (which displayed excitatory responses in control solution). This effect was reversible, with excitatory responses recorded in approximately 80% (35/44) of cells after bumetanide washout. This pattern was repeated for post-natal mWGE- and hESC-derived neurons with a loss of 94% and 93% during bumetanide application and recovery after washout in 100% and 78% of cells, respectively.

5.4.5. NS1619 Switches Inhibitory GABA Responses to Excitatory

When considering aspects of excitatory/inhibitory GABA responses it is important to consider not only the Cl^- equilibrium potential but also the V_m of the cell. If the V_m is less negative than the E_{Cl} then activation of $GABA_A$Rs will result in a net influx of Cl^- and an associated inhibitory hyperpolarisation of the membrane potential. Similarly, V_m values more negative than E_{Cl} will result in Cl^- efflux and excitatory depolarisation of the membrane potential. The Ca^{2+}-activated K^+ channel (BK_{Ca}) activator, NS1619, has been previously shown to hyperpolarise rat cortical neurons isolated from E18 fetuses (Gáspár *et al.*, 2008). In the fetal hWGE-derived neurons in this study, NS1619 was shown to switch inhibitory responses to extracellular GABA application to excitatory responses. This suggests that NS1619 could be used as a tool for increasing excitatory GABAergic signalling in these populations. If such an effect were to be observed in hESC-derived neurons, an increase in excitatory GABAergic signalling may result in an improved differentiation outcome. Using

bumetanide or NS1619 to modulate GABAergic signalling, as summarised in Figure 5.13, needs to be investigated further both in primary fetal neurons and hESC-derived neurons. To increase the control over cellular signalling mechanisms during differentiation could greatly reduce the variability observed between separate differentiation studies.

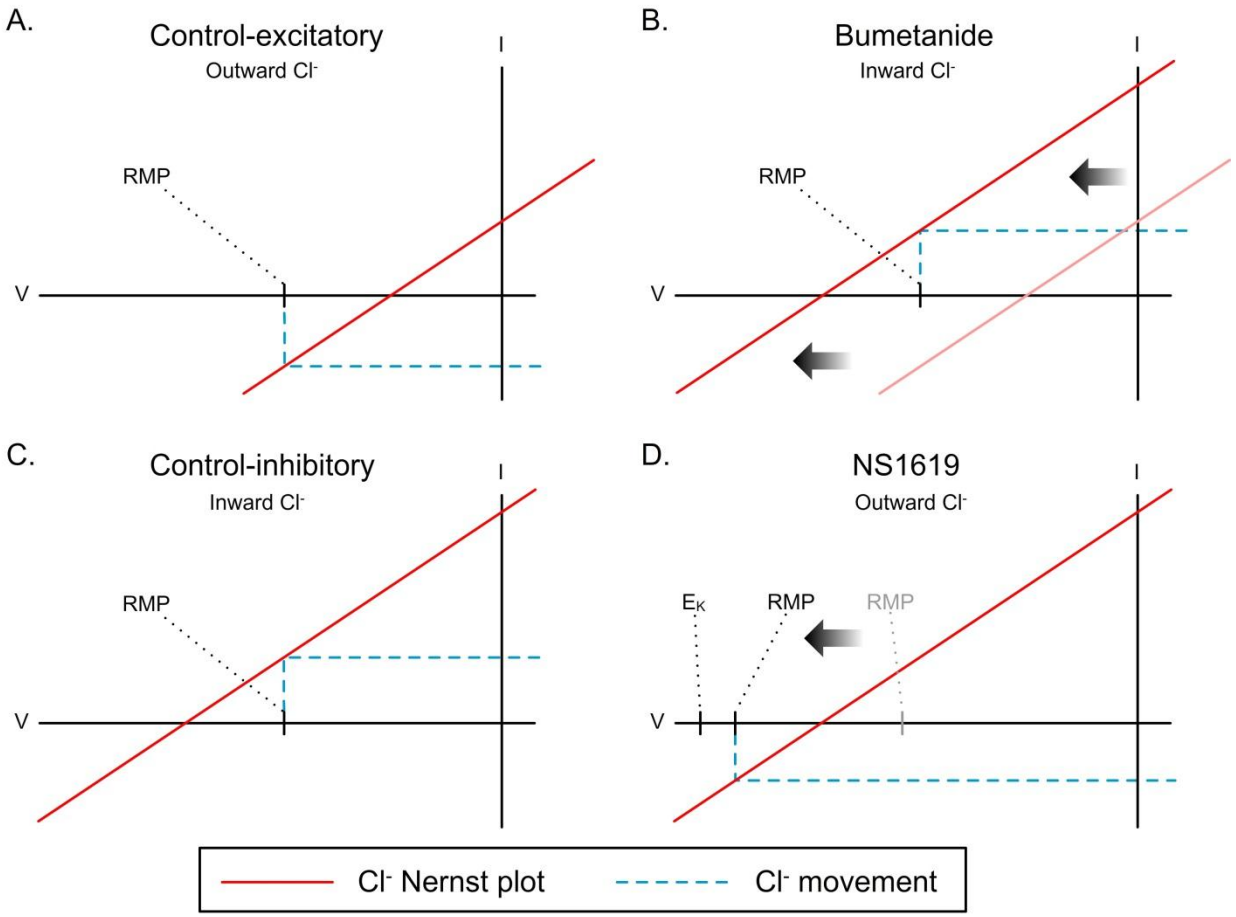

Figure 5.13. Visual representation of E_{Cl} in GABA Signalling: E_{Cl} is based on the intracellular and extracellular Cl^- concentrations. This value, along with the V_m, establishes whether $GABA_AR$ activation will result in hyperpolarisation (A. excitatory) or depolarisation (C. inhibitory). Inhibition of Cl^- uptake via NKCC1 using bumetanide (B.) shifts E_{Cl} to a less negative value and switches excitatory responses to inhibitory. Activation of BK_{Ca} channels via NS1619 application (D.) shifts V_m towards E_K switching inhibitory responses to excitatory.

Currently there are no well-defined specific inhibitors of the cation- Cl^- co-transporter KCC2. Two drugs, 4,4'-Diisothiocyano-2,2'-stilbenedisulfonic acid (DIDS)

and *R*(+)-[(2-*n*-butyl-6,7-dichloro-2-cyclopentyl-2,3-dihydro-1-oxo-1H-inden-5-yl)oxy] acetic acid (DIOA), are commonly used, but they lack the specificity required to distinguish effects on KCC2 from those of other Cl^- transporters (Rivera *et al.*, 2005; Delpire *et al.*, 2009). The advent and discovery of new drugs, such as the recently discovered N-(4-methylthiazol-2-yl)-2-(6-phenylpyridazin-3-ylthio)acetamide (D4), which specifically inhibit this transporter will hopefully allow for future studies to provide a greater understanding of the role and importance of KCC2 activity in neuronal development, similarly these drugs may become important tools for the control of endogenous GABAergic signalling during neuronal differentiation.

Chapter 6. Future Developments and General Discussion

The data presented in this thesis provide important and novel information about the development of ionotropic and metabotropic signalling mechanisms present in hESC-derived and primary neuronal cultures *in vitro*. Data are presented which indicate that several signalling mechanisms are functionally active in these populations and that there are observable changes in electrical signalling during hESC-differentiation down a neuronal lineage. Modulation of non-synaptic signalling is shown in multiple cell types providing the basis for further research into the effect of these pathways on development.

6.1. Functional Characterisation of an iPSC Line from a Huntington's Disease Patient

As previously discussed, the developing area of iPSC-development has provided cell biologists with a new tool for the study of genetic diseases during development *in vitro*. The following section outlines preliminary work carried out as part of a collaborative arrangement funded by the National Institute of Health (NIH) and the Cure Huntington's Disease Initiative (CHDI).

iPSC lines have been derived from both a patient suffering from Huntington's Disease (HD60i.4) and their non-HD sibling (HD33i.8) by Clive Svendson at Cedars-Sinai Medical Centre in the Univerisity of Wisconsin. Preliminary functional characterisation has been carried out on neurons derived from these iPSCs.

6.1.1. Huntington's Disease

Huntington's disease (HD) is an autosomal dominant trinucleotide repeat disorder resulting in progressive neurodegeneration, leading to a number of characteristic symptoms including the selective loss of medium spiny neurons from the striatum. The expansion of CAG repeats in the huntingtin gene (*HTT*) beyond 36 conveys the disease state due to alterations to the protein function and formation of protein aggregates. In the healthy brain, the ability to control voluntary movement is maintained by a complex network of inhibitory and excitatory inputs. Impulses driving movement through the upper motor neurons are inhibited by the cells of the basal ganglia during times of desired inactivity. Basal ganglionic inhibition is increased by excitatory input from the subthalamic nucleus. External globus pallidus cells can inhibit this subthalamic nucleus-excitation during desired activity. These inhibitory globus pallidus cells are usually themselves inhibited by the medium spiny neurons (MSNs) which project from the striatum into the globus pallidus. In Huntington's disease, approximately 95% of the observed neurodegeneration is attributed to loss of these MSNs, which results in reduced inhibitory control of involuntary movement through the pathway described above (Gelehrter, Collins et al. 1998; Bates and Murphy 2002). As the disease progresses degeneration of the cortex is also observed. The root cause of neurodegeneration in HD remains unknown (Landles & Bates, 2004).

Currently there are very few effective treatments of HD. Inhibitory neurotransmitters are used to reduce the random movements and antidepressants are used to alleviate the depression highly associated with disease progression, but these have unwanted side effects in many patients. The potential for

downregulation of the mutant *htt* by siRNA or correction by gene therapy has been suggested and drugs aimed at reducing or degrading the aggregations of the mutant protein have been hypothesised. No successful cure has yet been produced, and treatment is very much aimed at reducing the impact of the disorder on the patient's life rather than preventing neurodegeneration *per se* (Kim *et al.*, 2008).

6.1.2. Methods

Clive Svendson at Cedars-Sinai Medical Centre in the Univerisity of Wisconsin provided neural stem cell lines derived from the patient iPSC lines, HD33i.8 and HD60i.4, where 33 and 60 relate to the CAG repeat number in *htt* for each line, respectively. This work was carried out externally and only the culture and terminal differentiation of NSC lines was carried out within Cardiff University. The following method sections on the generation of iPSC (section 6.1.2.1. and neural stem cell (6.1.2.2. lines are included for the purpose of clarity.

6.1.2.1. Generation of iPSC Lines

Human fibroblast lines were obtained from an HD patient with 60 CAG repeats in *htt* and the non-HD sibling of the patient with 33 CAG repeats. Pluripotency reprogramming was induced by lentiviral transduction of Oct4, Sox2, Klf4, cMyc, Nanog and Lin28 as previously described (Yu *et al.*, 2007). Clonal colonies with iPSC morphology were expanded into stable iPS cell lines.

6.1.2.2. Generation of iPS-Derived Neural Stem Cell Lines

NSC lines were generated by collagenase treating iPS colonies and lifting them from feeder layers directly into Stemline media (Sigma) supplemented with 100 ng/ml basic fibroblast growth factor (bFGF, Chemicon), 100 ng/ml epidermal growth factor

(EGF, Chemicon), and 5 µg/ml heparin (Sigma) in polyhema-coated flasks to prevent attachment. iPS-derived NSCs were expanded as spherical aggregates and passaged weekly using the standard chopping technique (Svendsen *et al.*, 1998).

6.1.2.3. Terminal Differentiation of iPSC-Derived Neurons

NSC lines were plated onto glass coverslips for terminal differentiation using the method described in section 2.1.4. Growth media (SFDMII) was supplemented with the notch inhibitor N-[N-(3,5-Difluorophenacetyl)-L-alanyl]-S-phenylglycine t-butyl ester (DAPT, 2.5 µM , Sigma) and ascorbic acid (200 µM, Sigma).

6.1.2.4. Functional Characterisation of iPSC Lines

Neurons derived from the two iPSC lines were functionally characterised after 2 weeks of the terminal differentiation protocol. The preliminary electrophysiological characterisation was carried out as described in section 2.2.2.

6.1.3. Results

The preliminary functional analysis of the iPSC lines consisted of similar experiments to those carried out on the hESC-derived neurons in section 4.3.3. The capacitance, voltage-gated channel activity and action potential capabilities of these cells were measured. This work was carried out as a preliminary study to determine whether these cells were amenable to the experimental protocols used throughout the previous work within this thesis. The data are, therefore, not intended to provide conclusive evidence for an effect of the Huntingtin mutation in these cells. Further work, including a full characterisation at various time points throughout terminal differentiation, is planned as part of the on-going collaboration within HD iPSC disease modelling consortium funded by CHDI and the NIH.

6.1.3.1. iPSC-Derived Neurons Display Functional Neuronal Characteristics

Capacitance was measured for each cell from the iPSC-derived neurons from both lines. Box and whisker plots of these data are shown in Figure 6.1. The mean capacitance values were 18.6 and 8.7 pF for HD33i.8 and HD60i.4, respectively.

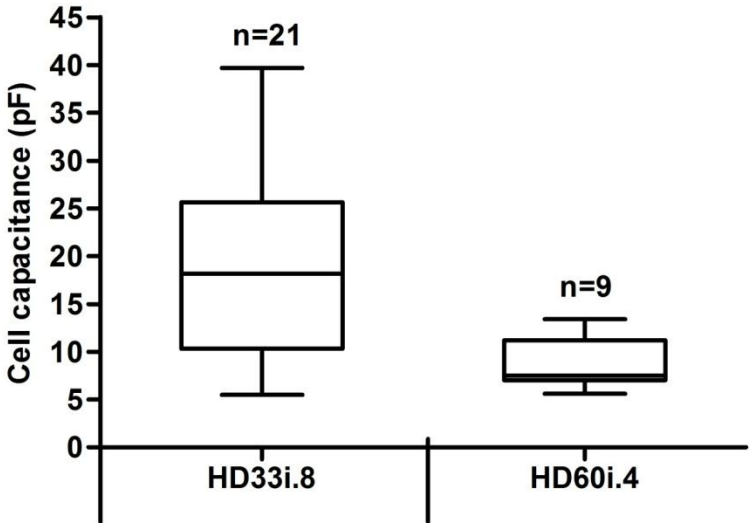

Figure 6.1. Cell capacitance in iPSC-derived neurons: The recorded capacitance (pF) for each cell during terminal differentiation of iPSC-derived neurons was recorded. Box plots of the data are show here from the two iPSC lines.

Voltage-gated channel activity similar to that observed in primary and hESC-derived neurons was observed in neurons derived from both iPSC-lines (Figure 6.2 and Figure 6.3).

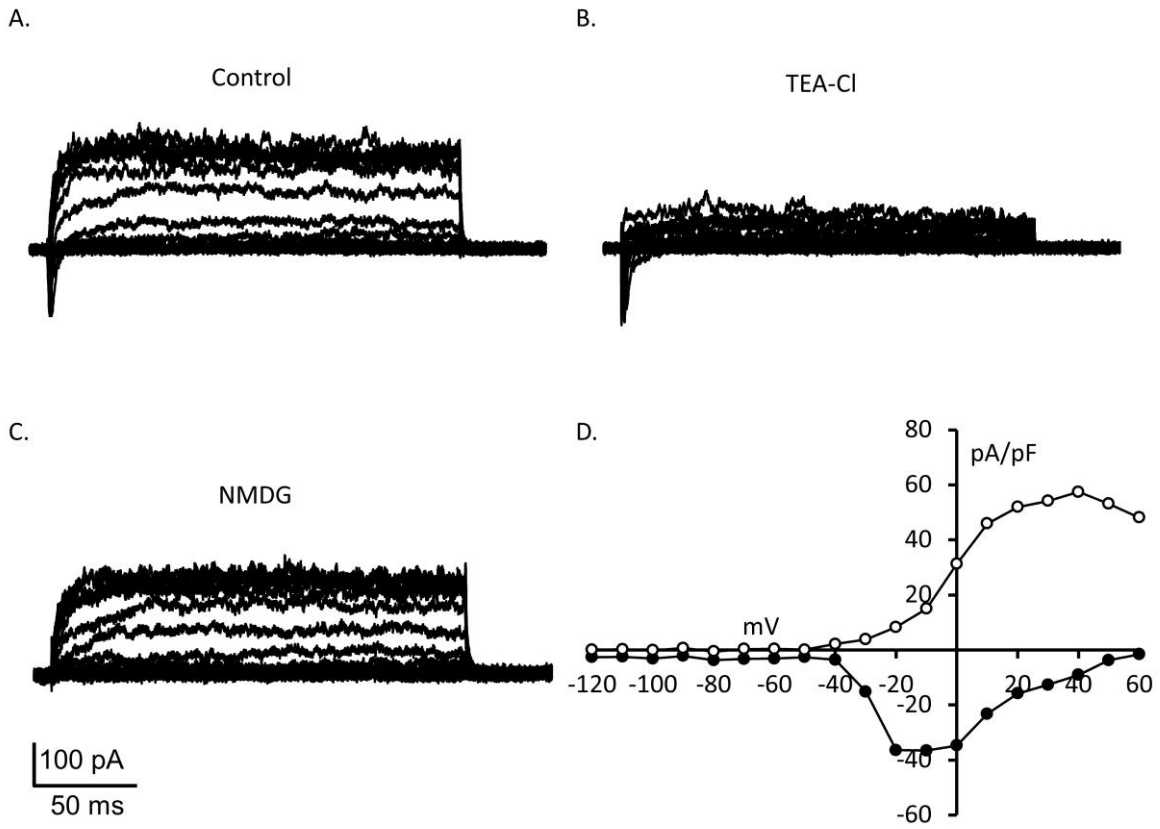

Figure 6.2. Voltage-activated currents in a neuron from the HD33i.8 line: Example traces showing the currents elicited by a voltage-step protocol are shown (A, B and C). A. Voltage-activated currents in control (ECS) solution. B. Voltage-activated currents in the presence of 20 mM TEA-Cl. C. Voltage-activated currents during the replacement of extracellular Na^+ with NMDG. D. The current-voltage curves for the mean outward plateau (open circles) and minimum inward peak (filled circles).

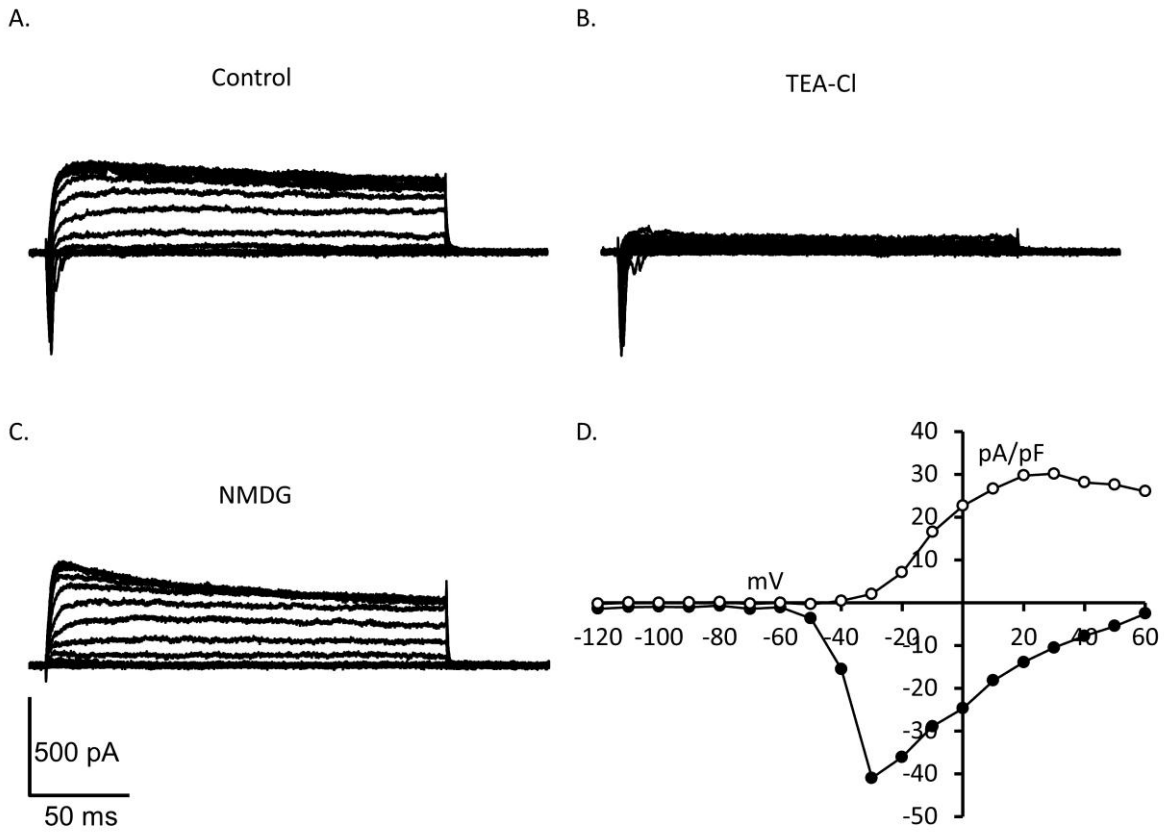

Figure 6.3. Voltage-activated currents in a neuron from the HD60i.4 line: Example traces showing the currents elicited by a voltage-step protocol are shown (A, B and C). A. Voltage-activated currents in control (ECS) solution. B. Voltage-activated currents in the presence of 20 mM TEA-Cl. C. Voltage-activated currents during the replacement of extracellular Na^+ with NMDG. D. The current-voltage curves for the mean outward plateau (open circles) and minimum inward peak (filled circles).

The K^+ and Na^+ current amplitudes for each iPS-line were calculated. Box-and-whisker plots of these data are shown in Figure 6.4. and Figure 6.5, respectively. The mean K^+ current amplitudes were 42.6 and 40.9 pA/pF and the mean Na^+ current amplitudes were -47.0 and -49.4 pA/pF for HD33i.8 and HD60i.4, respectively.

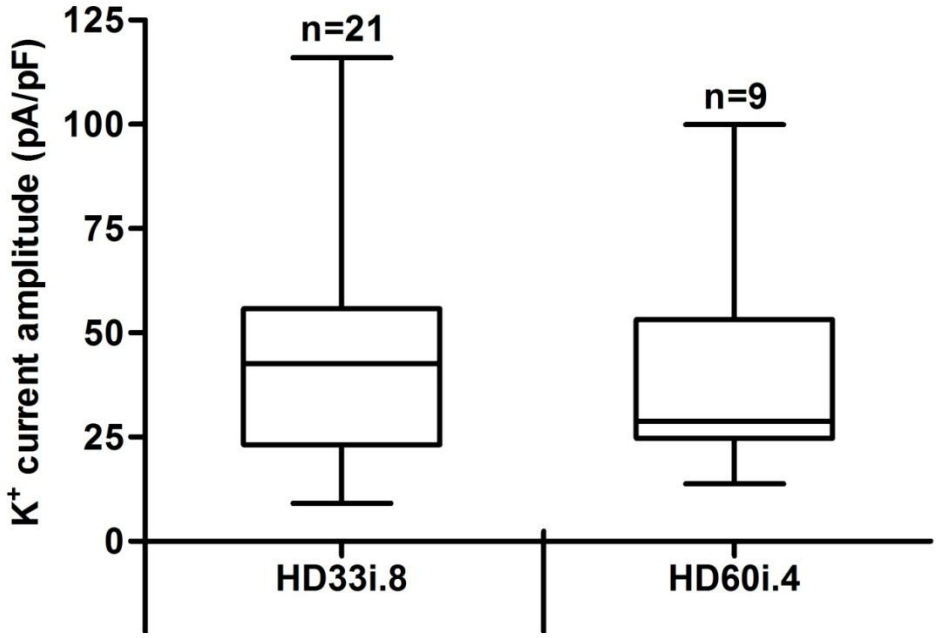

Figure 6.4. K^+ channel amplitudes in iPSC-derived neurons: Average K^+ current amplitude (pA/pF) for the two iPSC lines are shown (Boxes represent upper and lower quartiles, vertical bars represent the range, numbers indicated above bars).

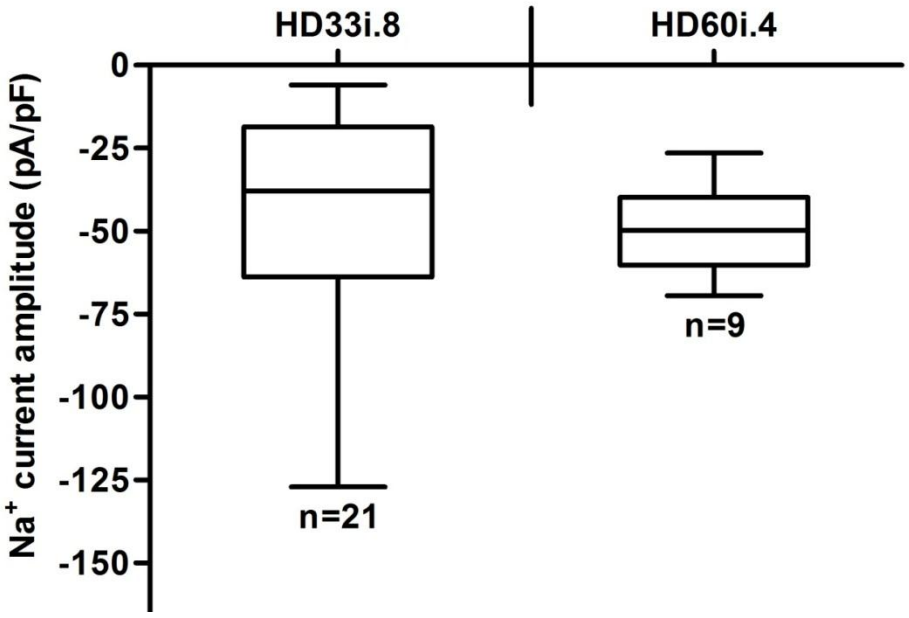

Figure 6.5. Na^+ channel amplitudes in iPSC-derived neurons: Average Na^+ current amplitude (pA/pF) for the two iPSC lines are shown (Boxes represent upper and lower quartiles, vertical bars represent the range, numbers indicated below bars).

The percentage of cells displaying Na^+ channel activity in neurons derived from the HD33i.8 (81%) and HD60i.4 (100%) iPSC-lines are shown in Figure 6.6.

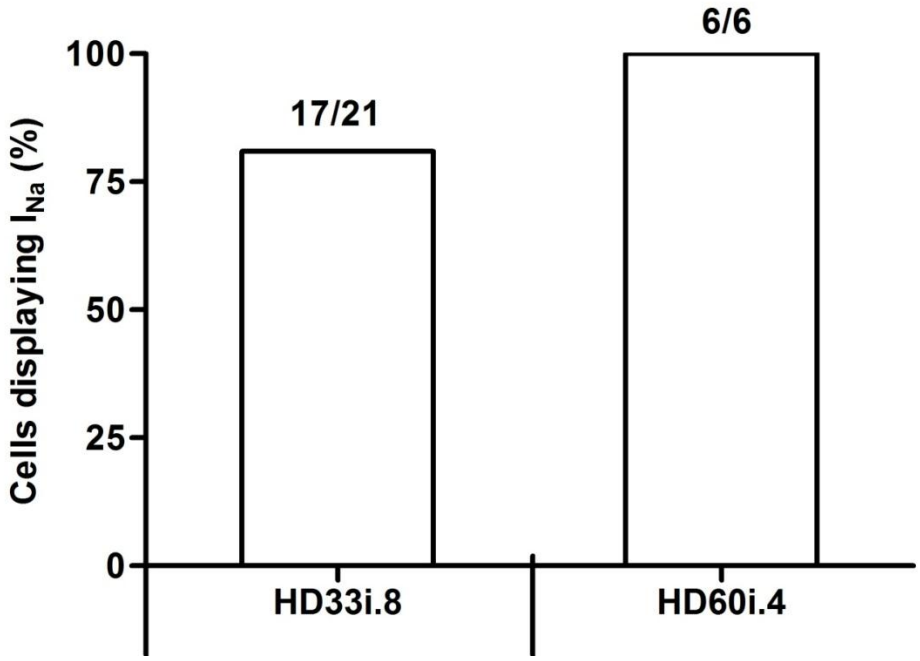

Figure 6.6. Percentage of cells with voltage-gated Na^+ channels in iPSC-derived neurons: The percentage of cells displaying voltage-gated Na^+ channel activity using the voltage-step protocol are shown for the two iPSC lines (numbers are given above each bar).

Action potential-like responses were evoked upon current stimulation in neurons derived from both iPSC-lines (Figure 6.7).

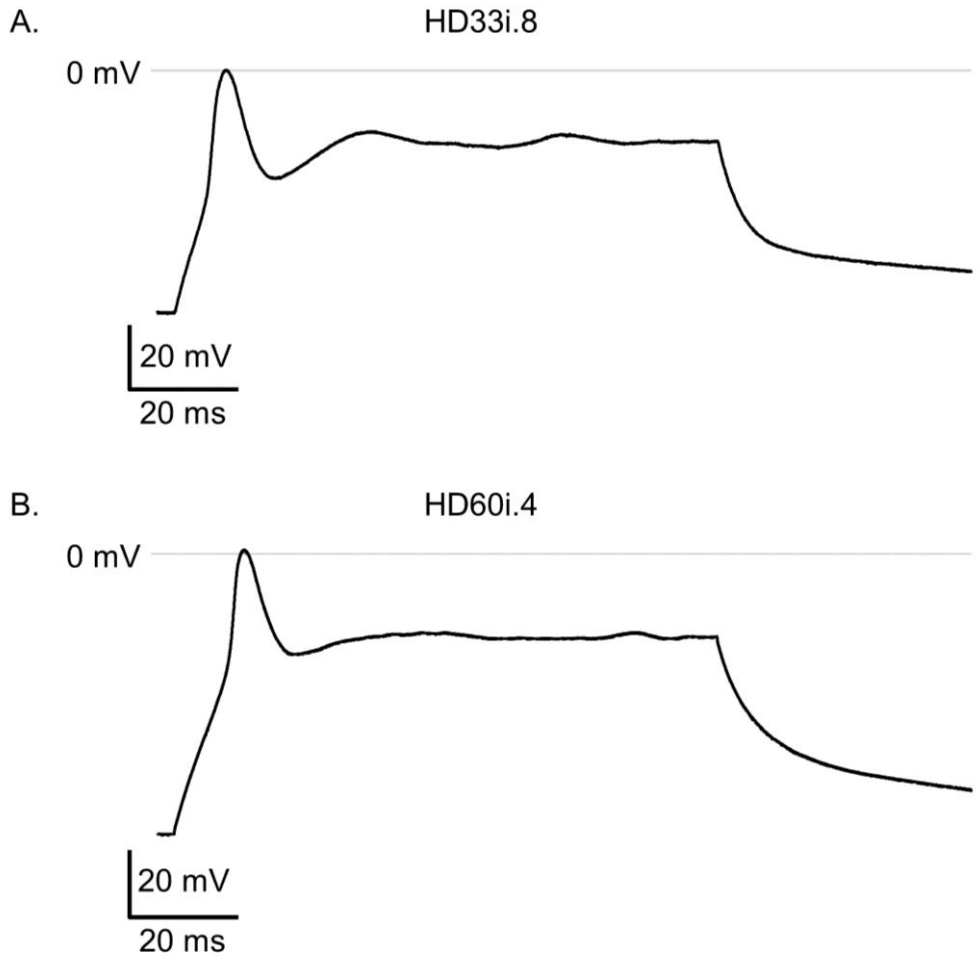

Figure 6.7 Induced action potentials in iPSC-derived neurons: An example iAP is shown from one cell from each iPSC-line.

The percentage of cells displaying iAPs in neurons derived from the HD33i.8 (41.6%) and HD60i.4 (60%) iPSC-lines are shown in Figure 6.8.

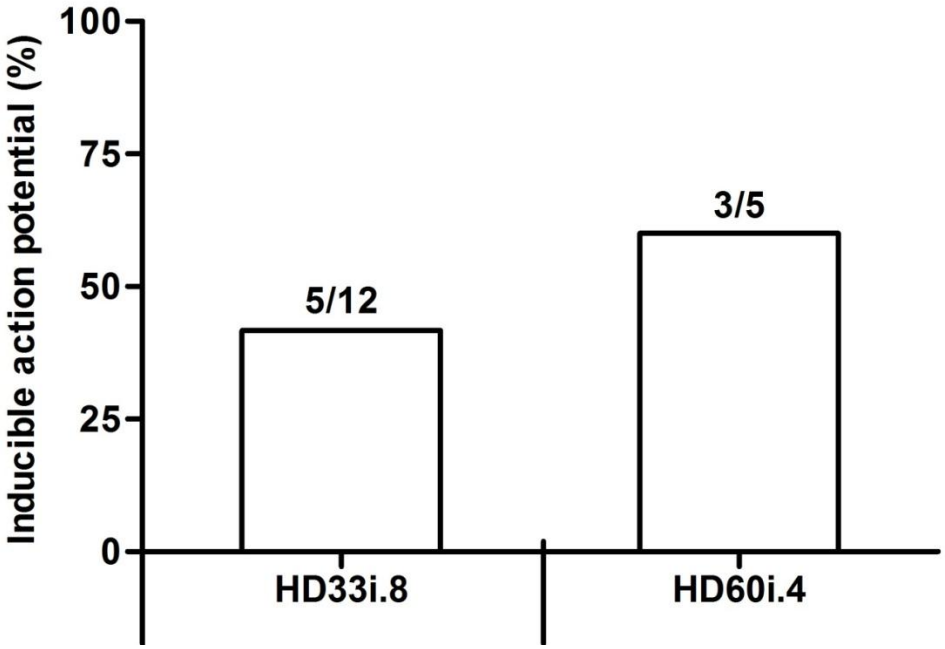

Figure 6.8 Percentage of cells with inducible action potentials in iPSC-derived neurons: The percentage of cells displaying iAPs using the current-step protocol are shown for both iPSC- lines (numbers are given above each bar).

The iAP thresholds for each iPS-line were calculated and box-and-whisker plots of these data are shown in Figure 6.9. The mean iAP thresholds were -38.2 and -35.7 mV for HD33i.8 and HD60i.4, respectively.

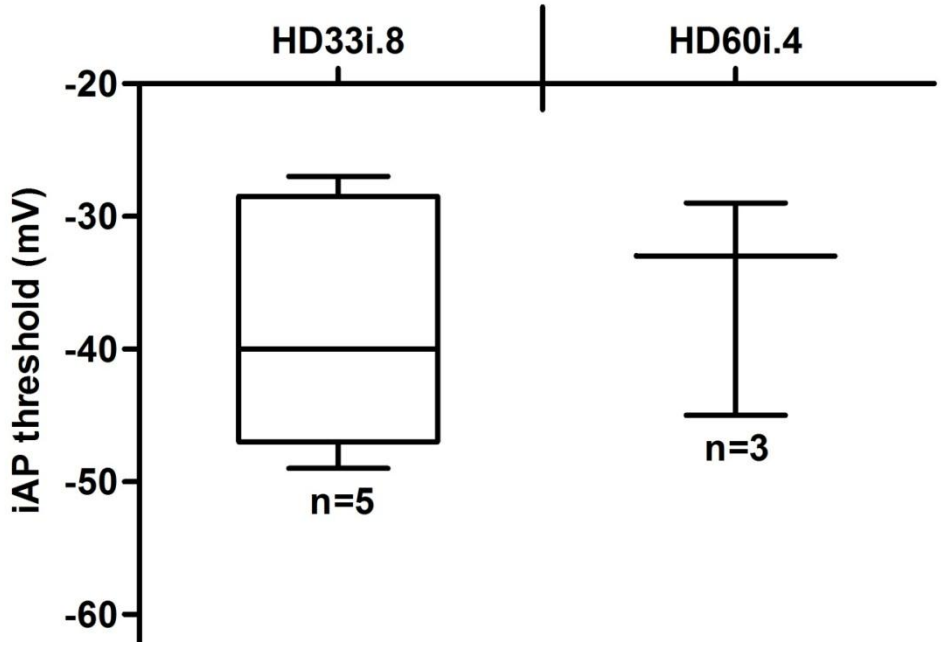

Figure 6.9 iAP threshold values in iPSC-derived: The average iAP threshold values for the two iPSC-lines are shown (Boxes represent upper and lower quartiles, vertical bars represent the range, numbers indicated below bars).

V_m was calculated for each iPS-line. Box-and-whisker plots of these data are shown in Figure 6.9. The mean V_m values were -46.7 and -49 mV for HD33i.8 and HD60i.4, respectively.

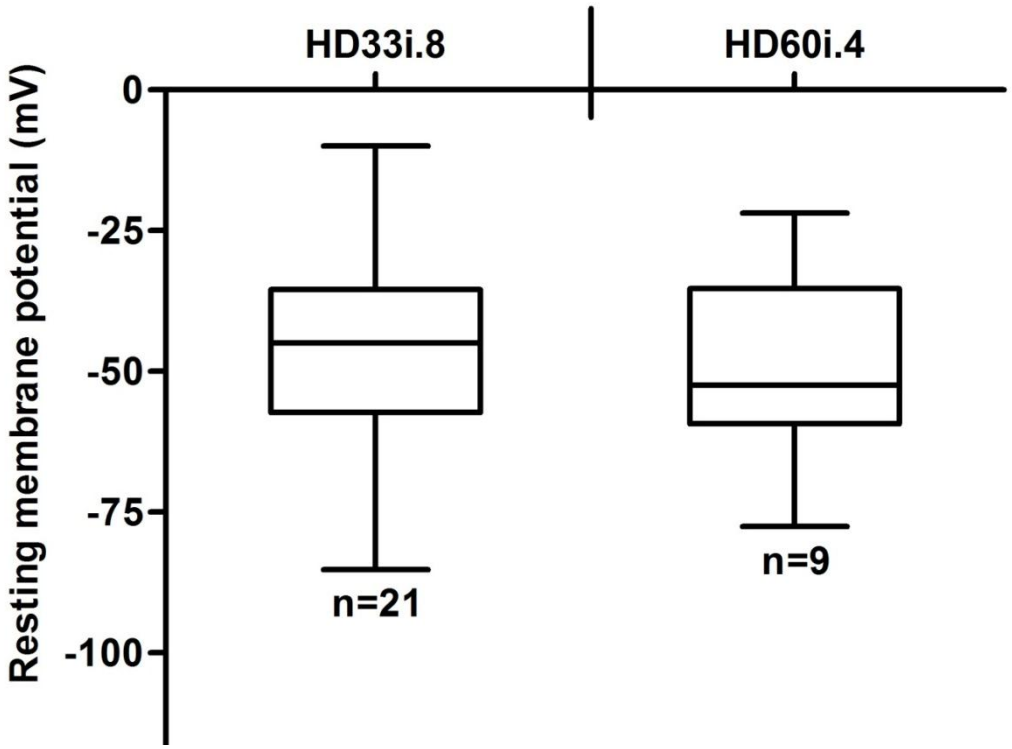

Figure 6.10 Resting membrane potential values in iPSC-derived neurons: The average V_m for the iPSC-lines are shown (Boxes represent upper and lower quartiles, vertical bars represent the range, numbers indicated below bars).

As was observed in hESC-derived neurons, none of the recorded cells from either HD33i.8 (*n* = 21) or HD60i.4 (*n* = 9) displayed spontaneous activity during recording of V_m.

6.1.4. Conclusions

The observation that Huntington's Disease carrying iPSC-derived neurons display functional characteristics similar to those observed in both primary and hESC-derived neurons suggests that these cells may be useful as tools for the study of this disease *in vitro*.

The presence of voltage-gated K^+ channels in all cells and Na^+ channels in the majority of cells is similar to the data obtained from primary and hESC-derived cells at 2 weeks PPD. Similarly, the ability of at least some of these cells to fire an action

potential upon current injection indicates a neuronal phenotype and suggests these cells may be amenable to electrical signalling. The relatively depolarised membrane potentials coupled with the apparent absence of spontaneous activity suggest that, at the measured stage of the differentiation protocol (week 2), these cells are not yet being influenced by such electrical signalling and that they may need further maturation in order to more optimally mimic primary tissue.

As has been mentioned, these data are preliminary findings which will form the basis of a larger study of the functional properties of these cells and any potential differences which are CAG-repeat number-dependent. However, they do indicate that these cells are functionally neuronal. Further characterisation, of not only their voltage-gated channel and action potential activity, but also their responses to various neurotransmitters, will provide data which can indicate an influence of the disease-state on neuronal function. In this regard, it has already been shown within our lab that neurons derived from the HD60i.4 and another iPSC line (HD180i.5/7 – from a patient with 180 CAG repeats) have compromised Ca^{2+} homeostasis during repeated extracellular applications of NMDA indicating an increases susceptibility to glutamatergic excitotoxicity, potentially leading to caspase activation and augmented cell death (manuscript submitted to Cell Stem Cell).

6.2. General Discussion

During development, cell signalling plays a crucial role in the control of apoptosis, proliferation, migration, fate-determination and also neuronal specific developmental properties such as voltage-gated ion channel expression, neurotransmitter specification, axon path-finding, neuronal survival and integration into existing neuronal circuitry.

6.2.1. Purinergic Signalling in Stem Cell Populations

The observation that purinergic receptors are present within undifferentiated hESC populations suggests that not only may purinergic signalling have the capacity to influence hESC development, but also that the results of previously published studies on the effects of purinergic signalling in similar, non-embryonic stem cell populations may be used to predict the effect in hESCs. That ATP can induce a transient rise in $[Ca^{2+}]_i$ provides a mechanism by which this signalling may be able to influence gene expression and protein activity (Webb *et al.*, 2005; Greer & Greenberg, 2008). This raises the possibility that agonists and antagonists of purinergic receptors may be utilised for the control of receptor activity during differentiation procedures which may provide new options for targeted differentiation protocols.

Purinergic signalling has also been shown to regulate neuronal progenitor proliferation and neuronal differentiation (Lin *et al.*, 2007). The potential for recruitment of stem-cell like populations from neurogenic regions of the adult brain offers a therapeutic option which is independent of the introduction of exogenous tissue or cells. That purinergic signalling may play a part in the control of such stem-cell populations is exciting as it suggests that regulation of such signalling, either through control of the relevant receptor activity using agonists and antagonists, or through modulation of downstream signalling cascades, could be clinically beneficial.

Furthermore, the presence of purinergic signalling in stem-cell populations and the link between cellular stress and the release of ATP (Bodin & Burnstock, 2001) has both *in vitro* and *in vivo* implications. During routine cell culture, regular periods of

physical stress are imposed upon cell populations, especially during dissociation. Similarly, during surgical procedures, large sections of the patients' tissue undergo severe physical trauma. The combination of these situations during neuronal transplantation, where NSCs cultured in the lab are routinely dissociated before being surgically transplanted into the adult brain (Brundin *et al.*, 2010), highlights the importance of understanding this mechanism further.

There is already evidence that purinergic signalling, specifically $P2Y_1$-meditated transient increases in $[Ca^{2+}]_i$, effects adult NSCs (Mishra *et al.*, 2006; Lin *et al.*, 2007). In these studies, $P2Y_1$ signalling was shown to stimulate proliferation in these cells and was hypothesised to modulate neurogenesis in the adult brain. Data presented in this thesis show that hESCs also have the capacity for ATP-mediated autocrine regulation.

6.2.2. Functional Characterisation of hESC-Derived Neurons

By measuring functional neuronal characteristics in hESC-derived neurons and comparing them with foetal hWGE- and neonatal mWGE-derive neurons, it has been shown functionally that these hESC-derived neurons are not as mature as primary-derived populations. The presence, and increased prevalence, of voltage-gated channel activity, specifically Na^+ and Ca^{2+} channels, confirms that these cells are differentiating down a neuronal lineage in terms of both their gene and protein expression, and with respect to their excitability. The ability to fire action potentials is a fundamental characteristic of a neuron. That these cells display this ability is further evidence of their neuronal fate-determination. However, the lack of spontaneous activity in these cells suggests that, using the current differentiation protocol, these cells are not maturing to a stage where spontaneous electrical

signalling is influencing their development. The differences in V_m and iAP threshold values between these cells and the neonatal mWGE-derived neurons suggest that hESC-derived neurons retain an immature functional phenotype during the terminal differentiation protocol. However, compared to the fetal hWGE-neurons, a greater percentage of these cells displayed neuronal characteristics suggesting they are developing to a more homogeneously neuronal population. That these cells appear to undergo a degree of maturation towards a neuronal fate and yet fail to display mature neuronal properties suggests that they are maintained in a neuronal precursor phenotype. This has implications regarding their use as both therapeutic agents, and as models of disease.

The majority of successful neuronal grafting has been carried out using either fetal-brain-derived NSC populations (Lindvall & Bjorklund, 2004; Kelly *et al.*, 2011; Trounson *et al.*, 2011). These populations, like the fetal hWGE-neurons studied in this chapter, have been shown to display neuronal characteristics, but have also been shown to be developmentally immature compared to adult neurons (Ogawa *et al.*, 2009). It is possible that the immaturity of hESC-derived neuroprogenitor populations may in fact improve their therapeutic potential as these cells may be at a developmental stage which would still permit further proliferation and recruitment into adult neuronal circuitry that would be otherwise less apparent in a more mature population. Further work regarding the functional development of these cells within host tissues is required. Understanding the effects of endogenous signalling pathways present *in vivo* which may modulate stem-cell-derived neuronal integration will hopefully enable improved graft-survival and clinical benefit in the future.

In terms of their use as disease models, that these cells display a more immature phenotype suggests they may not be ideal for modelling the mature neuronal populations of the adult brain. This area requires that populations be accurately represented both in terms of developmental progress and functional activity. An increased understanding of, and ability to regulate, *in vitro* differentiation will ultimately yield cells which are more developmentally similar to adult tissues.

However, to suggest that under current differentiation protocols hESC-derived neurons are not useful for disease modelling due to their immaturity would be to overlook a potentially valuable resource. The study of functionally immature cells which show a degree of similarity to those of the developing brain offers an insight into clinically relevant processes. Increased knowledge of developmental processes will undoubtedly shed light on an area of great clinical significance. Also, by studying and improving upon these incomplete developmental protocols, it is likely that a greater understanding of neuronal maturation will be gained.

6.2.3. GABAergic Signalling in Fetal hWGE-Derived Neurons

The observation that GABA signalling is present and active in fetal hWGE-, neonatal mWGE- and hESC-derived neuronal populations provides evidence for a mechanism enabling functional modulation of these cells via this neurotransmitter. Currently, a great deal of evidence has been provided that GABAergic signalling modulates developmental processes in the developing rodent brain (Ge, 2006; Cancedda *et al.*, 2007; Parga *et al.*, 2007). It has been shown previously that, during neuronal maturation, GABAergic signalling switches from excitatory (immature) to inhibitory (mature). The mechanism of this switch has been shown to be dependent of the balance between intracellular and extracellular Cl^- concentrations, primarily

controlled by the expression of the Cl^- transporters, NKCC1 and KCC2. Evidence that excitatory GABAergic signalling increases neural precursor proliferation, migration and neuronal differentiation (Ben-Ari, 2002) alongside the observation that, following neuronal trauma, adult neuronal populations undergo a switch back to inhibitory GABAergic signalling via down-regulation of KCC2, serves to highlight the importance of this signalling mechanism (Nabekura *et al.*, 2002).

The most striking and completely novel observation in this study was that fetal hWGE-derived neuronal populations appear to contain neurons which are already inhibitory in their response to GABA. The presence of cells displaying inhibitory-responses to GABA in mouse populations has only ever been shown in post-natal neurons. That these may already be present during fetal neuronal development in humans highlights the issues associated with the use of animal models for human development and suggests that the mechanism of GABA regulation during human neuronal development must be reconsidered.

Similarly, sustained *in vitro* culture of these fetal hWGE-derived neurons, whilst showing a reduction in excitatory GABAergic signalling, did not switch all cells towards an inhibitory response to GABA, as has been observed in mouse-derived populations previously. This may be indicative of a longer period of maturity in these cells, but again highlights an observable difference in an important signalling mechanism which may be reflected in further developmental differences.

The modulation of GABAergic signalling in stem-cell populations has been suggested as a tool for the control of the downstream effects on development in these populations (Represa & Ben-Ari, 2005; Delpire *et al.*, 2009). The potential benefit of

such control during *in vitro* neuronal differentiation is more than apparent. Similarly, the presence of excitatory GABAergic signalling in neurogenic regions of the adult brain further highlights the importance of understanding and potentially controlling this phenomenon. By efficiently modulating the excitatory/inhibitory nature of GABAergic signalling in neuronal populations it may be possible to enhance the endogenous recruitment of neurogenic populations in the brain, improve the functional integration of transplanted neurons into the host brain and optimise the differentiation of functionally mature neuronal populations for disease modelling.

The similarity between purinergic and GABAergic signalling in stem-cell populations is notable. Both are linked heavily with apoptosis (Zhang *et al.*, 2007), proliferation (Fiszman *et al.*, 1999; Liu *et al.*, 2005), migration (Bolteus & Bordey, 2004; Manent, 2005) and terminal differentiation (Tozuka *et al.*, 2005; Parga *et al.*, 2007). Both are present in embryonic and prenatal neuronal populations (Cancedda *et al.*, 2007). Both have been linked to control of neurogenic regions of the adult brain (Ge, 2006; Parga *et al.*, 2007). *In vitro* modulation of either has yielded measurable effects on the neuronal populations studied (Yamada *et al.*, 2004; Represa & Ben-Ari, 2005; Rivera *et al.*, 2005). Whilst these areas require much more research, it is apparent that such work may provide tangible benefits to both *in vitro* and *in vivo* applications.

6.2.4. iPSC-Derived Neurons Display Functional Neuronal Characteristics

The observation that iPSC-derived neurons behave in a similar manner to hESC-derived neurons *in vitro* suggests that any of the advances in hESC differentiation should be directly applicable to iPSC populations. Although both populations have

been shown to differentiate into functionally immature neurons, this does not mean they cannot be used to study the effects of the disease-state on neuronal development. Indeed, work on-going within our lab has uncovered an apparent functional phenotype in HD iPSCs which is dependent on the CAG repeat length responsible for the disease-state. This alone highlights the importance of further investigation into iPSC-derived neurons carrying known disease mutations.

6.3. Concluding Remarks

Ionotropic- and metabotropic-receptor mediated cell signalling during development, when compared with gene and protein expression, is an area which has been largely overlooked and is still relatively poorly understood. The absence of control over many of these signalling pathways during *in vitro* culture and differentiation provides a potential source of variability which could have tremendous effects on developmental outcome. The benefits of an increased knowledge and control over such pathways are apparent for both *in vitro* modelling and *in vivo* therapeutic strategies. The work described in this thesis provides a base for further study of both purinergic and GABAergic signalling within human stem-cell populations as well as a better understanding of the comparative functional properties of hESC-derived, iPSC-derived and primary human neuronal populations.

Chapter 7. References

Abe Y, Furukawa K, Itoyama Y & Akaike N. (1994). Glycine response in acutely dissociated ventromedial hypothalamic neuron of the rat: New approach with gramicidin perforated patch-clamp technique. *J Neurophysiol* **72,** 1530-1537.

Aboody K, Capela A, Niazi N, Stern JH & Temple S. (2011). Translating stem cell studies to the clinic for cns repair: Current state of the art and the need for a rosetta stone. *Neuron* **70,** 597-613.

Agnew WS, Levinson SR, Brabson JS & Raftery MA. (1978). Purification of the tetrodotoxin-binding component associated with the voltage-sensitive sodium channel from electrophorus electricus electroplax membranes. *Proc Natl Acad Sci U S A* **75,** 2606-2610.

Alexander GE, Crutcher MD & Delong MR. (1990). Basal ganglia-thalamocortical circuits - parallel substrates for motor, oculomotor, prefrontal and limbic functions. *Prefrontal Cortex* **85,** 119-146.

Alexander SPH, Mathie A & Peters JA. (2009). Guide to receptors and channels (grac), 4th edition. *Br J Pharmacol* **153,** S1-S1.

Arlotta P, Molyneaux BJ, Jabaudon D, Yoshida Y & Macklis JD. (2008). Ctip2 controls the differentiation of medium spiny neurons and the establishment of the cellular architecture of the striatum. *J Neurosci* **28,** 622-632.

Armstrong CM & Bezanilla F. (1977). Inactivation of sodium channel .2. Gating current experiments. *J Gen Physiol* **70,** 567-590.

Armstrong CM & Binstock L. (1965). Anomalous rectification in squid giant axon injected with tetraethylammonium chloride. *J Gen Physiol* **48,** 859-&.

Bachoud-Levi AC, Maison P, Bartolomeo P, Boisse MF, Dalla Barba G, Ergis AM, Baudic S, Degos JD, Cesaro P & Peschanski M. (2001). Retest effects and cognitive decline in longitudinal follow-up of patients with early hd. *Neurology* **56,** 1052-1058.

Bakay RAE & King FA. (1986). Transplanted fetal monkey neurons. *Lancet* **2,** 163-163.

Baker PF, Hodgkin AL & Shaw TI. (1961). Perfusion of giant nerve fibres of loligo. *Journal of Physiology-London* **157,** P25-&.

Barker RA & Barasi S. (1999). *The anatomical and functional organisation of the nervous system*. Blackwell Science, New York.

Bean RC, Shepherd WC, Chan H & Eichner J. (1969a). Discrete conductance fluctuations in lipid bilayer protein membranes. *J Gen Physiol* **53,** 741-&.

Bean RC, Shepherd WC & Eichner JT. (1969b). Divalent cation and polycation modification of excitability characteristics in lipid bilayer membranes. *Biophys J* **9,** A31-&.

Behar TN, Schaffner AE, Scott CA, Greene CL & Barker JL. (2000). GABA receptor antagonists modulate postmitotic cell migration in slice cultures of embryonic rat cortex. *Cereb Cortex* **10,** 899-909.

Behar TN, Schaffner AE, Scott CA, O'Connell C & Barker JL. (1998). Differential response of cortical plate and ventricular zone cells to GABA as a migration stimulus. *J Neurosci* **18,** 6378-6387.

Ben-Ari Y. (2002). Excitatory actions of GABA during development: The nature of the nurture. *Nat Rev Neurosci* **3,** 728-739.

Ben-David U & Benvenisty N. (2011). The tumorigenicity of human embryonic and induced pluripotent stem cells. *Nat Rev Cancer* **11,** 268-277.

Bezanilla F & Armstrong CM. (1977). Inactivation of sodium channel .1. Sodium current experiments. *J Gen Physiol* **70,** 549-566.

Bianchi BR, Lynch KJ, Touma E, Niforatos W, Burgard EC, Alexander KM, Park HS, Yu H, Metzger R, Kowaluk E, Jarvis MF & van Biesen T. (1999). Pharmacological characterization of recombinant human and rat p2x receptor subtypes. *Eur J Pharmacol* **376,** 127-138.

Bibel M, Richter J, Schrenk K, Tucker KL, Staiger V, Korte M, Goetz M & Barde YA. (2004). Differentiation of mouse embryonic stem cells into a defined neuronal lineage. *Nat Neurosci* **7,** 1003-1009.

Biella G, Di Febo F, Goffredo D, Moiana A, Taglietti V, Conti L, Cattaneo E & Toselli M. (2007). Differentiating embryonic stem-derived neural stem cells show a maturation-dependent pattern of voltage-gated sodium current expression and graded action potentials. *Neuroscience* **149,** 38-52.

Birnbaumer L. (1990). G proteins in signal transduction. *Annu Rev Pharmacol Toxicol* **30,** 675-705.

Bjorklund A, Dunnett SB, Stenevi U, Lewis ME & Iversen SD. (1980). Re-innervation of the denervated striatum by substantia nigra transplants - functional consequences as revealed by pharmacological and sensorimotor testing. *Brain Res* **199,** 307-333.

Bjorklund A & Stenevi U. (1979). Reconstruction of the nigrostriatal dopamine pathway by intra-cerebral nigral transplants. *Brain Res* **177,** 555-560.

Blanton MG, Lo Turco JJ & Kriegstein AR. (1990). Endogenous neurotransmitter activates n-methyl-d-aspartate receptors on differentiating neurons in embryonic cortex. *Proc Natl Acad Sci USA* **87,** 8027-8030.

Bleasdale JE, Thakur NR, Gremban RS, Bundy GL, Fitzpatrick FA, Smith RJ & Bunting S. (1990). Selective inhibition of receptor-coupled phospholipase c-dependent processes in human platelets and polymorphonuclear neutrophils. *J Pharmacol Exp Ther* **255,** 756-768.

Blum B & Benvenisty N. (2008). The tumorigenicity of human embryonic stem cells. *Advances in Cancer Research, Vol 100* **100,** 133-+.

Bodin P & Burnstock G. (2001). Purinergic signalling: ATP release. *Neurochem Res* **26,** 959-969.

Bolteus AJ & Bordey A. (2004). GABA release and uptake regulate neuronal precursor migration in the postnatal subventricular zone. *J Neurosci* **24,** 7623-7631.

Bongso A & Fong C-Y. (2009). Human embryonic stem cells: Their nature, properties, and uses. *Trends in Stem Cell Biology and Technology***,** 1-17.

Bootman MD, Collins TJ, Mackenzie L, Roderick HL, Berridge MJ & Peppiatt CM. (2002). 2-aminoethoxydiphenyl borate (2-apb) is a reliable blocker of store-operated ca2+ entry but an inconsistent inhibitor of insp3-induced ca2+ release. *The FASEB Journal* **16,** 1145-1150.

Bootman MD, Collins TJ, Peppiatt CM, Prothero LS, MacKenzie L, De Smet P, Travers M, Tovey SC, Seo JT, Berridge MJ, Ciccolini F & Lipp P. (2001). Calcium signalling--an overview. *Semin Cell Dev Biol* **12,** 3-10.

Born GVR. (1962). Aggregation of blood platelets by adenosine diphosphate and its reversal. *Nature* **194,** 927-&.

Brinley FJ & Mullins LJ. (1967). Sodium extrusion by internally dialyzed squid axons. *J Gen Physiol* **50,** 2303-&.

Brundin P, Barker RA & Parmar M. (2010). Chapter 14 - neural grafting in parkinson's disease: Problems and possibilities. In *Prog brain res*, pp. 265-294. Elsevier.

Brundin P, Pogarell O, Hagell P, Piccini P, Widner H, Schrag A, Kupsch A, Crabb L, Odin P, Gustavii B, Bjorklund A, Brooks DJ, David Marsden C, Oertel WH, Quinn NP, Rehncrona S & Lindvall O. (2000). Bilateral caudate and putamen grafts of embryonic mesencephalic tissue treated with lazaroids in parkinson's disease. *Brain* **123,** 1380-1390.

Burnstock G. (2002). Purinergic signaling and vascular cell proliferation and death. *Arterioscler Thromb Vasc Biol* **22,** 364-373.

Burnstock G. (2006). Purinergic signalling. *Br J Pharmacol* **147,** S172-S181.

Burnstock G & Kennedy C. (1986). A dual function for adenosine 5'-triphosphate in the regulation of vascular tone - excitatory cotransmitter with noradrenaline from perivascular nerves and locally released inhibitory intravascular agent. *Circ Res* **58,** 319-330.

Burnstock G & Ulrich H. (2011). Purinergic signaling in embryonic and stem cell development. *Cell Mol Life Sci* **68,** 1369-1394.

Burnstock G & Verkhratsky A. (2009). Evolutionary origins of the purinergic signalling system. *Acta Physiologica* **195,** 415-447.

Burnstock G & Williams M. (2000). P2 purinergic receptors: Modulation of cell function and therapeutic potential. *J Pharmacol Exp Ther* **295,** 862-869.

Cancedda L, Fiumelli H, Chen K & Poo M. (2007). Excitatory GABA action is essential for morphological maturation of cortical neurons in vivo. *J Neurosci* **27,** 5224-5235.

Carleton A, Petreanu LT, Lansford R, Alvarez-Buylla A & Lledo PM. (2003). Becoming a new neuron in the adult olfactory bulb. *Nat Neurosci* **6,** 507-518.

Castle NA, Wickenden AD & Zou A. (2001). Electrophysiological analysis of heterologously expressed kv and sk/ik potassium channels. In *Current protocols in pharmacology*. John Wiley & Sons, Inc.

Catterall WA. (2011). Voltage-gated calcium channels. *Cold Spring Harbor Perspectives in Biology* **3**.

Chandler WK, Hodgkin AL & Meves H. (1965). Effect of changing internal solution on sodium inactivation and related phenomena in giant axons. *Journal of Physiology-London* **180,** 821-&.

Chavas J & Marty A. (2003). Coexistence of excitatory and inhibitory GABA synapses in the cerebellar interneuron network. *J Neurosci* **23,** 2019-2031.

Chen LY & Liu L. (2009). Current progress and prospects of induced pluripotent stem cells. *Science in China Series C-Life Sciences* **52,** 622-636.

Cho T, Bae JH, Choi HB, Kim SS, McLarnon JG, Suh-Kim H, Kim SU & Min CK. (2002). Human neural stem cells: Electrophysiological properties of voltage-gated ion channels. *Neuroreport* **13,** 1447-1452.

Cooke BA. (1999). Signal transduction involving cyclic AMP-dependent and cyclic AMP-independent mechanisms in the control of steroidogenesis. *Mol Cell Endocrinol* **151,** 25-35.

Corlew R, Bosma MM & Moody WJ. (2004). Spontaneous, synchronous electrical activity in neonatal mouse cortical neurones. *J Physiol (Lond)* **560,** 377-390.

Cristante AF, Barros TEP, Tatsui N, Mendrone A, Caldas JG, Camargo A, Alexandre A, Teixeira WGJ, Oliveira RP & Marcon RM. (2009). Stem cells in the treatment of chronic spinal cord injury: Evaluation of somatosensitive evoked potentials in 39 patients. *Spinal Cord* **47,** 733-738.

Curtis HJ & Cole KS. (1942). Membrane resting and action potentials from the squid giant axon. *Journal of Cellular and Comparative Physiology* **19,** 135-144.

D'Ambrosi N, Murra B, Cavaliere F, Amadio S, Bernardi G, Burnstock G & Volonté C. (2001). Interaction between ATP and nerve growth factor signalling in the survival and neuritic outgrowth from pc12 cells. *Neuroscience* **108,** 527-534.

De Filippis L, Lamorte G, Snyder EY, Malgaroli A & Vescovi AL. (2007). A novel, immortal, and multipotent human neural stem cell line generating functional neurons and oligodendrocytes. *Stem Cells* **25,** 2312-2321.

Deckel AW, Moran TH & Robinson RG. (1986). Behavioral recovery following kainic acid lesions and fetal implants of the striatum occurs independent of dopaminergic mechanisms. *Brain Res* **363,** 383-385.

Deckel AW, Robinson RG, Coyle JT & Sanberg PR. (1983). Reversal of long-term locomotor abnormalities in the kainic acid model of huntingtons-disease by day-18 fetal striatal implants. *Eur J Pharmacol* **93,** 287-288.

Deisseroth K. (2004). Excitation-neurogenesis coupling in adult neural stem/progenitor cells. *Neuron* **42,** 535-552.

Deisseroth K, Singla S, Toda H, Monje M, Palmer TD & Malenka RC. (2004). Excitation-neurogenesis coupling in adult neural stem/progenitor cells. *Neuron* **42,** 535-552.

Delpire E, Days E, Lewis LM, Mi D, Kim K, Lindsley CW & Weaver CD. (2009). Small-molecule screen identifies inhibitors of the neuronal k-cl cotransporter kcc2. *Proceedings of the National Academy of Sciences* **106,** 5383-5388.

Dergham P, Ellezam B, Essagian C, Avedissian H, Lubell WD & McKerracher L. (2002). Rho signaling pathway targeted to promote spinal cord repair. *The Journal of Neuroscience* **22,** 6570-6577.

Dhara SK & Stice SL. (2008). Neural differentiation of human embryonic stem cells. *J Cell Biochem* **105,** 633-640.

Doetsch F & Hen R. (2005). Young and excitable: The function of new neurons in the adult mammalian brain. *Curr Opin Neurobiol* **15,** 121-128.

Dominguez-Bendala J, Ricordi C & Inverardi L. (2002). Stem cells and their clinical application. *Transplant Proc* **34,** 1372-1375.

Doyle DA, Cabral J, atilde, Morais o, Pfuetzner RA, Kuo A, Gulbis JM, Cohen SL, Chait BT & MacKinnon R. (1998). The structure of the potassium channel: Molecular basis of k+ conduction and selectivity. *Science* **280,** 69-77.

Drury AN & Szent-Gyorgyi A. (1929). The physiological activity of adenine compounds with especial reference to their action upon the mammalian heart. *Journal of Physiology-London* **68,** 213-237.

Dubyak GR & el-Moatassim C. (1993). Signal transduction via p2-purinergic receptors for extracellular ATP and other nucleotides. *American Journal of Physiology - Cell Physiology* **265,** C577-C606.

Dunnett SB, Bjorklund A, Stenevi U & Iversen SD. (1981). Behavioral recovery following transplantation of substantia nigra in rats subjected to 6-ohda lesions of the nigrostriatal pathway .1. Unilateral lesions. *Brain Res* **215,** 147-161.

Ebihara S, Shirato K, Harata N & Akaike N. (1995). Gramicidin-perforated patch recording: GABA response in mammalian neurones with intact intracellular chloride. *The Journal of Physiology* **484,** 77-86.

Evans RJ, Lewis C, Buell G, Valera S, North RA & Surprenant A. (1995). Pharmacological characterization of heterologously expressed ATP-gated cation channels (p2x purinoceptors). *Mol Pharmacol* **48,** 178-183.

Fiszman ML, Borodinsky LN & Neale JH. (1999). GABA induces proliferation of immature cerebellar granule cells grown in vitro. *Dev Brain Res* **115,** 1-8.

Flint AC, Dammerman RS & Kriegstein AR. (1999). Endogenous activation of metabotropic glutamate receptors in neocortical development causes neuronal ca oscillations. *Proc Natl Acad Sci USA* **96,** 12144-12149.

Freed CR, Greene PE, Breeze RE, Tsai W-Y, DuMouchel W, Kao R, Dillon S, Winfield H, Culver S, Trojanowski JQ, Eidelberg D & Fahn S. (2001). Transplantation of embryonic dopamine neurons for severe parkinson's disease. *N Engl J Med* **344,** 710-719.

Fritschy J-M & Mohler H. (1995). GABA_{a}-receptor heterogeneity in the adult rat brain: Differential regional and cellular distribution of seven major subunits. *The Journal of Comparative Neurology* **359,** 154-194.

Fuchs E & Gould E. (2000). In vivo neurogenesis in the adult brain: Regulation and functional implications. *Eur J Neurosci* **12,** 2211-2214.

Galli R, Gritti A & Vescovi AL. (2008). Adult neural stem cells. *Methods Mol Biol***,** 67-84.

Ganguly K, Schinder AF, Wong ST & Poo M. (2001). GABA itself promotes the developmental switch of neuronal gabaergic responses from excitation to inhibition. *Cell* **105,** 521-532.

Gao B-X & Ziskind-Conhaim L. (1998). Development of ionic currents underlying changes in action potential waveforms in rat spinal motoneurons. *J Neurophysiol* **80,** 3047-3061.

Gáspár T, Katakam P, Snipes JA, Kis B, Domoki F, Bari F & Busija DW. (2008). Delayed neuronal preconditioning by ns1619 is independent of calcium activated potassium channels. *J Neurochem* **105,** 1115-1128.

Gaura V, Bachoud-Levi AC, Ribeiro MJ, Nguyen JP, Frouin V, Baudic S, Brugieres P, Mangin JF, Boisse MF, Palfi S, Cesaro P, Samson Y, Hantraye P, Peschanski M & Remy P. (2004). Striatal neural grafting improves cortical metabolism in huntington's disease patients. *Brain* **127,** 65-72.

Ge S. (2006). GABA regulates synaptic integration of newly generated neurons in the adult brain. *Nature* **439,** 589-593.

Goffredo D, Conti L, Di Febo F, Biella G, Tosoni A, Vago G, Biunno I, Moiana A, Bolognini D, Toselli M & Cattaneo E. (2008). Setting the conditions for efficient, robust and reproducible generation of functionally active neurons from adult subventricular zone-derived neural stem cells. *Cell Death Differ* **15,** 1847-1856.

Gold MR & Martin AR. (1984). Gamma-aminobutyric acid and glycine activate cl-channels having different characteristics in cns neurons. *Nature* **308,** 639-641.

Goldman L & Schauf CL. (1972). Inactivation of sodium current in myxicola giant axons - evidence for coupling to activation process. *J Gen Physiol* **59,** 659-&.

Goldstein SAN, Bayliss DA, Kim D, Lesage F, Plant LD & Rajan S. (2005). International union of pharmacology. Lv. Nomenclature and molecular relationships of two-p potassium channels. *Pharmacol Rev* **57,** 527-540.

Gouaux E & MacKinnon R. (2005). Principles of selective ion transport in channels and pumps. *Science* **310,** 1461-1465.

Greer PL & Greenberg ME. (2008). From synapse to nucleus: Calcium-dependent gene transcription in the control of synapse development and function. *Neuron* **59,** 846-860.

Greig AVH, Linge C, Cambrey A & Burnstock G. (2003). Purinergic receptors are part of a signaling system for keratinocyte proliferation, differentiation, and apoptosis in human fetal epidermis. **121,** 1145-1149.

Grimm I, Ullsperger SN & Zimmermann H. (2010). Nucleotides and epidermal growth factor induce parallel cytoskeletal rearrangements and migration in cultured adult murine neural stem cells. *Acta Physiologica* **199,** 181-189.

Grynkiewicz G, Poenie M & Tsien RY. (1985). A new generation of ca-2+ indicators with greatly improved fluorescence properties. *J Biol Chem* **260,** 3440-3450.

Habela CW, Ernest NJ, Swindall AF & Sontheimer H. (2009). Chloride accumulation drives volume dynamics underlying cell proliferation and migration. *J Neurophysiol* **101,** 750-757.

Hagell P, Schrag A, Piccini P, Jahanshahi M, Brown R, Rehncrona S, Widner H, Brundin P, Rothwell JC, Odin P, Wenning GK, Morrish P, Gustavii B, Bjorklund A, Brooks DJ, Marsden CD, Quinn NP & Lindvall O. (1999). Sequential bilateral transplantation in parkinson's disease - effects of the second graft. *Brain* **122,** 1121-1132.

Hamill OP, Marty A, Neher E, Sakmann B & Sigworth FJ. (1981). Improved patch-clamp techniques for high-resolution current recording from cells and cell-free membrane patches. *Pflugers Archiv European Journal of Physiology* **391,** 85-100.

Hauser RA, Freeman TB, Snow BJ, Nauert M, Gauger L, Kordower JH & Olanow CW. (1999). Long-term evaluation of bilateral fetal nigral transplantation in parkinson disease. *Arch Neurol* **56,** 179-187.

Haydar TF, Wang F, Schwartz ML & Rakic P. (2000). Differential modulation of proliferation in the neocortical ventricular and subventricular zones. *J Neurosci* **20,** 5764-5774.

Hebert JM & Fishell G. (2008). The genetics of early telencephalon patterning: Some assembly required. *Nature Reviews Neuroscience* **9,** 678-685.

Hellstraom NAK, Bjork-Eriksson T, Blomgren K & Kuhn HG. (2009). Differential recovery of neural stem cells in the subventricular zone and dentate gyrus after ionizing radiation. *Stem Cells* **27,** 634-641.

Hodgkin AL & Huxley AF. (1939). Action potentials recorded from inside a nerve fibre. *Nature* **144,** 710-711.

Hodgkin AL & Huxley AF. (1945). Resting and action potentials in single nerve fibres. *Journal of Physiology-London* **104,** 176-195.

Hodgkin AL & Huxley AF. (1952a). A quantitative description of membrane current and its application to conduction and excitation in nerve. *Journal of Physiology-London* **117,** 500-544.

Homolya L, Steinberg TH & Boucher RC. (2000). Cell to cell communication in response to mechanical stress via bilateral release of atp and utp in polarized epithelia. *The Journal of Cell Biology* **150,** 1349-1360.

Horn R, Marty A & Korn SJ. (1988). Perforated patch recording to prevent wash-out. *Biophys J* **53,** A360-A360.

Huang R-Q & Dillon GH. (2002). Functional characterization of gabaa receptors in neonatal hypothalamic brain slice. *J Neurophysiol* **88,** 1655-1663.

Hunt PN, McCabe AK & Bosma MM. (2005). Midline serotonergic neurones contribute to widespread synchronized activity in embryonic mouse hindbrain. *J Physiol (Lond)* **566,** 807-819.

Isacson O, Brundin P, Kelly PAT, Gage FH & Bjorklund A. (1984). Functional neuronal replacement by grafted striatal neurons in the ibotenic acid-lesioned rat striatum. *Nature* **311,** 458-460.

Isacson O, Dunnett SB & Bjorklund A. (1986). Graft-induced behavioral recovery in an animal-model of huntington disease. *Proc Natl Acad Sci U S A* **83,** 2728-2732.

Iwasaki S, Momiyama A, Uchitel OD & Takahashi T. (2000). Developmental changes in calcium channel types mediating central synaptic transmission. *The Journal of Neuroscience* **20,** 59-65.

Jain M, Armstrong RJE, Barker RA & Rosser AE. (2001). Cellular and molecular aspects of striatal development. *Brain Res Bull* **55,** 533-540.

Jaksch M, Múnera J, Bajpai R, Terskikh A & Oshima RG. (2008). Cell cycle-dependent variation of a cd133 epitope in human embryonic stem cell, colon cancer, and melanoma cell lines. *Cancer Res* **68,** 7882-7886.

Jentsch TJ, Stein V, Weinreich F & Zdebik AA. (2002). Molecular structure and physiological function of chloride channels. *Physiol Rev* **82,** 503-568.

Joannides AJ, Fiore-Hériché C, Battersby AA, Athauda-Arachchi P, Bouhon IA, Williams L, Westmore K, Kemp PJ, Compston A, Allen ND & Chandran S. (2007a). A scaleable and defined system for generating neural stem cells from human embryonic stem cells. *Stem Cells* **25,** 731-737.

Joannides AJ, Webber DJ, Raineteau O, Kelly C, Irvine K-A, Watts C, Rosser AE, Kemp PJ, Blakemore WF, Compston A, Caldwell MA, Allen ND & Chandran S. (2007b). Environmental signals regulate lineage choice and temporal maturation of neural stem cells from human embryonic stem cells. *Brain* **130,** 1263-1275.

Joannides AJ, Webber DJ, Raineteau O, Kelly C, Irvine KA, Watts C, Rosser AE, Kemp PJ, Blakemore WF, Compston A, Caldwell MA, Allen ND & Chandran S. (2007c). Environmental signals regulate lineage choice and temporal maturation of neural stem cells from human embryonic stem cells. *Brain* **130,** 1263-1275.

Johnson MA, Weick JP, Pearce RA & Zhang S-C. (2007). Functional neural development from human embryonic stem cells: Accelerated synaptic activity via astrocyte coculture. *The Journal of Neuroscience* **27,** 3069-3077.

Kahan BD. (2009). Forty years of publication of transplantation proceedings--the second decade: The cyclosporine revolution. *Transplant Proc* **41,** 1423-1437.

Kallen RG, Cohen SA & Barchi RL. (1993). Structure, function and expression of voltage-dependent sodium-channels. *Mol Neurobiol* **7,** 383-428.

Kelly CM, Precious SV, Torres EM, Harrison AW, Williams D, Scherf C, Weyrauch UM, Lane EL, Allen ND, Penketh R, Amso NN, Kemp PJ, Dunnett SB & Rosser AE. (2011). Medical terminations of pregnancy: A viable source of tissue for cell replacement therapy for neurodegenerative disorders. *Cell Transplant* **20,** 503-513.

Kempermann G & Gage FH. (1999). New nerve cells for the adult brain. *Sci Am* **280,** 48-53.

Kim M, Lee S-T, Chu K & Kim SU. (2008). Stem cell-based cell therapy for huntington disease: A review. *Neuropathology* **28,** 1-9.

King BF, Wildman SS, Ziganshina LE, Pintor J & Burnstock G. (1997). Effects of extracellular ph on agonism and antagonism at a recombinant p2x2 receptor. *Br J Pharmacol* **121,** 1445-1453.

King BF, Ziganshina LE, Pintor J & Burnstock G. (1996). Full sensitivity of p-2x2 purinoceptor to ATP revealed by changing extracellular ph. *Br J Pharmacol* **117,** 1371-1373.

Klinger M, Freissmuth M & Nanoff C. (2002). Adenosine receptors: G protein-mediated signalling and the role of accessory proteins. *Cell Signal* **14,** 99-108.

Komuro H & Rakic P. (1996). Intracellular ca2+ fluctuations modulate the rate of neuronal migration. *Neuron* **17,** 275-285.

Koyanagi M, Takahashi J, Arakawa Y, Doi D, Fukuda H, Hayashi H, Narumiya S & Hashimoto N. (2008). Inhibition of the rho/rock pathway reduces apoptosis during transplantation of embryonic stem cell-derived neural precursors. *J Neurosci Res* **86,** 270-280.

Landles C & Bates GP. (2004). Huntingtin and the molecular pathogenesis of huntington's disease. *EMBO Rep* **5,** 958-963.

Lazarowski ER & Boucher RC. (2001). Utp as an extracellular signaling molecule. *Physiology* **16,** 1-5.

Le Gros Clark W. (1940). Neuronal differentiation in implanted foetal cortical tissue. *Journal of Neurology and Psychiatry* **3,** 263-272.

Lin JHC, Takano T, Arcuino G, Wang X, Hu F, Darzynkiewicz Z, Nunes M, Goldman SA & Nedergaard M. (2007). Purinergic signaling regulates neural progenitor cell expansion and neurogenesis. *Dev Biol* **302,** 356-366.

Lindvall O & Bjorklund A. (2004). Cell therapy in parkinson's disease. *NeuroRX* **1,** 382-393.

Lindvall O & Kokaia Z. (2006). Stem cells for the treatment of neurological disorders. *Nature* **441,** 1094-1096.

Liu X, Wang Q, Haydar TF & Bordey A. (2005). Nonsynaptic GABA signaling in postnatal subventricular zone controls proliferation of gfap-expressing progenitors. *Nature Neurosci* **8,** 1179-1187.

LoTurco JJ, Owens DF, Heath MJ, Davis MB & Kriegstein AR. (1995). GABA and glutamate depolarize cortical progenitor cells and inhibit DNA synthesis. *Neuron* **15,** 1287-1298.

Ludbrook J. (1991). On making multiple comparisons in clinical and experimental pharmacology and physiology. *Clin Exp Pharmacol Physiol* **18,** 379-392.

Ma DK, Bonaguidi MA, Ming G-l & Song H. (2009). Adult neural stem cells in the mammalian central nervous system. *Cell Res* **19,** 672-682.

Manent JB. (2005). A noncanonical release of GABA and glutamate modulates neuronal migration. *J Neurosci* **25,** 4755-4765.

Marinissen MJ & Gutkind JS. (2001). G-protein-coupled receptors and signaling networks: Emerging paradigms. *Trends Pharmacol Sci* **22,** 368-376.

Markakis EA & Redmond JDE. (2005). Know thyself: Autologous cell transplantation strategies for brain repair. *Exp Neurol* **196,** 6-8.

Marrale J, Morrissey M & Haddad F. (2007). A literature review of autograft and allograft anterior cruciate ligament reconstruction. *Knee Surg Sports Traumatol Arthrosc* **15,** 690-704.

Marty A & Finkelstein A. (1975). Pores formed in lipid bilayer membranes by nystatin - differences in its one-sided and 2-sided action. *J Gen Physiol* **65,** 515-526.

Maruyama T, Kanaji T, Nakade S, Kanno T & Mikoshiba K. (1997). 2apb, 2-aminoethoxydiphenyl borate, a membrane-penetrable modulator of ins(1,4,5)p-3-induced ca2+ release. *J Biochem (Tokyo)* **122,** 498-505.

McDonald JW & Becker D. (2003). Spinal cord injury - promising interventions and realistic goals. *Am J Phys Med Rehabil* **82,** S38-S49.

Menasche P. (2009). Cell therapy: Results in cardiology. *Bull Acad Natl Med* **193,** 559-568.

Mennerick S & Zorumski CF. (2000). Neural activity and survival in the developing nervous system. *Mol Neurobiol* **22,** 41-54.

Ming G-l & Song H. (2011). Adult neurogenesis in the mammalian brain: Significant answers and significant questions. *Neuron* **70,** 687-702.

Ming G, Henley J, Tessier-Lavigne M, Song H & Poo M. (2001). Electrical activity modulates growth cone guidance by diffusible factors. *Neuron* **29,** 441-452.

Mishra SK, Braun N, Shukla V, Fullgrabe M, Schomerus C, Korf H-W, Gachet C, Ikehara Y, Sovigny J, Robson SC & Zimmermann H. (2006). Extracellular nucleotide signaling in adult neural stem cells: Synergism with growth factor-mediated cellular proliferation. *Development* **133,** 675-684.

Murray J, Merrill J & Harrison J. (1956). Renal homotransplantation in identical twins. *J Am Soc Nephrol* **12,** 201-204.

Nabekura J, Ueno T, Okabe A, Furuta A, Iwaki T, Shimizu-Okabe C, Fukuda A & Akaike N. (2002). Reduction of kcc2 expression and gabaareceptor-mediated excitation after in vivo axonal injury. *The Journal of Neuroscience* **22,** 4412-4417.

Narahashi T, Moore JW & Scott WR. (1964). Tetrodotoxin blockage of sodium conductance increase in lobster giant axons. *J Gen Physiol* **47,** 965-&.

Neary JT, Lenz G, Kang Y, Rodnight R & Avruch J. (2001). Role of mitogen-activated protein kinase cascades in p2y receptor-mediated trophic activation of astroglial cells. *Drug Development Research* **53,** 158-165.

Neary JT, McCarthy M, Kang Y & Zuniga S. (1998). Mitogenic signaling from p1 and p2 purinergic receptors to mitogen-activated protein kinase in human fetal astrocyte cultures. *Neurosci Lett* **242,** 159-162.

Neher E, Sakmann B & Steinbach JH. (1978). Extracellular patch clamp - method for resolving currents through individual open channels in biological-membranes. *Pflugers Archiv-European Journal of Physiology* **375,** 219-228.

Nguyen L, Malgrange B, Breuskin I, Bettendorff L, Moonen G, Belachew S & Rigo JM. (2003). Autocrine/paracrine activation of the gabaa receptor inhibits the proliferation of neurogenic polysialylated neural cell adhesion molecule - positive (psa - ncam!+) precursor cells from postnatal striatum. *Society for Neuroscience Abstract Viewer and Itinerary Planner* **2003,** Abstract No. 562.515.

Nichols CG & Lopatin AN. (1997). Inward rectifier potassium channels. *Annu Rev Physiol* **59,** 171-191.

Normile D. (2009). Recipe for induced pluripotent stem cells just got clearer. *Science* **325,** 803-a-.

North RA. (2002). Molecular physiology of p2x receptors. *Physiol Rev* **82,** 1013 - 1067.

O'Brien T & Barry FP. (2009). Stem cell therapy and regenerative medicine. *Mayo Clin Proc* **84,** 859-861.

O'Rahilly R & Muller F. (1999). *The embryonic human brain: An atlas of developmental stages*. Wiley-Liss Inc., New York.

Obrietan K & Vandenpol AN. (1995). GABA neurotransmission in the hypothalamus - developmental reversal from ca2+ elevating to depressing. *J Neurosci* **15,** 5065-5077.

Ogawa D, Okada Y, Nakamura M, Kanemura Y, Okano HJ, Matsuzaki Y, Shimazaki T, Ito M, Ikeda E, Tamiya T, Nagao S & Okano H. (2009). Evaluation of human fetal neural stem/progenitor cells as a source for cell replacement therapy for neurological disorders: Properties and tumorigenicity after long-term in vitro maintenance. *J Neurosci Res* **87,** 307-317.

Oikawa T, Tasaki I, Spyropoulos CS & Teorell T. (1961). Methods for perfusing giant axon of loligo pealii. *Acta Physiol Scand* **52,** 195-&.

Olesen S-P, Munch E, Moldt P & Drejer J. (1994). Selective activation of ca2+ - dependent k+ channels by novel benzimidazolone. *Eur J Pharmacol* **251,** 53-59.

Olga A S. (1998). Comparison of glycine- and GABA-evoked currents in two types of neurons isolated from the rat striatum. *Neurosci Lett* **243,** 9-12.

Olsen RW & Sieghart W. (2008). International union of pharmacology. Lxx. Subtypes of gamma-aminobutyric acid(a) receptors: Classification on the basis of subunit composition, pharmacology, and function. Update. *Pharmacol Rev* **60,** 243-260.

Olsson M, Björklund A & Campbell K. (1998). Early specification of striatal projection neurons and interneuronal subtypes in the lateral and medial ganglionic eminence. *Neuroscience* **84,** 867-876.

Owens DF, Boyce LH, Davis MBE & Kriegstein AR. (1996). Excitatory GABA responses in embryonic and neonatal cortical slices demonstrated by gramicidin perforated-patch recordings and calcium imaging. *J Neurosci* **16,** 6414-6423.

Palma E, Amici M, Sobrero F, Spinelli G, Di Angelantonio S, Ragozzino D, Mascia A, Scoppetta C, Esposito V, Miledi R & Eusebi F. (2006). Anomalous levels of cl^- transporters in the hippocampal subiculum from temporal lobe epilepsy patients make GABA excitatory. *Proceedings of the National Academy of Sciences* **103,** 8465-8468.

Pankratov Y, Lalo U, Verkhratsky A & North R. (2006). Vesicular release of ATP at central synapses. *PflÃ¼gers Archiv European Journal of Physiology* **452,** 589-597.

Parent A & Hazrati LN. (1995). Functional-anatomy of the basal ganglia .1. The cortico-basal ganglia-thalamo-cortical loop. *Brain Research Reviews* **20,** 91-127.

Parga JA, Rodriguez-Pallares J, Guerra MJ & Labandeira-Garcia JL. (2007). Effects of GABA and GABA receptor inhibition on differentiation of mesencephalic precursors into dopaminergic neurons in vitro. *Developmental Neurobiology* **67,** 1549-1559.

Perlow MJ, Freed WJ, Hoffer BJ, Seiger A, Olson L & Wyatt RJ. (1979). Brain grafts reduce motor abnormalities produced by destruction of nigrostriatal dopamine system. *Science* **204,** 643-647.

Piccini P, Brooks DJ, Bjorklund A, Gunn RN, Grasby PM, Rimoldi O, Brundin P, Hagell P, Rehncrona S, Widner H & Lindvall O. (1999). Dopamine release from nigral transplants visualized in vivo in a parkinson's patient. *Nat Neurosci* **2,** 1137-1140.

Picken Bahrey HL & Moody WJ. (2003a). Voltage-gated currents, dye and electrical coupling in the embryonic mouse neocortex. *Cereb Cortex* **13,** 239-251.

Picken Bahrey HL & Moody WJ. (2003b). Early development of voltage-gated ion currents and firing properties in neurons of the mouse cerebral cortex. *J Neurophysiol* **89,** 1761-1773.

Plant LD, Rajan S & Goldstein SAN. (2005). K2p channels and their protein partners. *Curr Opin Neurobiol* **15,** 326-333.

Ralevic V & Burnstock G. (1998). Receptors for purines and pyrimidines. *Pharmacol Rev* **50,** 413-492.

Redmond DE, Sladek JR, Roth RH, Collier TJ, Elsworth JD, Deutch AY & Haber S. (1986). Fetal neuronal grafts in monkeys given methylphenyltetrahydropyridine. *Lancet* **1,** 1125-1127.

Rego AC, Lambert JJ & Nicholls DG. (2001). Developmental profile of excitatory gabaa responses in cultured rat cerebellar granule cells. *Neuroreport* **12,** 477-482.

Represa A & Ben-Ari Y. (2005). Trophic actions of GABA on neuronal development. *Trends Neurosci* **28,** 278-283.

Resende RR, Britto LRG & Ulrich H. (2008). Pharmacological properties of purinergic receptors and their effects on proliferation and induction of neuronal differentiation of p19 embryonal carcinoma cells. *Int J Dev Neurosci* **26,** 763-777.

Reubinoff BE, Itsykson P, Turetsky T, Pera MF, Reinhartz E, Itzik A & Ben-Hur T. (2001). Neural progenitors from human embryonic stem cells. *Nat Biotechnol* **19,** 1134-1140.

Reynolds BA & Weiss S. (1992). Generation of neurons and astrocytes from isolated cells of the adult mammalian central nervous system. *Science* **255,** 1707-1710.

Rivera C, Voipio J & Kaila K. (2005). Two developmental switches in gabaergic signalling: The k+-cl- cotransporter kcc2 and carbonic anhydrase cavii. *Journal of Physiology-London* **562,** 27-36.

Rodrigues CAV, Fernandes TG, Diogo MM, da Silva CL & Cabral JMS. (2011). Stem cell cultivation in bioreactors. *Biotechnology Advances* **In Press, Corrected Proof**.

Rojas E & Luxoro M. (1963). Micro-injection of trypsin into axons of squid. *Nature* **199,** 78-&.

Rubenstein JLR, Shimamura K, Martinez S & Puelles L. (1998). Regionalization of the prosencephalic neural plate. *Annu Rev Neurosci* **21,** 445-477.

Ryu JK, Choi HB, Hatori K, Heisel RL, Pelech SL, McLarnon JG & Kim SU. (2003). Adenosine triphosphate induces proliferation of human neural stem cells: Role of calcium and p70 ribosomal protein s6 kinase. *J Neurosci Res* **72,** 352-362.

Sakmann B, Edwards F, Konnerth A & Takahashi T. (1989). Patch clamp techniques used for studying synaptic transmission in slices of mammalian brain. *Q J Exp Physiol Cogn Med Sci* **74,** 1107-1118.

Sato C, Ueno Y, Asai K, Takahashi K, Sato M, Engel A & Fujiyoshi Y. (2001). The voltage-sensitive sodium channel is a bell-shaped molecule with several cavities. *Nature* **409,** 1047-1051.

Sauzeau V, le Jeune Hln, Cario-Toumaniantz C, Vaillant N, Gadeau A-P, Desgranges C, Scalbert E, Chardin P, Pacaud P & Loirand G. (2000). P2y1, p2y2, p2y4, and p2y6 receptors are coupled to rho and rho kinase activation in vascular myocytes. *American Journal of Physiology - Heart and Circulatory Physiology* **278,** H1751-H1761.

Savitz SI, Dinsmore JH, Wechsler LR, Rosenbaum DM & Caplan LR. (2004). Cell therapy for stroke. *NeuroRx* **1,** 406-414.

Scemes E, Duval N & Meda P. (2003). Reduced expression of p2y1 receptors in connexin43-null mice alters calcium signaling and migration of neural progenitor cells. *The Journal of Neuroscience* **23,** 11444-11452.

Schaarschmidt G, Wegner F, Schwarz SC, Schmidt H & Schwarz J. (2009). Characterization of voltage-gated potassium channels in human neural progenitor cells. *PLoS ONE* **4,** e6168.

Scheffler B, Edenhofer F & Brüstle O. (2006). Merging fields: Stem cells in neurogenesis, transplantation, and disease modeling. *Brain Pathol* **16,** 155-168.

Schwartz PH, Bryant PJ, Fuja TJ, Su H, O'Dowd DK & Klassen H. (2003). Isolation and characterization of neural progenitor cells from post-mortem human cortex. *J Neurosci Res* **74,** 838-851.

Seger R & Krebs EG. (1995). The mapk signaling cascade. *The FASEB Journal* **9,** 726-735.

Sekerli M, Del Negro CA, Lee RH & Butera RJ. (2004). Estimating action potential thresholds from neuronal time-series: New metrics and evaluation of methodologies. *Biomedical Engineering, IEEE Transactions on* **51,** 1665-1672.

Sen A, Kallos MS & Behie LA. (2004). New tissue dissociation protocol for scaled-up production of neural stem cells in suspension bioreactors. *Tissue Eng* **10,** 904-913.

Shen J & DiCorleto PE. (2008). ADP stimulates human endothelial cell migration via p2y1 nucleotide receptor-mediated mitogen-activated protein kinase pathways. *Circ Res* **102,** 448-456.

Shimomura O, Johnson FH & Saiga Y. (1962). Extraction, purification and properties of aequorin, a bioluminescent protein from luminous hydromedusan, aequorea. *Journal of Cellular and Comparative Physiology* **59,** 223-&.

Shukla V, Zimmermann H, Wang L, Kettenmann H, Raab S, Hammer K, Sévigny J, Robson SC & Braun N. (2005). Functional expression of the ecto-atpase ntpdase2 and of nucleotide receptors by neuronal progenitor cells in the adult murine hippocampus. *J Neurosci Res* **80,** 600-610.

Song HJ, Stevens CF & Gage FH. (2002). Neural stem cells from adult hippocampus develop essential properties of functional cns neurons. *Nature Neurosci* **5,** 438-445.

Sørensen CE & Novak I. (2001). Visualization of ATP release in pancreatic acini in response to cholinergic stimulus. *J Biol Chem* **276,** 32925-32932.

Soslau G & Youngprapakorn D. (1997). A possible dual physiological role of extracellular ATP in the modulation of platelet aggregation. *Biochimica et Biophysica Acta (BBA) - Molecular Cell Research* **1355,** 131-140.

Spitzer NC. (2006). Electrical activity in early neuronal development. *Nature* **444,** 707-712.

Starzl TE. (2000). History of clinical transplantation. *World J Surg* **24,** 759-782.

Strubing C, Ahnerthilger G, Shan J, Wiedenmann B, Hescheler J & Wobus AM. (1995). Differentiation of pluripotent embryonic stem-cells into the neuronal lineage in-vitro gives rise to mature inhibitory and excitatory neurons. *Mech Dev* **53,** 275-287.

Surprenant A, Rassendren F, Kawashima E, North RA & Buell G. (1996). The cytolytic p2z receptor for extracellular ATP identified as a p2x receptor (p2x7). *Science* **272,** 735-738.

Svendsen CN, ter Borg MG, Armstrong RJE, Rosser AE, Chandran S, Ostenfeld T & Caldwell MA. (1998). A new method for the rapid and long term growth of human neural precursor cells. *J Neurosci Methods* **85,** 141-152.

Takahashi K & Yamanaka S. (2006). Induction of pluripotent stem cells from mouse embryonic and adult fibroblast cultures by defined factors. *Cell* **126,** 663-676.

Tasaki I & Hagiwara S. (1957). Demonstration of 2 stable potential states in the squid giant axon under tetraethylammonium chloride. *J Gen Physiol* **40,** 859-885.

Thomson JA, Itskovitz-Eldor J, Shapiro SS, Waknitz MA, Swiergiel JJ, Marshall VS & Jones JM. (1998). Embryonic stem cell lines derived from human blastocysts. *Science* **282,** 1145-1147.

Tozuka Y, Fukuda S, Namba T, Seki T & Hisatsune T. (2005). Gabaergic excitation promotes neuronal differentiation in adult hippocampal progenitor cells. *Neuron* **47,** 803-815.

Trounson A, Thakar R, Lomax G & Gibbons D. (2011). Clinical trials for stem cell therapies. *BMC Medicine* **9,** 52.

Uchida N, Buck DW, He D, Reitsma MJ, Masek M, Phan TV, Tsukamoto AS, Gage FH & Weissman IL. (2000). Direct isolation of human central nervous system stem cells. *Proceedings of the National Academy of Sciences* **97,** 14720-14725.

Valeyev AY, Hackman JC, Holohean AM, Wood PM, Katz JL & Davidoff RA. (1999). GABA-induced cl^- current in cultured embryonic human dorsal root ganglion neurons. *J Neurophysiol* **82,** 1-9.

Varju P, Katarova Z, Madarász E & Szabó G. (2001). GABA signalling during development: New data and old questions. *Cell Tissue Res* **305,** 239-246.

Várnai P, Hunyady L & Balla T. (2009). Stim and orai: The long-awaited constituents of store-operated calcium entry. *Trends Pharmacol Sci* **30,** 118-128.

Verfaillie CM. (2002). Hematopoietic stem cells for transplantation. *Nat Immunol* **3,** 314-317.

von Kugelgen I & Wetter A. (2000). Molecular pharmacology of p2y-receptors. *Naunyn Schmiedebergs Arch Pharmacol* **362,** 310 - 323.

Wachs F-P, Couillard-Despres S, Engelhardt M, Wilhelm D, Ploetz S, Vroemen M, Kaesbauer J, Uyanik G, Klucken J, Karl C, Tebbing J, Svendsen C, Weidner N, Kuhn H-G, Winkler J & Aigner L. (2003). High efficacy of clonal growth and expansion of adult neural stem cells. *Lab Invest* **83,** 949-962.

Wang DD, Krueger DD & Bordey A. (2003). GABA depolarizes neuronal progenitors of the postnatal subventricular zone via gabaa receptor activation. *J Physiol (Lond)* **550,** 785-800.

Wang L, Jacobsen SE, Bengtsson A & Erlinge D. (2004). P2 receptor mRNA expression profiles in human lymphocytes, monocytes and cd34+ stem and progenitor cells. *BMC Immunology* **5,** 16.

Webb SE, Moreau M, Leclerc C & Miller AL. (2005). Calcium transients and neural induction in vertebrates. *Cell Calcium* **37,** 375-385.

Wei Q, Costanzi S, Liu Q-Z, Gao Z-G & Jacobson KA. (2011). Activation of the p2y1 receptor induces apoptosis and inhibits proliferation of prostate cancer cells. *Biochem Pharmacol* **82,** 418-425.

Wernig M, Benninger F, Schmandt T, Rade M, Tucker KL, Bussow H, Beck H & Brustle O. (2004). Functional integration of embryonic stem cell-derived neurons in vivo. *The Journal of Neuroscience* **24,** 5258-5268.

Wisden W & Seeburg PH. (1992). Gabaa receptor channels: From subunits to functional entities. *Curr Opin Neurobiol* **2,** 263-269.

Xu Y, Shi Y & Ding S. (2008). A chemical approach to stem-cell biology and regenerative medicine. *Nature* **453,** 338-344.

Yamada J, Okabe A, Toyoda H, Kilb W, Luhmann HJ & Fukuda A. (2004). Cl- uptake promoting depolarizing GABA actions in immature rat neocortical neurones is mediated by nkcc1. *Journal of Physiology-London* **557,** 829-841.

Yamada M, Tanemura K, Okada S, Iwanami A, Nakamura M, Mizuno H, Ozawa M, Ohyama-Goto R, Kitamura N, Kawano M, Tan-Takeuchi K, Ohtsuka C, Miyawaki A, Takashima A, Ogawa M, Toyama Y, Okano H & Kondo T. (2007). Electrical stimulation modulates fate determination of differentiating embryonic stem cells. *Stem Cells* **25,** 562-570.

Yegutkin GG. (2008). Nucleotide- and nucleoside-converting ectoenzymes: Important modulators of purinergic signalling cascade. *Biochimica et Biophysica Acta (BBA) - Molecular Cell Research* **1783,** 673-694.

Yu J, Vodyanik MA, Smuga-Otto K, Antosiewicz-Bourget J, Frane JL, Tian S, Nie J, Jonsdottir GA, Ruotti V, Stewart R, Slukvin II & Thomson JA. (2007). Induced pluripotent stem cell lines derived from human somatic cells. *Science* **318,** 1917-1920.

Zhang F, Li C, Wang R, Han D, Zhang QG, Zhou C, Yu HM & Zhang GY. (2007). Activation of GABA receptors attenuates neuronal apoptosis through inhibiting the tyrosine phosphorylation of nr2a by src after cerebral ischemia and reperfusion. *Neuroscience* **150,** 938-949.

Zhang S-C, Wernig M, Duncan ID, Brustle O & Thomson JA. (2001). In vitro differentiation of transplantable neural precursors from human embryonic stem cells. *Nat Biotech* **19,** 1129-1133.

Zhou B-Y, Ma W & Huang X-Y. (1998). Specific antibodies to the external vestibule of voltage-gated potassium channels block current. *The Journal of General Physiology* **111,** 555-563.

Zirm E. (1906). Eine erfolgreiche totale keratoplastik. *Graefe's Archive for Clinical and Experimental Opthalmology* **64,** 1145-1147.

Zito K & Svoboda K. (2002). Activity-dependent synaptogenesis in the adult mammalian cortex. *Neuron* **35,** 1015-1017.

Annex

This section annexes two papers accepted for publication and one submitted manuscript which contain works which I have contributed to but which have not been discussed at any great length in this thesis.